Atmospheric Gravity Waves and Soaring Flight

Physical principles and practical applications

Dieter Etling

as free publication available online at:

www.schwerewelle.de

Atmospheric Gravity Waves and Soaring Flight

Physical principles and practical applications

Dieter Etling

Institute of Meteorology and Climatology
Leibniz University Hannover
D-30419 Hannover, Germany

etling@muk.uni-hannover.de

Hannover, January 2014

Cover picture: Atmospheric gravity waves triggered by a small ridge named Ith in Northern Germany. Photograph by Andreas Gidde, Aeroclub Hameln

Table of contents

Preface

Glider pilots need lift for staying airborne. This lift is provided by vertical atmospheric motion from various meteorological phenomena including thermals and mountain waves. While the latter source of lift is treated in this booklet, we will not provide practical information about wave soaring, as this is treated in books written by glider pilots. Instead, it is the intention of this text to provide non specialists with some basic physical principles of atmospheric gravity waves.

The idea for this topic arose from the author's participation at yearly meetings of a group of glider pilots who exchange their experiences of wave soaring over small mountainous areas in Northern Germany. The author is not a pilot himself, but a meteorologist with a teaching position at the Leibniz University of Hannover, Germany. During these meetings, he tried to provide some explanations on the physical principles behind the formation of atmospheric gravity waves. It turned out that glider pilots know much more about mountain waves (a special class of gravity waves very favorable for wave soaring) than many meteorologists, but wanted further to understand the physical reasons for wave formation.

Initially, it was planned to provide a popular treatment of gravity waves without mathematical formulas. But during the early stages of writing, it turned out that some formal treatment of wave physics is necessary in order to understand the wave properties as observed by glider pilots. These wave principles are provided in Chapters 2 – 6. Gravity waves suitable for soaring flight are presented in Chapters 7 – 10, which contain little formal treatment. The booklet begins with an introduction to soaring and mountain waves in Chapter 1 and ends with a short history of soaring flight in Chapter 11. The material is provided for free to everyone interested in wave soaring or in atmospheric gravity waves in general. However, the reader has to take into account, that a professional layout as that provided by publishers is lacking.

Acknowledgements: This text could not have been written without various information provided by glider pilots. Firstly, I would like to mention Jörg Dummann, who is not only organizing the yearly meetings of wave soaring enthusiasts and runs the website `www.schwerewelle.de` as a forum for flight reports and other wave information, but has also encouraged me to write this text. Various glider pilots from this wave soaring community provided me with information and pictures, especially Karl-Heinz Dannhauer, Andreas Gidde, Rene Heise, Hendrik Hoeth, Carsten Lindemann and Christoph Maul. My former students Christoph Knigge and Niklas Kubitschke allowed me to use figures from their Diploma and PhD Theses. Richard Foreman helped with the language editing. And last but not least, Lennart Böske, student of meteorology, converted my hand-written equations and formulas and my hand-drawn figures into a nearly professional final layout.

1 Introduction

1.1 Soaring flight and meteorology

It is our experience that under the influence of gravity all bodies will fall. Some details on the motion of mass particles due to gravity forces will be given in Section 2.2. Let us consider, for example, a sphere with a diameter of 1 m and the weight of a modern sailplane of 250 kg. If we release this sphere from a height of 1000 m above ground, it will take only 14 seconds to hit the surface with a final speed of 140 m/s or 500 km/h if we neglect the influence of friction against the surrounding air. If friction is taken into account, the sphere will fall more slowly, but the terminal velocity will still be in the range of 100 m/s or 360 km/h. Sailplanes have sinking rates of about 1 m/s or even less. Hence, it will take about 1000 seconds or 16 minutes for a plane to reach the landing site from an initial altitude of 1000 m in still air. From these numbers, it follows that some vertical atmospheric motion will be necessary in order to keep gliders aloft for a longer time and that motion should exceed the sink speed of the gliders. Hence, we are looking for atmospheric motion with upward vertical velocities of more than 1 - 2 m/s.

The WMO monograph, Weather and Soaring Flight (OSTIV, 2009), lists various meteorological phenomena favorable for soaring (see Figure 1.1). In general, vertical motion can be divided into that induced by heating of the surface (thermal convection) and the lift due to flow convergence or orography, including ridge lift and mountain waves. The latter will be discussed shortly in the next section. These sources for atmospheric lift do not only differ with respect to

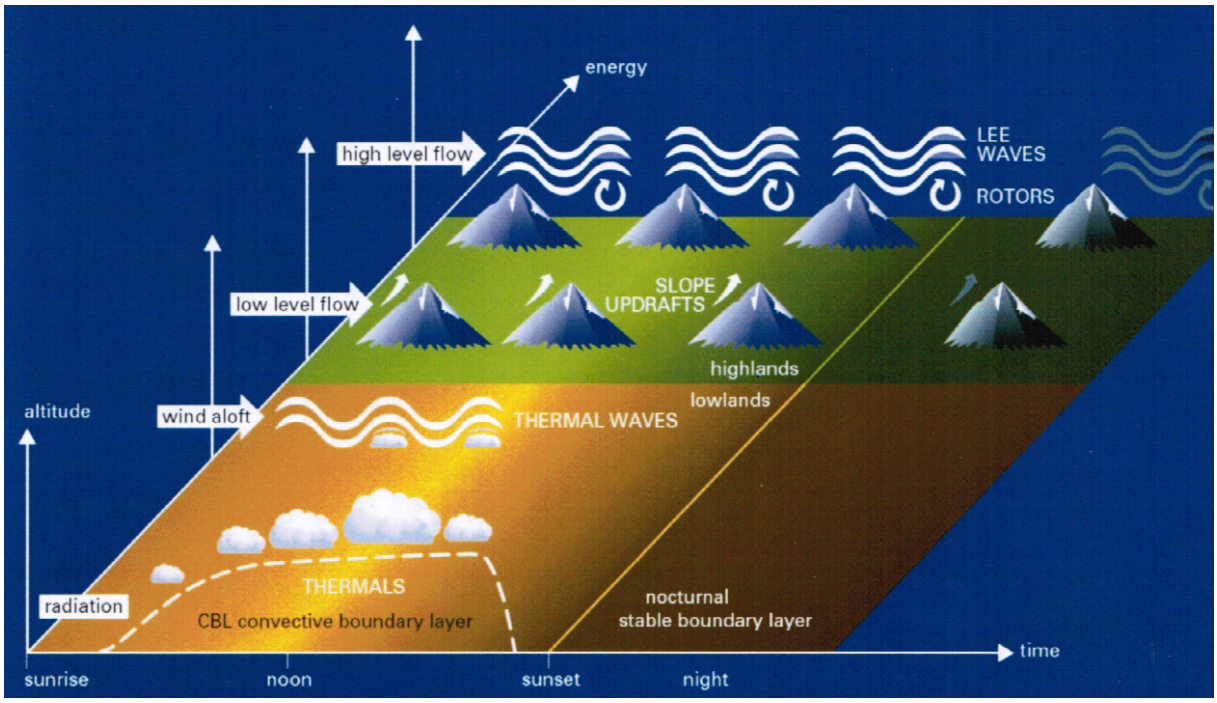

Fig. 1.1: Various meteorological phenomena to support soaring flight.
Source: OSTIV (2009), WMO-No. 1038

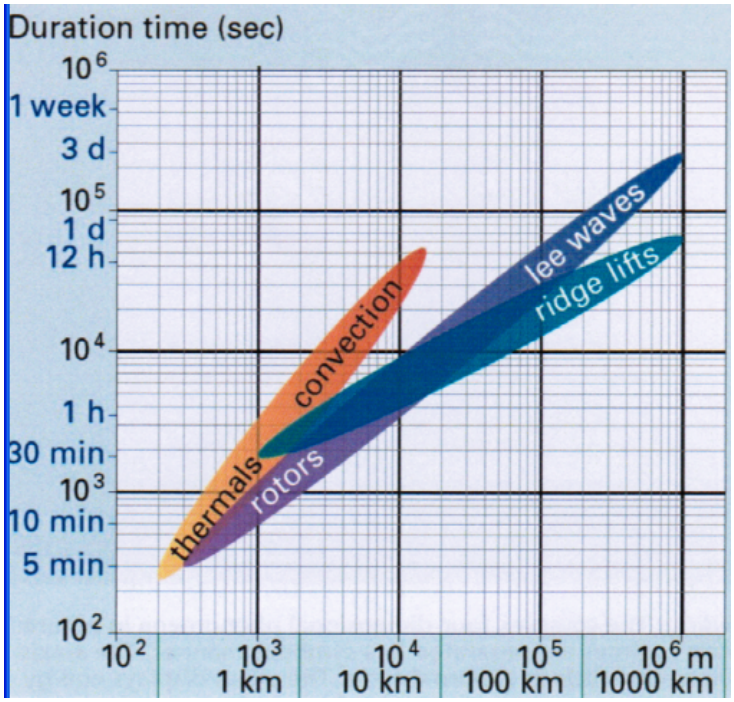

Fig. 1.2: Temporal and spatial scales of atmospheric motion useful for soaring flight.
Source: OSTIV (2009), WMO-No. 1038

their physical origin, but also with respect to their spatial and temporal time scales as shown in Figure 1.2. The various meteorological phenomena to support soaring flight are also discussed in any book on soaring. Here we mention only the monographs by Reichmann (1988) and Eckey (2012) and the special books on thermal soaring (Hertenstein, 2005) and wave soaring (Hertenstein, 2011).

1.2 Mountain waves

Mountain waves are a special class of atmospheric gravity wave found in the lee of mountains. A schematic diagram of mountain waves in the lee of the Hruby Jesenik ridge in the Czech Republic is shown in Figure 1.3. Similar schematics of mountain waves can be also found in any book on soaring flight. Shown is a cross section of the wave system which would extend over several kilometres in the direction parallel to the mountain ridge. The blue lines indicate pathways of air parcels approaching the ridge from the left (the luff side). Areas of upward wave motion are indicated by red crosses and symbolic sail planes. The special phenomenon of rotors beneath the wave crests near the ground is also indicated, with areas of very turbulent air motion indicated by cumulus clouds. The cumulus clouds can be contrasted with so-called lenticularis clouds shown in the upper part of the waves, which are indicators of smooth quasi laminar air flow. The wavelength in this particular case is between 4 and 8 km but will vary for other mountain areas. The mountain wave system extends parallel to the mountain ridge as can be seen in many satellite cloud pictures, for example, in Figure 1.4.

Importantly, unless the updrafts are thermals, the up and downdraft areas of the waves are practically fixed in space over long time scales (hours or even days). Hence, glider pilots can use these quasi-stationary areas of upward vertical air motion to balance or even counteract the sink rate of their planes. In fact, many world records for soaring flight have been obtained in mountain wave systems. We might mention the long distance record of 3009 km or the altitude record of 15460 m both flown in the lee of the Andes wave system. The PERLAN project (see `www.perlanproject.org`) even plans to reach altitudes of 100,000 ft or 30 km by using lee waves reaching out into the stratosphere.

Earlier record flights with respect to distance or altitude have also been flown in other high mountain areas like the Sierra Nevada in the USA, the Alps of Southern New Zealand or the European Alps. Some of these flights are documented in the monographs by Whelan (2000) and Delore and Dew (2005).

The Mountain Wave Project of the OSTIV (`www.mountain-wave-project.com`) collects world wide data on mountain waves and rotors in order to support the preparation of wave soaring. Not only high mountain ranges give rise to wave flights, but small mountain areas with heights less than 1000 m (see, e.g., Fig. 1.3) can also have lee wave systems supporting long distance and high altitude flights. We might mention the altitude record of about 10 km above the Southern Uplands of Scotland, where ridge heights are almost 1000 m. Altitudes of about 7 km have been reached in wave systems in low mountain areas of Germany, where some ridges are only 200 - 300 m high (Dummann, 2009). Various flights in the wave system of the Harz Mountains in Northern Germany are described by Dannhauer (2011).

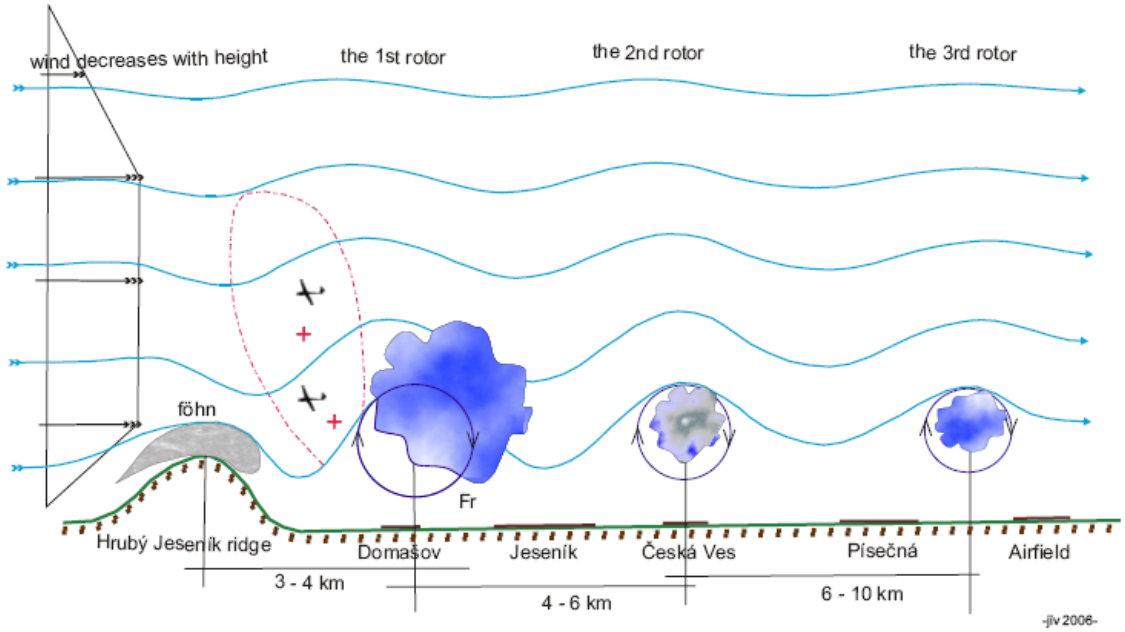

Fig. 1.3: Schematic of the lee waves in the area of the Hruby ridge near Jesenik, Czech Republic. The height of the mountain ridge is about 1000 m above the surrounding terrain.
Source: Aeroclub Jesenik

These wave flights tell us that high mountain areas are not necessary to induce atmospheric wave systems to be used for soaring flight. Hence, wave flights have been performed by hundreds of glider pilots during thousands of hours by using lower mountain ranges nearby their home. In Germany, those pilots are organized by the so-called "Mittelgebirgsleewelle (lee waves in low mountain ranges)" project (Dummann, 2009). Wave flights are reported on the website "`www.schwerewelle.de`" and a yearly meeting on wave soaring takes place. Attendance of these meetings shows that glider pilots have a very good understanding of all practical aspects of wave flight including the (dangerous) phenomenon of rotors, which are regularly connected to the mountain wave system. However, many pilots would also like to understand the physical mechanisms behind mountain waves. There are of course excellent monographs on atmospheric gravity waves including mountain waves like those by Nappo (2012) and Sutherland (2010), but these are intended for graduate students or atmospheric scientists as they require fundamental understanding of fluid mechanics and calculus. Special books on wave flight for soaring pilots by Dannhauer (2011), Hertenstein (2011) or Palmer (2004) are very instructive but are not aimed at explaining mountain wave physics. Hence, it is the intention of these notes to provide some basic physical principles behind atmospheric gravity waves, including mountain waves.

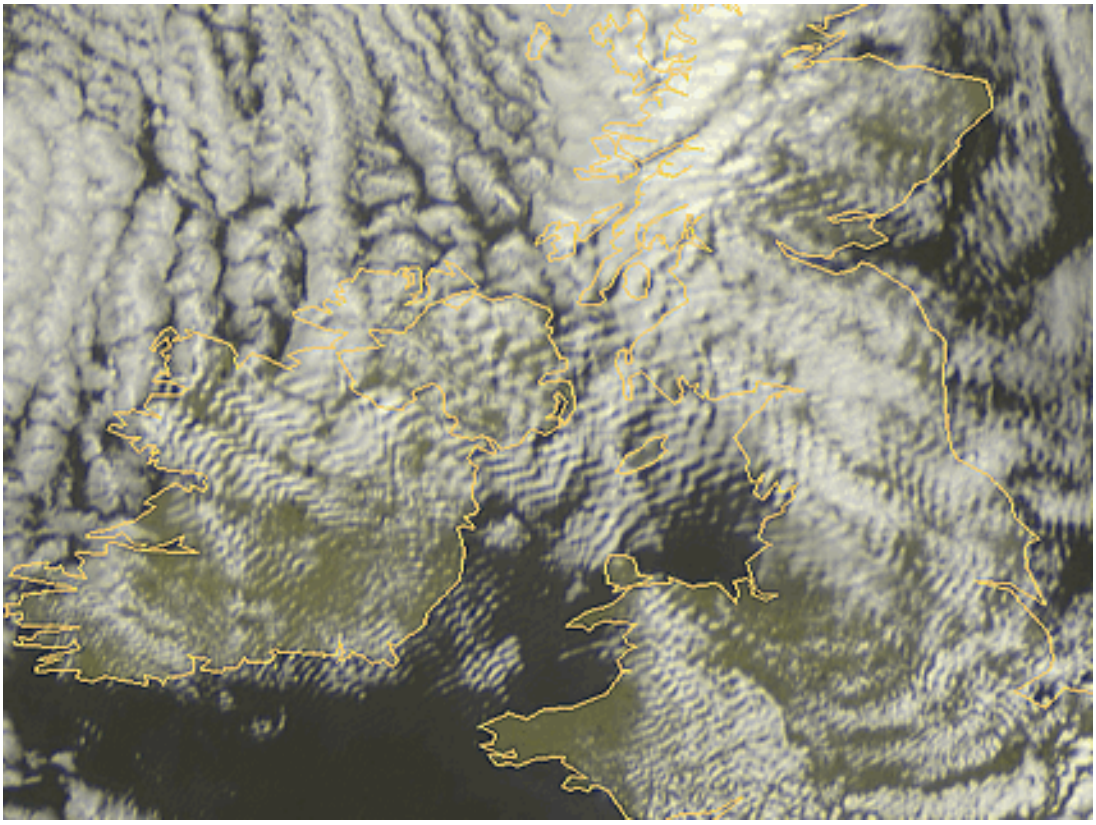

Fig. 1.4: Satellite picture of mountain waves around Ireland and the British Isles. The waves are indicated by bands of cumulus clouds orientated approximately parallel to the mountain ridges.
Source: EUMETSAT

2 Forces and motion

2.1 Some formalities

In order to understand wave motion in the atmosphere, we have to consider the basic physical laws governing this motion. In the following, we define a fluid particle (given the subscript "p") by its mass m_p, volume V_p and density $\rho_\mathrm{p}(= m_\mathrm{p}/V_\mathrm{p})$. The motion of this particle is described by the second law of Newton (Isaac Newton, 1642 - 1727, one of the great scientists in history) which can be stated in words as

mass times acceleration equals the sum of the forces applied to the particle

In the form of a physical equation, this can be written as:

$$m_\mathrm{p} a = \sum F_i \,, \qquad i = 1, 2, 3, ... \tag{2.1}$$

Here, a denotes the particle acceleration and F_i the forces. The acceleration is the temporal change of the particle velocity. The forces acting on fluid particles in the atmosphere (or in any fluid) are gravity, pressure and frictional forces. We will introduce these forces more formally in the next sections.

In order to discuss forces and accelerations, we have to introduce a coordinate system which provides the direction in which forces and accelerations are acting. This is usually done with a simple rectangular Cartesian coordinate system as shown in Figure 2.1. Here, the horizontal coordinates, which are supposed to be parallel to the earth's surface, are denoted by x and y, while the vertical coordinate is denoted by z. For later discussions, we also need the definition of differences in fluid properties. These will be denoted by "d" and can be interpreted as follows: let the density within a fluid at two positions x_1 and x_2 in the x-direction be named $\rho(x_1)$ and $\rho(x_2)$, then the difference between these densities $\rho(x_2) - \rho(x_1)$ will be denoted by "$d\rho$". The differences between the positions x_1 and x_2 will be denoted by $dx = x_2 - x_1$ (see Fig. 2.2). If we are interested in the temporal change of a fluid property, say the change of density, we have to take the difference $\rho(t_2) - \rho(t_1)$ at times t_1 and t_2. The change in time will then be defined by "dt" $= t_2 - t_1$ (see Fig. 2.2).

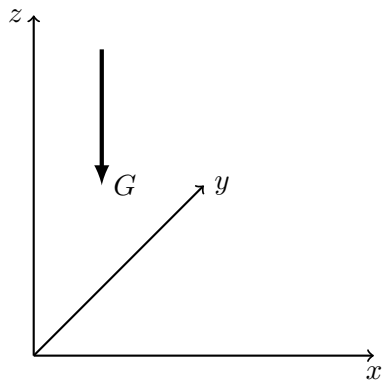

Fig. 2.1: The coordinate system and the direction of the force due to gravity.

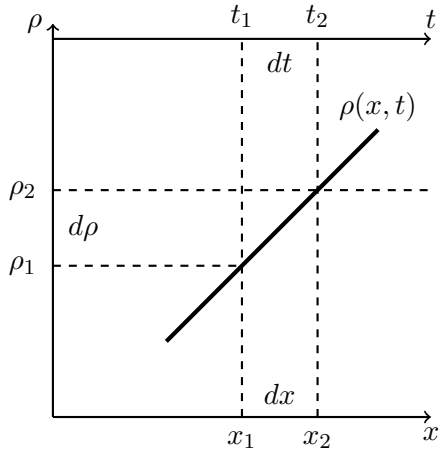

Fig. 2.2: Change in a fluid property (here: density $d\rho$) in space (dx) or time (dt).

Let us give an example: As the velocity of a fluid particle is defined as the temporal change of its space coordinates with time, we have for the horizontal velocity component u:

$$u = \frac{dx}{dt} = \frac{(x(t_2) - x(t_1))}{(t_2 - t_1)}, \tag{2.2}$$

and for the vertical velocity component w:

$$w = \frac{dz}{dt} = \frac{(z(t_2) - z(t_1))}{(t_2 - t_1)}. \tag{2.3}$$

A change in a fluid property in space will be called a "gradient". For example, if the fluid density changes in the vertical (as in stratified fluids, to be discussed later) we have

$$\frac{d\rho}{dz} = \frac{(\rho(z_2) - \rho(z_1))}{(z_2 - z_1)}. \tag{2.4}$$

2.2 Gravity force

The gravity force acts on all bodies on earth. It is directed toward the earth's center or perpendicular to the earth's surface as displayed in Figure 2.1. Formally, this can be written as

$$G = -m_\mathrm{p} g, \tag{2.5}$$

where g is the gravitational constant with a value of about $9.81\,\mathrm{m/s^2}$, and has the dimensions of an acceleration. If only the gravity force is acting on a particle, Newton's law gives

$$m_\mathrm{p} \frac{dw}{dt} = -m_\mathrm{p} g, \tag{2.6}$$

or dividing by the particle mass m_p:

$$\frac{dw}{dt} = -g. \tag{2.7}$$

The last version is the formal description of the well known statement by Galileo Galilei (1564 - 1642) that all bodies fall at equal rates. This is of course only true if no other forces are acting

on the fluid particles. Everyday experience shows us that a stone falls faster than a feather or a leaf and sailplanes may not fall at all toward the earth's surface. This is due to pressure and friction forces acting on the body which cannot be neglected in real applications of Newton's law to falling bodies. For our purposes to explain atmospheric gravity waves, we can to a first approximation neglect frictional forces. Hence, as the next step we will investigate the influence of pressure forces on falling bodies.

With respect to our goal of explaining gravity waves, we might consider at this stage the possibility of harmonic oscillations due to gravity. These are possible if there is a compensating force which counteracts the falling of a mass. Two well known examples will be given: the pendulum and a sphere in a bowl presented schematically in Figure 2.3. For the case of the pendulum, the mass is fixed to a string of length l which is fixed at some height z. At rest, gravity is equally balanced by the tension in the string. If the mass is deflected by an angle φ from its equilibrium position, which is straight down, only the component of gravity parallel to the string can compensate the string tension: $F = mg\cos(\varphi)$. The other component, $F_s = mg\sin(\varphi)$ has no opposing force, hence Newton's law for the acceleration in the s-direction can be written as:

$$m\frac{du_s}{dt} = mg\sin(\varphi), \tag{2.8}$$

where $u_s = ds/dt$. For small angles ($\varphi < 20°$) we can write $\sin(\varphi) \approx s/l$. Hence equation 2.8 can be approximated by

$$\frac{d^2s}{dt^2} + \frac{g}{l}s = 0. \tag{2.9}$$

This is the well known pendulum equation which has the solution

$$s(t) = s_o\cos(\omega t), \tag{2.10}$$

where $\omega = \sqrt{g/l}$ is the pendulum frequency and s_o is the initial position of the pendulum.

A similar argument leads to the same equation for a sphere moving in a circular bowl with radius l. Hence, a sphere deflected from its equilibrium position will also perform a harmonic oscillation according to eq. 2.10.

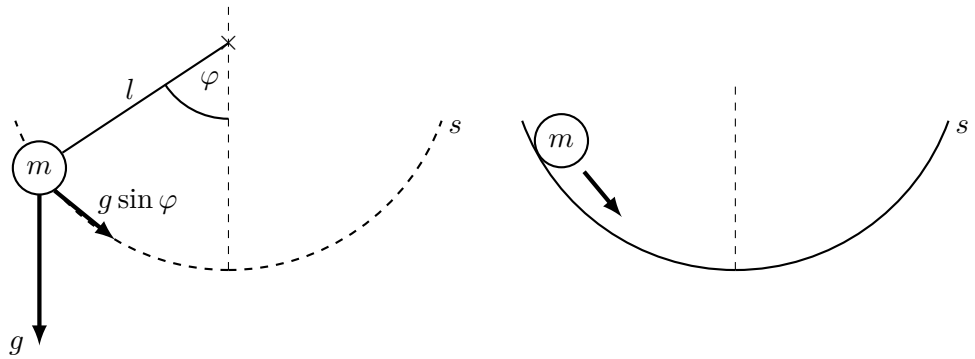

Fig. 2.3: Pathways (s) followed by a mass m under the influence of gravity. Left: a pendulum of length l. Right: sphere in a bowl.

2.3 Pressure Forces

Forces applied in the normal direction to the surface of masses are called pressure forces and will be denoted by F_p in the following. For example, if you lean against a wall, you exert a pressure force on the wall, but neither the wall nor yourself will move due to the principle "action = reaction" and hence the wall also exerts a pressure force of opposite sign on you. The more general case of pressure forces acting on a mass particle is illustrated in Figure 2.4 where, for simplicity, only two surfaces of a cube are shown. If we want to know whether the mass will be accelerated by pressure forces, we have to take the sum of the forces acting on the x and z surfaces. In Figure 2.4, the forces in the vertical direction are assumed to be equal but of opposite sign so that there will be no motion in the vertical direction. In the horizontal direction, the force in the positive x-direction is assumed to be larger than the opposing pressure force in the negative x-direction. Hence, according to Newton's law, the particle will be accelerated in the positive x-direction as indicated in the figure.

The force per unit surface area is called pressure and is usually denoted by the symbol "p". As forces are expressed in Newtons (N), pressure has the units of Newtons per square meter ($\mathrm{N/m^2}$) which is called a "Pascal (Pa)". It can be shown that the acceleration of a body with mass m due to pressure forces in each spatial direction can be written using pressure p as variable by

$$m\frac{du}{dt} = -V\frac{dp}{dx}, \qquad m\frac{dw}{dt} = -V\frac{dp}{dz}, \tag{2.11}$$

where V is the volume of the body and dp/dx and dp/dz are the pressure gradients across the body's diameter. We might remark that pressure forces are also called volume forces as they act only on the surface of fluid particles like friction forces, which are not treated here. This is in contrast to gravity forces, which do not depend on the volume of particles but only on their mass.

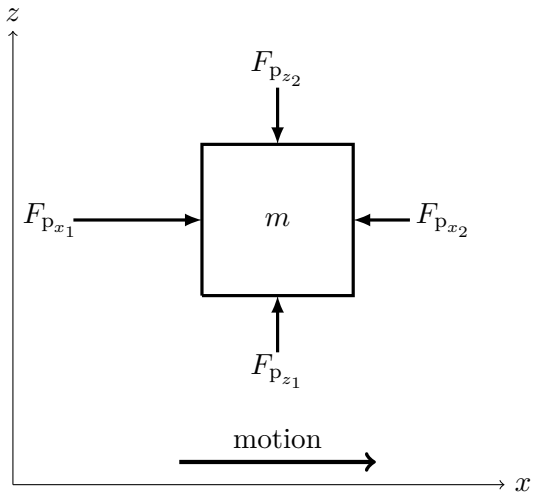

Fig. 2.4: Action of pressure forces F_p on a body. The resulting direction of motion is indicated by the arrow at the bottom.

2.4 Hydrostatic Pressure

Next we consider the balance between gravity and the pressure force as is illustrated in Figure 2.5. On the left part of the figure, a cube of mass m and volume $V = ah$, where a is the surface area and h is the height, is placed on a solid surface so that the cube cannot move downward due to gravity because the wall exerts an opposing pressure force on it. At the surface, gravity and pressure forces are in equilibrium, which can be expressed as

$$G = F_\mathrm{p} \qquad \text{or} \qquad mg = p_0 a, \tag{2.12}$$

where p_0 is the pressure at the wall. If we replace the mass m by the density ρ and the volume V by surface area, a times height h, we have

$$\rho a h g = p_0 a \qquad \text{or} \qquad p_0 = \rho g h. \tag{2.13}$$

This pressure resulting from the gravity force acting on a solid horizontal surface is called the static pressure. When the mass above the wall is a fluid or a gas, it is called the hydrostatic pressure.
Let us give an example: if a lake has a water depth of 10 m and if we neglect air pressure acting on the water, the hydrostatic pressure at the bottom of the lake will be $p = 1000\,\mathrm{kg/m^3} \times 10\,\mathrm{m/s^2} \times 10\,\mathrm{m} = 100000\,\mathrm{N/m^2} = 100000\,\mathrm{Pa} = 1000\,\mathrm{hPa}$, which is equal to the air pressure we observe at the earth's surface.

The above formula provides the pressure at a solid horizontal wall exerted by a body of height h due to the action of gravity. If we consider a fluid (water) or a gas (the atmosphere), we might be also interested in the variation of pressure in the vertical coordinate. Let us consider the situation on the right hand side of Figure 2.5, where a fluid column of height H is shown and we are interested in the pressure at an intermediate height h.

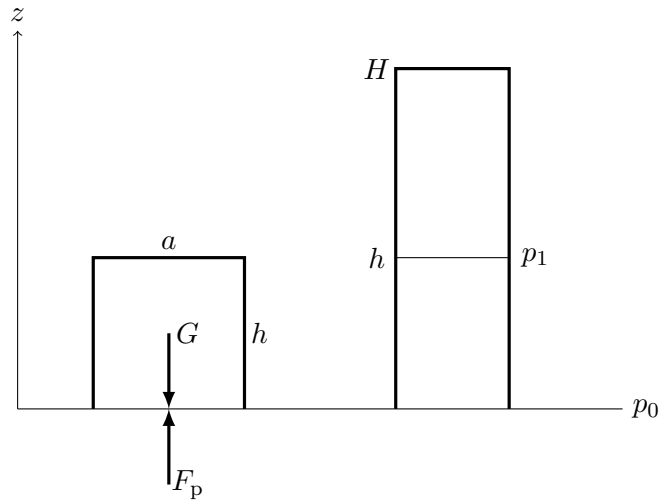

Fig. 2.5: Left part: forces acting on a cube of mass m resting on a surface. G = gravity force, F_p = pressure force. Right part: pressure distribution in a fluid column of height H.

According to the derivation above, the pressure at height h (denoted by p_1) is $p_1 = \rho g(H-h)$. At the surface, the pressure (denoted by p_0) is $p_0 = \rho g H$. Hence, for the pressure difference between $z = h$ and $z = 0$ we have

$$p_1 - p_0 = -\rho g h = -\rho g(z_1 - z_0). \tag{2.14}$$

Here, we have replaced h by the more general height difference, $z_1 - z_0$. If we apply this relation to more arbitrary differences, dp and dz, we have

$$\frac{dp}{dz} = -g\rho. \tag{2.15}$$

This is the so-called hydrostatic pressure law which states that, under the influence of gravity, the pressure in a fluid at rest decreases with height. The density of the fluid need not to be constant as in the case of water, but can vary with height as in the case of the atmosphere. The height variation of pressure, $p(z)$, resulting from integrating the hydrostatic law is as follows. For constant density, pressure decreases linearly with height (or for lakes and oceans it increases with depth), whereas for the atmosphere where density decreases with height, the pressure follows an exponential decay shown in Figure 2.6.

An example of the pressure distribution for the ICAO standard atmosphere is given in Figure 2.6. It can be seen that for each height, there is only one pressure value. Hence, pressure and height are unequivocally related to each other and therefore height can be also deduced from the measurement of static pressure. This fact has long been known and is the basis of altitude measurements in aviation (determination of the altitude of airplanes from GPS is of course the modern method).

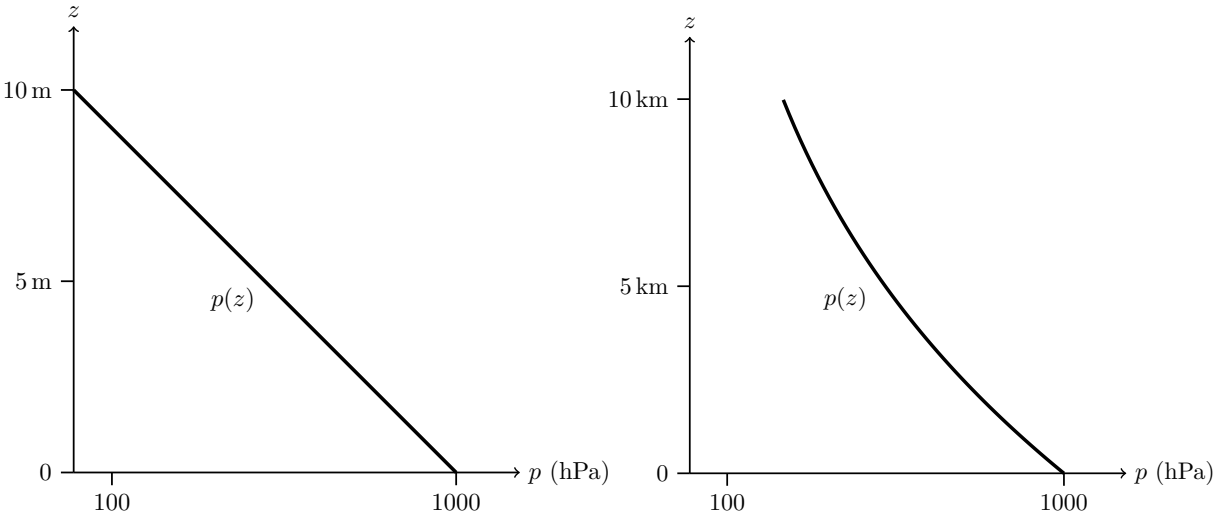

Fig. 2.6: Vertical variation of hydrostatic pressure in a lake (left) and in the atmosphere (right). The surface pressure in both cases is 1000 hPa.

2.5 Dynamic pressure

The relation between fluid acceleration and the pressure gradient given in Section 2.3 can also be inverted in the sense of Newton's law, "action = reaction". Not only a pressure gradient leads to fluid particle acceleration but also acceleration (or deceleration) in the fluid induces a pressure force. The resulting pressure is called the "dynamic pressure" and will be denoted by p_d.

Let us consider the following example: if a water jet from your garden hose spurts against a wall, the ejected water will be decelerated while impinging on the wall because it cannot penetrate a solid surface. There will be a pressure force acting on the wall exerted from the impinging water jet, which you can feel yourself if you spurt the jet against your hand.

The relation between dynamic pressure p_d and the fluid velocity u is given by the famous Bernoulli equation, named after the Swiss physicist D. Bernoulli (1700-1782), which can be expressed in its simple form as

$$p_\mathrm{d} + \rho\frac{u^2}{2} = \text{constant}. \tag{2.16}$$

The consequences of the Bernoulli law for fluid motion are illustrated in Figure 2.7, where velocity and pressure variation for the flow through a constriction in a channel is shown. As the mass flux through any cross section of the channel must be constant, the fluid accelerates through the constriction where the maximum velocity is reached and is accompanied by a reduction in dynamic pressure. The Bernoulli principle can, in practice, be found on any airplane in the so-called Pitot-tube, which measures the aircraft speed relative to the surrounding air based on the relation given above.

Actually, dynamic pressure forces are very important in fluids as they communicate the movement of fluid particles relative to solid walls (e.g. bending pipes) or among themselves throughout the fluid volume. In aviation, for example, these pressure forces lead to aerodynamic lift of airfoils and hence make flight possible.

2.6 Mass conservation and continuity principle

In the previous chapters, we have presented the laws for fluid motion which are based on Newton's principle, but these are not sufficient to describe all fluid physics. As an additional restriction, we have to follow the law of mass conservation which can be stated for the mass m_p for any

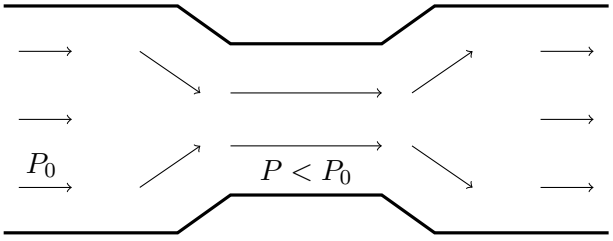

Fig. 2.7: Velocity and pressure distribution in a constriction of a fluid channel according to Bernoulli's equation. The arrow length is proportional to the fluid velocity. P_0 denotes the upstream pressure.

particle as m_p = constant. If we observe the particle mass during the course of time, this can be written as

$$\frac{dm_\mathrm{p}}{dt} = 0 \tag{2.17}$$

and is called the mass conservation law. It does not mean that the particle density cannot change since mass can also be defined as the product of particle volume V_p and density ρ_p ($m_\mathrm{p} = \rho_\mathrm{p} V_\mathrm{p}$). Hence, if the particle volume is changed due to some external forces acting on the particle surface (see Figure 2.8), the density also changes, but the product of the two remains constant. If the fluid particle density can be changed, the fluid is called "compressible" and the most prominent compressible fluid is air.

Liquids such as water are barely compressible under normal circumstances and in many applications in fluid mechanics are assumed to be incompressible. This means that the density or volume of fluid particles remains constant with time and can be formally written as

$$\frac{dV_\mathrm{p}}{dt} = 0, \qquad \frac{d\rho_\mathrm{p}}{dt} = 0 \tag{2.18}$$

and is called the incompressibility condition in the literature. This does not mean however that the density of the entire fluid is constant, but only that the density of individual fluid particles is constant with time. Cases of incompressible fluids with density varying in space are presented in Section 3.2 under the topic of stratified fluids.

The incompressibility condition states that the density or volume of fluid particles does not change in time. This does not exclude the change of the outer shape of a fluid particle. An example for this is given in Figure 2.8, where a square particle is stretched or squeezed by the action of fluid motion resulting in a rectangular form with the same volume as the original square form. To conserve particle volume (or density), the fluid motion is restricted by the so-called continuity condition relating the horizontal velocity divergence defined by du/dx (a divergence

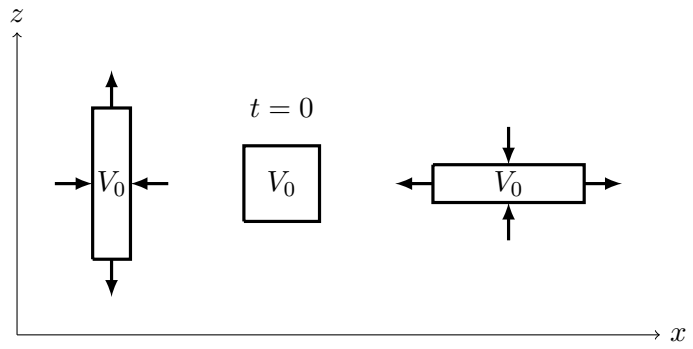

Fig. 2.8: Deformation of a fluid particle due to horizontal convergence/vertical divergence (left) and due to horizontal divergence/vertical convergence (right) of the fluid motion. The shape of the particle before deformation is shown in the middle. The case shown here is for incompressible fluids as the particle volume V_0 remains constant. The same scheme also applies for compressible fluids but with the additional possibility of a variable particle volume.

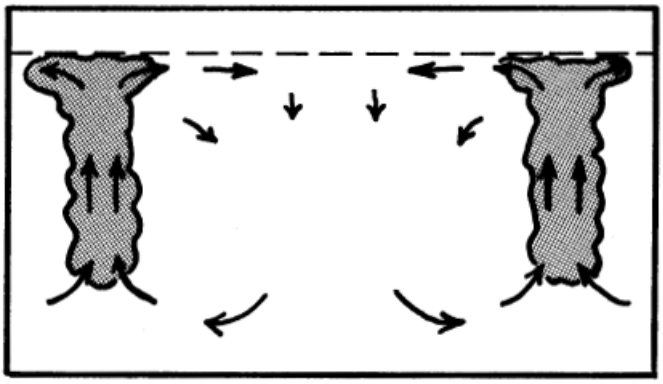

Fig. 2.9: Schematic of the circulation within a field of cumulus clouds according to the continuity principle.

with a negative sign is called convergence), and the vertical velocity divergence (or convergence) defined by dw/dz through

$$\frac{du}{dx} + \frac{dw}{dz} = 0. \tag{2.19}$$

This relation is called the *continuity equation* and is one of the most often used approximations in the field of fluid mechanics. It is even applied to atmospheric motion under some restrictions and will be also used for the formal treatment of waves in this monograph.

The continuity principle for fluid motion is well known to glider pilots when they are performing thermal flight as is illustrated in Figure 2.9 where the principal circulation in a field of cumulus clouds is shown. The strong and narrow updrafts within the clouds have to be compensated by weaker and wider downdrafts in the cloud-free areas.

3 Archimedes' principle and buoyancy forces

3.1 Archimedes forces

Let us now consider the behaviour of a solid particle submerged in a fluid at rest shown in Figure 3.1. In the following, we denote the properties of the particle by a subscript "p" and those of the environmental fluid by a subscript "f". The particle is held at its initial position by two weightless strings exerting a net force F_S. It is supposed that the density of the fluid ρ_f as well as the density of the particle ρ_p are also kept constant. Applying Newton's law for the situation with a fixed position at time $t = 0$, one obtains:

$$\rho_p \frac{dw}{dt} = -\rho_p g - \frac{dp_f}{dz} + F_S = 0. \tag{3.1}$$

Here, p_f is the static pressure of the fluid which can be calculated by the hydrostatic law as

$$\frac{dp_f}{dz} = -\rho_f g. \tag{3.2}$$

Inserting this into Newton's law yields for the equilibrium situation:

$$\rho_p \frac{dw}{dt} = -\rho_p g + \rho_f g = -g(\rho_p - \rho_f) + F_S = 0. \tag{3.3}$$

If we release the strings while keeping the particle in its initial position, the external force F_S vanishes and one has

$$\rho_p \frac{dw}{dt} = -g(\rho_p - \rho_f) \tag{3.4}$$

or

$$\frac{dw}{dt} = -g\frac{(\rho_p - \rho_f)}{\rho_p}. \tag{3.5}$$

This is the so-called Archimedes' principle, named after Greek philosopher Archimedes (around 200 BC), which says that a body of density ρ_p submerged into a fluid with density ρ_f experiences a vertical force (also called *buoyancy force*) proportional to the density differences multiplied by gravity g. The term on the right hand side of the first equation is a force per unit volume and a force per unit mass appears on the right hand side in the second equation. The latter version is most often used in applications of Archimedes' principle to fluid motion where this force is called the *buoyancy force*. This force is directed upward if the particle density

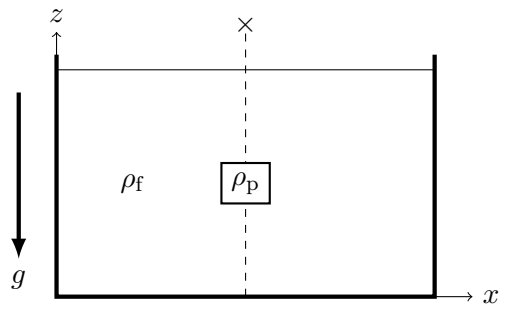

Fig. 3.1: A body with density ρ_p is submerged in a fluid with density ρ_f. The body is fixed in position by two weightless strings (dashed lines).

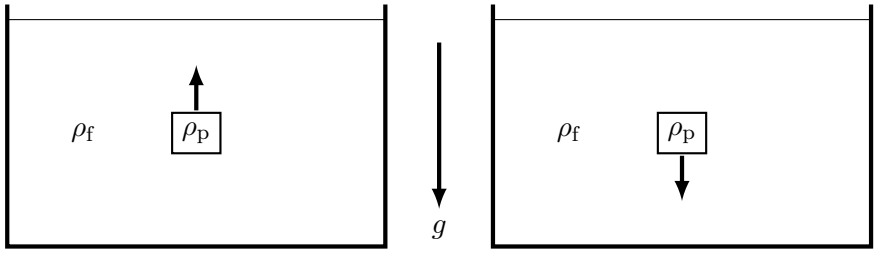

Fig. 3.2: Acceleration of a particle with density ρ_p submerged in a fluid with density ρ_f due to Archimedes' principle. Left: $\rho_p < \rho_f$, right: $\rho_p > \rho_f$.

is less than that of the surrounding fluid, and downward if the particle is denser than the fluid. Hence, after the supporting strings in our configuration are removed at time $t = 0$, the following motion will be observed (see Figure 3.2). If the particle is less dense than the fluid density, it will be accelerated upward, if it more dense than the surrounding fluid it will move downward. From everyday experience, we know if we throw a stone into the water, it will sink and if we press a ball down into the water and release it, the ball will move up to the water surface. Glider pilots experience Archimedes' principle through rising warm air parcels (thermals).

In both cases, the solid particle submerged in a fluid will move away from its original position as time proceeds. No oscillations around its initial position will be observed, as would be desired to explain gravity waves in the atmosphere. In order to describe this behaviour, we have to introduce the concept of a stratified fluid as will be done in the next section.

3.2 Stratified fluids

So far, we have considered for simplicity a so-called homogeneous fluid where the fluid density ρ_f is constant in space and time. If the fluid density has different values in space, say $\rho_f(x, y, z)$, the fluid is called inhomogeneous, but if the fluid density varies only in the vertical direction, i.e. $\rho_f(z)$, a fluid is called stratified. In a stratified fluid, layers of constant density are oriented in planes parallel to the horizontal coordinates as indicated in Figure 3.3 (in the following, we

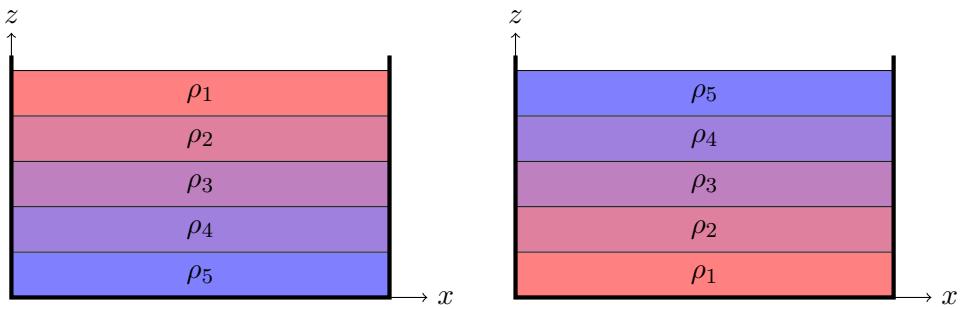

Fig. 3.3: Layers of constant density in a stratified fluid. Left: stable stratification, right: unstable stratification. The layer densities are arranged according to $\rho_1 < \rho_2 < \rho_3 < \rho_4 < \rho_5$.

show only the x coordinate). It can be shown for a fluid at rest, that the density surfaces have to be horizontal (or perpendicular to the gravity force g) or otherwise horizontal motion would be initiated.

The hydrostatic pressure law is also valid in the case of stratified fluids and can be written now as

$$\frac{dp_\mathrm{f}}{dz} = -g\rho_\mathrm{f}(z). \tag{3.6}$$

The resulting vertical pressure distribution is no longer linear as with a constant density fluid, but can have any form so long as the pressure decreases with increasing height.

In Figure 3.3, two situations are displayed. In one case, the fluid density decreases with height, which is called stable stratification. In the other case, density is increasing with height, which is called unstable stratification. The reason for this naming will become clear later on.

3.3 Archimedes' principle in a stratified fluid

The principle of Archimedes as introduced in Section 3.1 is also valid for stratified fluids, but now one has to consider the difference between the particle density and the fluid density at each vertical level, $\rho_\mathrm{p} - \rho_\mathrm{f}(z)$, in order to determine the buoyancy forces and the resulting vertical acceleration. We first find an equilibrium level z where both densities are equal and there is no buoyancy force so that the submerged particle will remain at this level as shown in Figure 3.4 for a particle with density ρ_3.

Let us consider what happens if we lift the particle from its equilibrium level to a layer with a different fluid density. For unstable stratification illustrated in Figure 3.4 (right side), lifting the particle to the layer with ρ_4 gives the Archimedes force A (or buoyancy force) on the particle as

$$A = -g(\rho_3 - \rho_4) > 0. \tag{3.7}$$

Hence, according to Newton's law, the particle will be accelerated upward away from its initial position. If the particle is shifted downward to the density level ρ_2,

$$A = -g(\rho_3 - \rho_2) < 0 \tag{3.8}$$

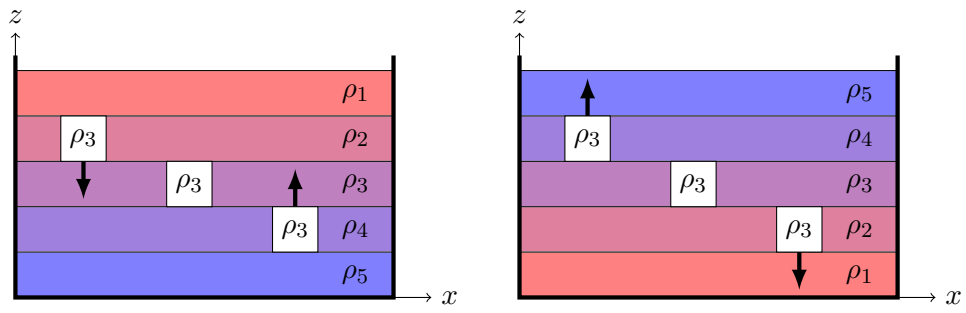

Fig. 3.4: The motion of a particle with density ρ_3 after being brought to another fluid density level. Left: stable stratification. Right: unstable stratification.

and the particle will be accelerated downward away from its starting position. In any case, the motion of the particle will be directed away from its level of equilibrium. This is called an unstable equilibrium and hence this kind of stratification is also called unstable.

For stable stratification shown in Figure 3.4 (left side), lifting the particle to the density level ρ_2 gives

$$A = -g(\rho_3 - \rho_2) < 0 \tag{3.9}$$

and the particle will be accelerated downward back to the direction of its equilibrium position. If the particle is shifted down to the density level ρ_4, then

$$A = -g(\rho_3 - \rho_4) > 0 \tag{3.10}$$

and hence it will be accelerated upward in the direction of its equilibrium level. In any case, the motion of the particle shifted initially away from its equilibrium position will be directed back toward this level. This kind of equilibrium is called stable equilibrium and hence the fluid stratification is also called stable.

3.4 Oscillations in a stratified fluid

For further discussion, we assume that the fluid density decreases linearly with height as displayed in Figure 3.5 and the equilibrium level is taken at $z = 0$ for convenience. For investigation of the motion of a lifted particle, we assume that the particle density does not change in time, i.e. $d\rho_\mathrm{p}/dt = 0$, thus using the incompressibility condition. Hence, in our diagram in Figure 3.5, the path of the particle will be along the vertical line $\rho_\mathrm{p} = \text{constant}$.

If we lift the particle to a small height z above its equilibrium level at $z = 0$, the density of the surrounding fluid at this height will be given by

$$\rho_\mathrm{f}(z) = \rho_\mathrm{f}(0) + \left(\frac{d\rho_\mathrm{f}}{dz}\right) z, \tag{3.11}$$

where at $z = 0$, $\rho_\mathrm{f} = \rho_\mathrm{p}$. Hence, the Archimedes force can de written as

$$A = -g(\rho_\mathrm{p} - \rho_\mathrm{f}(z)) = -g\left(\rho_\mathrm{p} - \rho_\mathrm{f}(0) - \frac{d\rho_\mathrm{f}}{dz} z\right) = g\frac{d\rho_\mathrm{f}}{dz} z, \tag{3.12}$$

and may be called Archimedes' law for continuously stratified fluids.

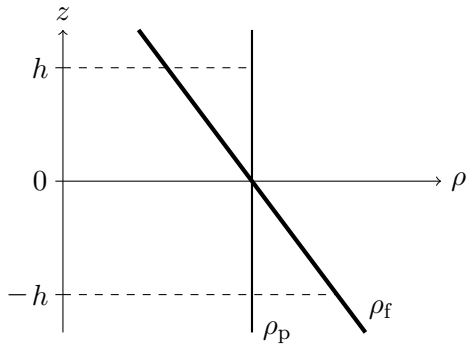

Fig. 3.5: Vertical profile of fluid density ρ_f in a stably stratified fluid and pathway of a particle with density ρ_p after leaving its equilibrium position at $z = 0$.

Newton's second law, $\rho_\mathrm{p} dw/dt = A$, then gives

$$\frac{dw}{dt} = \frac{g}{\rho_\mathrm{p}} \frac{d\rho_\mathrm{f}}{dz} z. \tag{3.13}$$

In the following, we are interested in what kind of vertical motion the fluid particle will experience once it is moved some small height z from its equilibrium position. As the vertical velocity w is defined as the temporal change of the particle position z by $w = dz/dt$, then

$$\frac{d^2z}{dt^2} = \frac{g}{\rho_\mathrm{p}} \frac{d\rho_\mathrm{f}}{dz} z \quad \text{or} \tag{3.14}$$

$$\frac{d^2z}{dt^2} + N^2 z = 0. \tag{3.15}$$

This equation for the temporal change of the particle's vertical position z has the same form as the well known equations for a pendulum (see Section 2.2) with the solution of a harmonic oscillator, where N^2 denotes the square of the oscillation frequency. In our case, this frequency is called the Brunt-Vaisala frequency, named after the British meteorologist Brunt and the Finish meteorologist Vaisala (written Väisälä in the original language), denoted by N and defined as

$$N = \sqrt{-\frac{g}{\rho_\mathrm{f}} \frac{d\rho_\mathrm{f}}{dz}}. \tag{3.16}$$

Note that in a stably stratified fluid, $d\rho_\mathrm{f}/dz < 0$ (see Fig. 3.3) and hence N is a real number. If we lift the particle initially to a small height h and release it from there, the solution of this equation is (see any standard textbook on calculus or oscillations)

$$z(t) = h \cos(Nt), \tag{3.17}$$

where the oscillation period τ is given by $\tau = 2\pi/N$. The vertical position of an oscillating particle according to equation 3.17 is sketched in 3.6, with details on the cosine function (cos) provided in Appendix AIII. It is important to note that vertical oscillations of fluid particles in a stably stratified fluid can be achieved by the action of gravity just as for the mechanical pendulum discussed in Section 2.2.

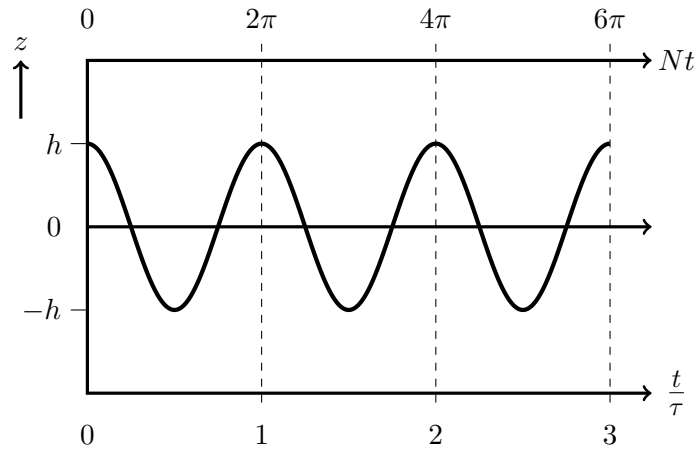

Fig. 3.6: Vertical position of a particle in a stably stratified fluid after being lifted to the height h above its equilibrium position $z = 0$. The variation in time according to equation 3.17 is shown for three oscillation periods τ.

3.5 Stratification and Archimedes' principle in the atmosphere

So far we have investigated the behavior of a mass particle in a stratified fluid where we have assumed that the particle density does not change in time ($d\rho_\mathrm{p}/dt = 0$). Now a gas like the atmosphere is always compressible if we apply some external pressure forces. High pressure results in a high particle density, low pressure in low density. As the static pressure of the atmosphere decreases with height, a lifted air parcel becomes less dense than it was at its original position and vice versa as shown in Figure 3.7. That does not necessarily mean that the parcel becomes buoyant with respect to its surroundings since the environment is also subject to air pressure decreasing with height. In meteorology, it is uncommon to consider parcel density with respect to Archimedes' law because density is hardly ever measured. Using the laws for ideal gases, air density is related to temperature and pressure which are the standard variables measured in meteorology. In fact, atmospheric stratification and buoyancy forces are defined with respect to air temperature as outlined below. Air temperature, denoted by T, is usually measured in degree Celsius (°C) for meteorological applications. However, the laws of thermodynamics require T to be defined in degree Kelvin (K), where $T(\mathrm{K}) = 273\,(\mathrm{K}) + T(°\mathrm{C})$. However, differences in air temperature have the same value, whether measured in (K) or (°C), hence $dT(\mathrm{K}) = dT(°\mathrm{C})$.

Stratification in the atmosphere is related to the vertical change in air temperature by the following rules which are derived in any textbook on meteorology. In neutral stratification, corresponding to an unstratified fluid, the air temperature decreases by 1 K or 1 °C per 100 m height difference:

$$dT/dz = -1\,\mathrm{K}/100\,\mathrm{m} = -\Gamma \quad \text{(neutral stratification)} \tag{3.18}$$

The symbol Γ is the *adiabatic lapse* rate which means that if an air parcel is lifted under adiabatic conditions (no heating or cooling due to external sources like radiation), its temperature

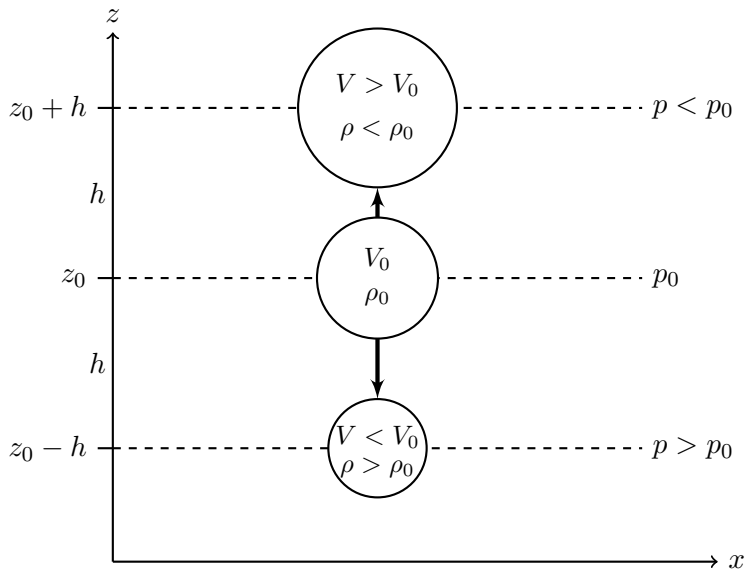

Fig. 3.7: Volume and density change of an air parcel lifted vertically from its initial position at $z = z_0$ due to atmospheric pressure p decreasing with height.

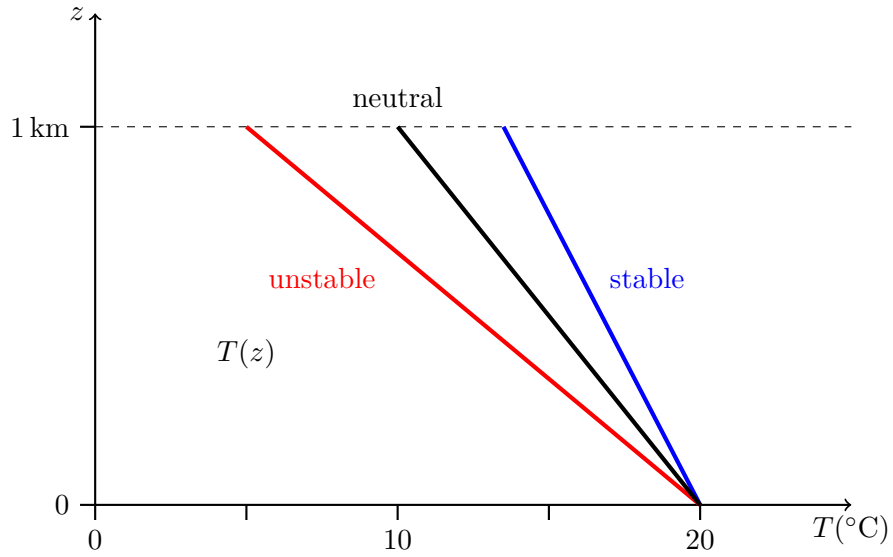

Fig. 3.8: Variation of air temperature $T(z)$ with height for different stratification. The temperature gradient in the stable case corresponds to the ICAO standard atmosphere.

decreases by 1 K/100 m in the vertical direction. In a stratified atmosphere, the actual vertical temperature gradient is either less or exceeds Γ according to the following rules:

$$\text{stable stratification:} \qquad dT/dz \leq -\Gamma, \tag{3.19}$$

$$\text{unstable stratification:} \qquad dT/dz \geq -\Gamma. \tag{3.20}$$

For example, consider the ICAO standard atmosphere defined by a temperature lapse rate of $dT/dz = -0.35\,\mathrm{K}/100\,\mathrm{m}$ in the lowest kilometres. This is less than $-1\,\mathrm{K}/100\,\mathrm{m}$ and hence this standard atmosphere is stably stratified as illustrated in Figure 3.8.

Archimedes' principle could be expressed by the differences in air temperature between an air parcel and its environment, but then one has to consider the adiabatic lapse rate Γ for the parcel temperature. For this reason, another temperature has been introduced in meteorology which is called potential temperature denoted by θ. The derivation of this temperature as based on the first law of thermodynamics for adiabatic processes found in any textbook on meteorology, with the result that

$$\theta = T\left(\frac{1000\,\mathrm{hPa}}{p}\right)^{0.26}, \tag{3.21}$$

where p is the pressure (in units hPa) of the air parcel under consideration. The potential temperature has the property of being constant for an adiabatic process like mechanical lifting of an air parcel giving

$$\frac{d\theta_\mathrm{p}}{dt} = 0, \tag{3.22}$$

which is equivalent to $d\rho_\mathrm{p}/dt = 0$ in an incompressible fluid. With this temperature, the Archimedes force A and the buoyancy force B can be expressed by

$$A = g(\theta_\mathrm{p} - \theta_\mathrm{a}), \tag{3.23}$$

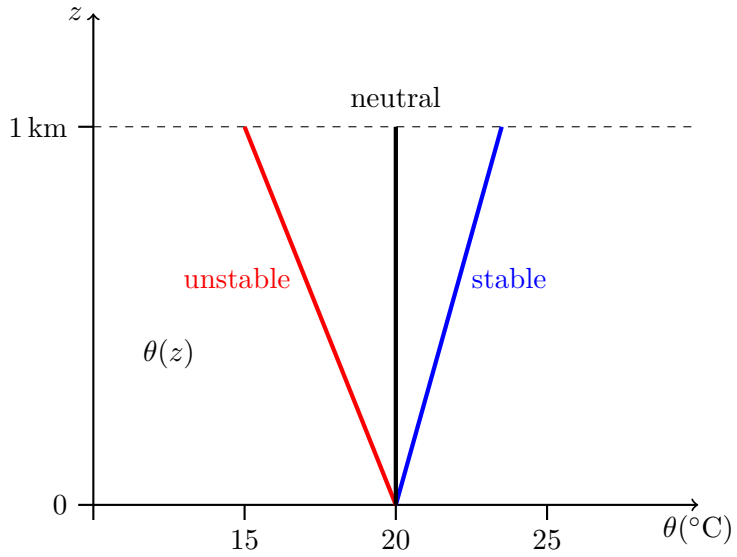

Fig. 3.9: Variation of potential temperature $\theta(z)$ with height for different stratification. The temperature gradient in the stable case corresponds to the ICAO standard atmosphere.

$$B = g\frac{(\theta_\mathrm{p} - \theta_\mathrm{a})}{\theta_\mathrm{p}}, \tag{3.24}$$

where θ_a is the actual potential temperature of the surrounding air. The vertical gradient of potential temperature can be related to the normal temperature lapse rate by

$$\frac{d\theta}{dz} = \frac{dT}{dz} + \Gamma. \tag{3.25}$$

With this relation, the stratification of the atmosphere can also be defined by using potential temperature θ instead of air temperature T:

$$\text{Stable stratification:} \quad \frac{d\theta}{dz} > 0, \tag{3.26}$$

$$\text{Neutral stratification:} \quad \frac{d\theta}{dz} = 0, \tag{3.27}$$

$$\text{Unstable stratification:} \quad \frac{d\theta}{dz} < 0. \tag{3.28}$$

These are illustrated in Figure 3.9.

Finally, the important Brunt-Vaisala frequency N can be defined for the atmosphere as

$$N = \sqrt{\frac{g}{\theta}\frac{d\theta}{dz}} = \sqrt{\frac{g}{T}\left(\frac{dT}{dz} + \Gamma\right)}. \tag{3.29}$$

Tab. 3.1: Brunt-Vaisala frequency N and oscillation period τ in a stably stratified atmosphere for different vertical gradients of air temperature T and potential temperature θ.

dT/dz (K/100 m)	$d\theta/dz$ (K/100 m)	N (1/s)	τ (s)
- 0.65	0.35	0.011	570
0.0	1.0	0.018	350
2.0	3.0	0.031	200

For the ICAO standard atmosphere as before where $dT/dz = -0.65\,\mathrm{K}/100\,\mathrm{m}$, this leads to $d\theta/dz = 0.35\,\mathrm{K}/100\,\mathrm{m}$. The resulting Brunt-Vaisala frequency is $N = 0.011\,1/s$ which gives an oscillation period τ $(= 2\pi/N)$ of about 10 minutes and is the typical period for vertical oscillations of air parcels in a stably stratified atmosphere. N and τ for other temperature gradients are given in Table 3.1.

4 Waves

4.1 General wave properties

So far, we have discussed oscillations of a fluid particle around its equilibrium position and thereby assumed that except for buoyancy, no other forces like friction or pressure forces are acting. By neglecting these forces, no interaction of an oscillating fluid particle with the surrounding fluid is possible. Allowing pressure forces to come into play makes the interaction of all fluid particles in a stratified flow possible, such as organized interactions in the form of waves. We may loosely define a wave as a periodic oscillation in time and space, with properties sketched in Figure 4.1. For simplicity, we consider only a one-dimensional wave in the x-direction. A wave in the atmosphere may be defined based on observed quantities like temperature, pressure or wind speed and will appear as an oscillation superimposed on some background state, which in Figure 4.1 is denoted by T_0. For a variable denoted by T, a wave can be formally described by

$$T(x,t) = T_0 + T_\mathrm{a} \sin\left\{\frac{2\pi}{L}(x - ct) + \varphi\right\}, \tag{4.1}$$

where T_a is the *wave amplitude* and L the *wavelength* (the distance between two maxima or minima). The wave moves with a *phase speed* c in the x-direction, while the *phase* φ provides information on the offset against the origin of the coordinate system. The use of the sine function is arbitrary as the cosine function could have also been used as both are related by a simple phase shift, $\sin(x) = \cos(x + a)$. Hence, one can find both forms for describing harmonic waves in the literature. Some details on sine and cosine functions are given in Appendix AIII.

In the following, we will omit for convenience the phase shift φ and the background T_0 from further discussion. We may first ask what an observer at a fixed position $x = x_0$ would measure

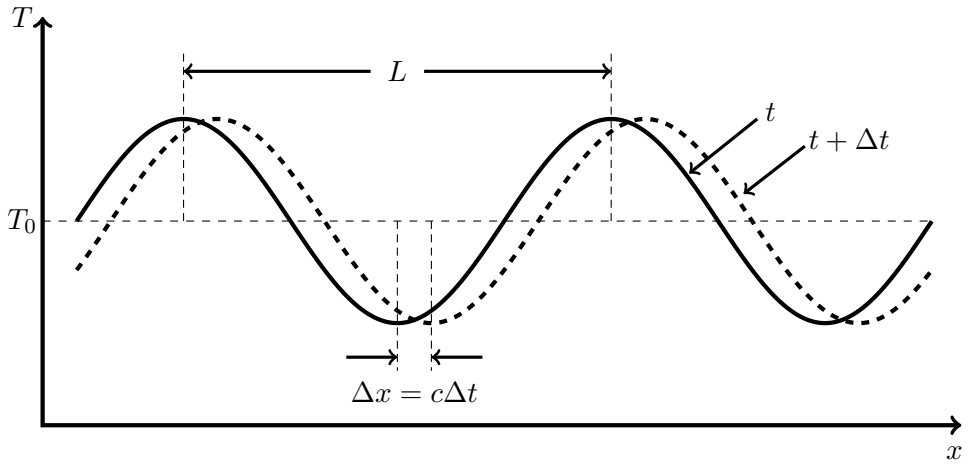

Fig. 4.1: Schematic of a simple sine wave $T(x,t)$ superimposed on a constant background state T_0. The full and dashed lines show the wave positions at different times t and $t + \Delta t$.

when a wave moves past their position at $x = x_0$? If

$$T(x_0, t) = T_\mathrm{a} \sin\left\{\frac{2\pi}{L} x_0 - \frac{2\pi c}{L} t\right\} \tag{4.2}$$

or

$$T(x_0, t) = T_\mathrm{a} \sin\left\{\frac{2\pi}{L} x_0 - \frac{2\pi}{\tau} t\right\}, \tag{4.3}$$

where τ ist the *wave period* defined as

$$\tau = \frac{L}{c}, \tag{4.4}$$

one would locally observe a harmonic oscillation of T with period τ.

It has been a matter of convenience to replace the terms $2\pi/L$ and $2\pi/\tau$ in the wave definitions by a so-called *wave number* k and an *angular frequency* ω:

$$k = \frac{2\pi}{L}, \qquad \omega = \frac{2\pi}{\tau}. \tag{4.5}$$

With these definitions, a wave is usually described using the phase speed c by

$$T(x, t) = T_\mathrm{a} \sin\{k(x - ct)\} \tag{4.6}$$

or frequency ω by

$$T(x, t) = T_\mathrm{a} \sin\{kx - \omega t)\}. \tag{4.7}$$

Here, the phase speed c is related to wave number k and frequency ω by

$$\omega = ck. \tag{4.8}$$

4.2 Transversal and longitudinal waves

Once the direction of wave propagation is known, one might be interested in which directions the fluid properties like temperature, pressure or velocity are oscillating. We distinguish between two types of waves: longitudinal and transversal waves, the properties of which are sketched in Figure 4.2. In a longitudinal wave, the oscillations are in the plane of wave propagation (i.e. in the direction of wave vector and phase speed). In a transversal wave, the oscillations are in planes perpendicular to the wave propagation.

Well known examples of longitudinal waves are sound waves in the atmosphere or in any other fluid. An example of transversal waves are pure gravity waves in fluids (see Section 5.1) or electromagnetic waves in physics. Many waves are also of a mixed type which means that oscillations occur in longitudinal and transversal directions. An example are water waves described in Section 4.4.

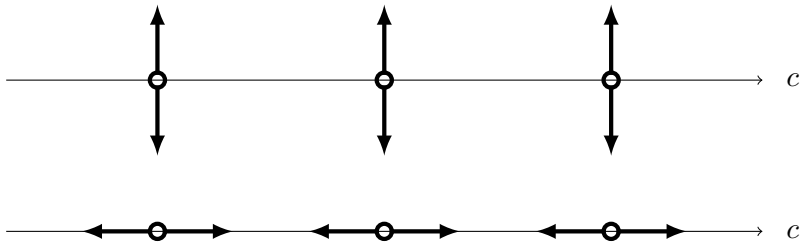

Fig. 4.2: Oscillations of fluid particles as indicated by thick arrows in a wave propagating in the c-direction. Top: transversal wave, bottom: longitudinal wave.

4.3 Stationary and standing waves

Waves do not necessarily move with their phase speed c with respect to a fixed coordinate system. If the phase lines (e.g., locations of maxima or minima) are fixed in space, we distinguish stationary and standing waves. In a stationary wave, the frequency ω and phase speed c are zero. If we use temperature T again as the observed fluid variable, this kind of wave is formally described by

$$T(x) = T_\mathrm{a} \sin(kx) = T_\mathrm{a} \sin\left(\frac{2\pi}{L}x\right). \tag{4.9}$$

An observer at some fixed position, $x = x_0$, would not observe any temporal change in the temperature field in this example (see, e.g., Figure 5.9 in Section 5.4) as there is only a spatial variation of temperature in the x-direction. These stationary waves are found as mountain waves in the atmosphere and are of great importance for wave soaring (see Chapter 7).

In contrast to stationary waves, standing waves are characterized by fixed positions of maxima, minima or zeros in the field of temperature (or any other wave variable) but with local oscillations of the form:

$$T(x,t) = T_\mathrm{a}(t) \sin(kx) = T_\mathrm{a}(t) \sin\left(\frac{2\pi}{L}x\right). \tag{4.10}$$

The temporal variation of the amplitude $T_\mathrm{a}(t)$ is given by:

$$T_\mathrm{a}(t) = T_\mathrm{max} \sin(\omega t) = T_\mathrm{max} \sin\left(\frac{2\pi}{\tau}t\right). \tag{4.11}$$

This wave behaviour is found in the vibrating strings of music instruments, where zero amplitudes (nodes) are mechanically fixed at the end of the strings. Standing waves can be also found as surface water waves in enclosed basins.

4.4 Water waves

One might wonder why a text on atmospheric gravity waves and soaring flight includes a chapter on water waves. The reason is that only a few specialists and interested laymen, including glider pilots, know about internal gravity waves in the atmosphere. Even less people are aware that the same type of waves can be found in the interior of oceans and lakes. But nearly everybody

has seen waves on the water surfaces of oceans, lakes, ponds or rivers. One could say that, from the perspective of the general public, waves in fluids are at nearly all times referring to water waves. Hence, we will start with these waves in order to get some feeling about the physical mechanism of water waves and the related motion of water particles. Some examples of water waves are shown in Figure 4.3.

While we are all aware of the wave motion on the water surface, we may also be interested in the motion of water particles below the surface, as induced by the waves. The theory of water waves is treated in any textbook on waves (e.g. Lighthill, 2001 or Sutherland, 2010), but most often some deeper knowledge of calculus and fluid mechanics is necessary to follow these texts. Here we try to understand the basic physics of water waves by first considering the situation in a vertical plane as shown in Figure 4.4.

We denote the undisturbed water surface by $z = 0$ and the total depth by H. The water waves are represented by a periodic disturbance of the water surface denoted by $h(x, t)$, which is assumed to be of the simple form

$$h(x,t) = h_0 \sin(kx - \omega t) = h_0 \sin k(x - ct), \tag{4.12}$$

where $k = 2\pi/L$ is the wave number introduced in Section 4.1.

Now we imagine that at some time $t = 0$, we could fix the water surface $h(x)$ to its sinusoidal position. What kind of forces are acting on the water particles? Let us first consider the gravity force and the vertical pressure force. As there is no initial motion, Newton's law (see Section 2.1) requires that gravity and pressure forces must be in equilibrium, i.e.

$$\frac{dp}{dz} = -g\rho. \tag{4.13}$$

This is valid for all water particles between the surface h and the bottom at $z = -H$. If we would now release the wavy water surface from its initial position, this still holds, as no additional forces are acting in the vertical direction. Hence, according to Newton's law, there would be no fluid

Fig. 4.3: Examples of surface water waves. Left: ring waves due to the impact of rain drops. Right: Typical irregular waves on an ocean surface.

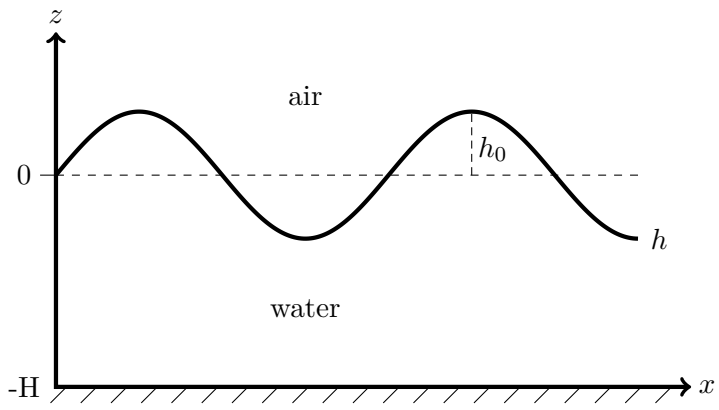

Fig. 4.4: Vertical cross section through a water column with waves at the air-water interface. The undisturbed water surface at $z = 0$ is indicated by the dashed line. The water bottom is located at $z = -H$.

acceleration in the vertical, but what we would observe is the sinking of the wave ridges and the rising of the wave troughs. What is then the reason for this? To answer this question, we have to consider the horizontal components of the forces, i.e. the pressure forces.

First, we calculate the pressure p itself from the hydrostatic law above. As the water density ρ is constant, we obtain the simple linear pressure profile as already calculated in Section 2.4:

$$p(z) = g\rho(h - z). \tag{4.14}$$

As h is varying in the horizontal (x) direction, then

$$p(x, z) = g\rho(h(x) - z). \tag{4.15}$$

The horizontal pressure force is not the pressure itself but, as outlined in Section 2.3, the horizontal pressure gradient (or the pressure difference) across a water particle. Hence, for the horizontal acceleration, we have

$$\frac{du}{dt} = -\frac{1}{\rho}\frac{dp}{dx} = -g\frac{dh}{dx}. \tag{4.16}$$

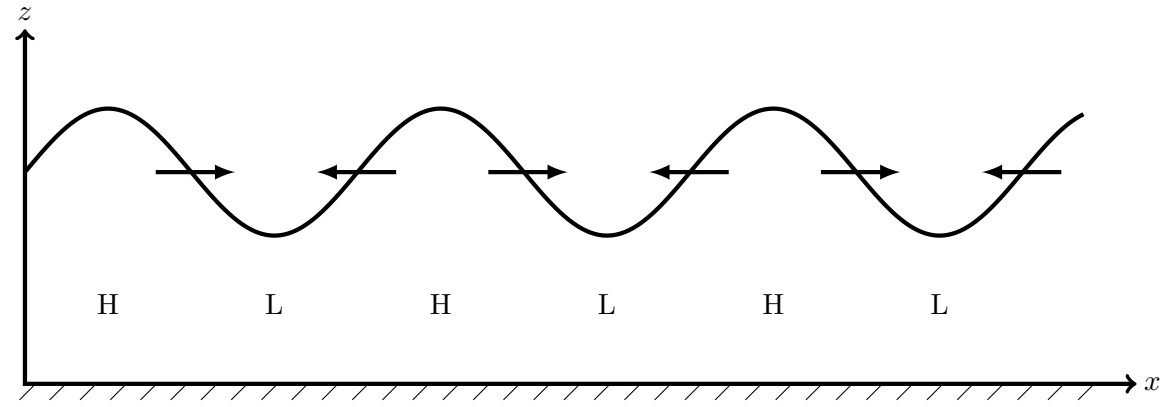

Fig. 4.5: Distribution of hydrostatic pressure (H = high, L = low) and hydrostatic pressure forces (arrows) in surface water waves.

From Figure 4.5, we can see that the pressure gradient, and hence the pressure force, is strongest on the flanks of the surface wave. The direction of the pressure forces and hence of the initial accelerations are also depicted in Figure 4.5. Therefore, if we release the wavy surface from its initial position, there will be some motion induced by horizontal pressure forces which are directed from the wave crests to the wave troughs. As a consequence of mass continuity (see Section 2.6), the amplitude of wave crests and wave troughs will decrease. Hence, particles located at these positions will move down or up, but this vertical motion is not induced by gravity but by dynamic pressure forces resulting from the horizontal accelerations in order to satisfy the continuity principle. Therefore, we might say that the restoring force of water waves is not induced by gravity directly, but the horizontal hydrostatic pressure force, which is of course related directly to gravity by the hydrostatic law (see above).

Now we may ask if water waves are of the longitudinal or transversal type? As the waves propagate in the horizontal direction (x direction in our examples), water particles would move in the vertical (z direction) in case of transversal waves and in the horizontal in case of a longitudinal wave. The derivation of particle motion as induced by surface water waves can be found in any textbook on waves (see e.g. Lighthill, 2001 or Sutherland, 2010) with the result shown in Figure 4.6.

In general, it has been found that particles move in elliptical orbits, where the relation of the horizontal to vertical axis depends on the ratio of the wavelength L to the water depth H. If the wavelength is much smaller than the water depth (say $H/L = 10$), the waves are called "deep water" waves. If in contrast the water depth is much smaller than the wavelength (say $H/L = 0.1$), the waves are called "shallow water" waves. In both cases, the water need not be deep or shallow in any absolute sense, but only in relation to the wavelength.

The calculation of particle orbits (see e.g. Lighthill, 2001 or Sutherland, 2010) show that for deep water waves, the particle orbits are circles with radius h_0 at the water surface, decreasing to zero at a depth of about $z = -L$ as shown in the left part of Figure 4.6.

For shallow water waves, particle orbits are very flat ellipses with the horizontal axis much larger than the vertical axis, as shown in the right part of Figure 4.6. The vertical excursion is equal to h_0 at the surface and vanishes at the water bottom at $z = -H$. The horizontal

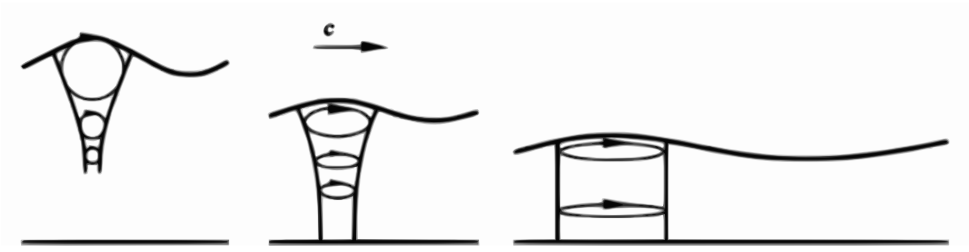

Fig. 4.6: Orbits of particle motion below a wavy water surface. Left: deep water; middle: intermediate water; right: shallow water.

Fig. 4.7: A wave on the interface of a two layer fluid. Blue: heavy fluid.

excursion is constant throughout the whole water column and is related to the wave height h_0 by $x_{\max} = h_0 L/(2\pi H)$.

As an example, we consider the motion of a cork on the water surface. If the wave height is $h_0 = 0.5\,\mathrm{m}$, the cork (or a swimmer) moves up and down by at most an amplitude of 1 m. In the horizontal, it would be moved by 1 m in the case of deep water waves and several meters in the case of shallow water waves. The nearly horizontal motion for the case of shallow water waves is also called sloshing and can be felt even at the water bottom. This brings us back to the question of whether water waves are of a longitudinal or transversal type. As particle motion includes both horizontal and vertical movement, water waves are a combination of transversal and longitudinal wave motion. In the case of shallow water waves, the motion is mainly in the horizontal direction and hence shallow water waves may be called longitudinal waves.

Finally, we present the results for the phase speed of water waves which are:

$$\text{deep water waves:} \quad c = \sqrt{\frac{g}{k}} = \sqrt{\frac{gL}{2\pi}}, \tag{4.17}$$

$$\text{shallow water waves:} \quad c = \sqrt{gH}. \tag{4.18}$$

Hence, for deep water waves, the phase speed increases with increasing wavelength. These waves are also called “dispersive waves”. For shallow water waves, the phase speed is independent of the wavelength, but depends only on the water depth. The phase speed for shallow water waves is also applicable to Tsunami waves and can, to a first approximation, be used to estimate their propagation speed and hence time of arrival at distant coasts. For example, if we take the mean depth of an ocean with 4000 m, the resulting Tsunami phase speed would be about 200 m/s or 720 km/h.

4.5 “Water waves” in the atmosphere

While this title may appear to be nonsense, it is not to be taken literally. Actually, the problem of water waves is just a special case of so-called interfacial waves between two fluid layers of different densities ρ_l and ρ_u, where the denser fluid occupies the lower layer (index l) and hence the fluid is stably stratified. Take for example water as the lower layer and oil as the upper layer (index u) as shown in Figure 4.7, with the corresponding density profile shown in Figure 4.8. The interface between the two fluids can support waves with the same properties of water waves

as described in Section 4.4. But now the hydrostatic pressure gradient, which acts as a restoring force, has to be calculated with the so-called reduced gravity given by

$$g' = -\frac{g}{\rho_\mathrm{l}} \left(\rho_\mathrm{u} - \rho_\mathrm{l}\right) \tag{4.19}$$

instead of full gravity g. This must also be done in all resulting formula, such as for the phase speed. For the atmosphere, two layers of constant potential temperature θ have to be considered as shown in Figure 4.8. The reduced gravity is now given by

$$g' = \frac{g}{\theta_\mathrm{l}} \left(\theta_\mathrm{u} - \theta_\mathrm{l}\right). \tag{4.20}$$

From the perspective of the lower layer, the waves appear at the upper boundary of this layer, hence these interfacial waves are also called "external gravity waves", which is to be contrasted with "internal gravity waves" to be discussed later.

The phase speeds of interfacial waves are now given by (see e.g. Sutherland, 2010):

$$c = \sqrt{g' \frac{L}{2\pi}} \quad \text{for } L \ll H, \tag{4.21}$$

$$c = \sqrt{g' H} \quad \text{for } L \gg H \tag{4.22}$$

and correspond to the results for deep and shallow water waves given in Section 4.4.

Let us give the following examples for external gravity waves at an inversion as sketched in Figure 4.8. A typical inversion height is $H = 500\,\mathrm{m}$ and a typical temperature jump is $\theta_\mathrm{u} - \theta_\mathrm{l} = 6\,^\circ\mathrm{C}$. If we consider a wavelength of $L = 5000\,\mathrm{m}$, we have $H/L = 0.1$ and hence can apply the phase speed formula for "shallow water" waves. The resulting phase speed is $c = 10\,\mathrm{m/s}$ (36 km/h) which might be contrasted to the phase speed of Tsunami waves (720 km/h) on ocean surfaces as estimated in Section 4.4.

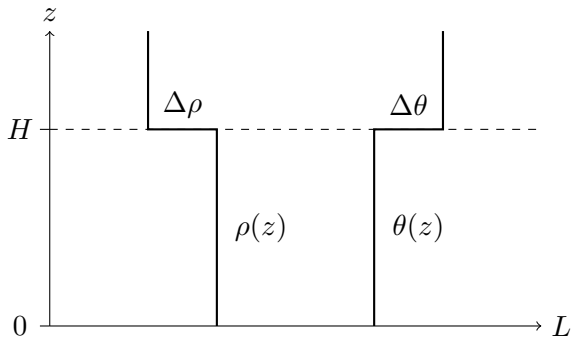

Fig. 4.8: Vertical variation of density ρ and potential temperature θ in a stably stratified two layer fluid.

5 Internal gravity waves

5.1 Waves in unbounded domains

In the following, we restrict the discussion to internal gravity waves to the atmosphere, although the same results would be obtained for stratified lakes or oceans. Internal gravity waves can be observed in a continuously stratified atmosphere characterized by a Brunt-Vaisala frequency $N(z)$. First, we consider the simple case of constant N, implying the potential temperature increases linearly with height. If the atmosphere is at rest and is not restricted by lower and upper boundaries (an ideal assumption), it can be shown (see, e.g., Nappo, 2012 or Sutherland, 2010) that the linearized wave equations (see Appendix AI, AII) have as possible solutions so-called plane waves, where the temperature perturbations θ (or density perturbations) are given by the wave relation

$$\theta(x,z,t) = \theta_0 \sin(kx + lz - \omega t). \tag{5.1}$$

Here, $k = 2\pi/L_x$ and $l = 2\pi/L_z$ are the horizontal and vertical wave numbers with L_x and L_z denoting horizontal and vertical wavelength.

The phase lines are orientated perpendicular to the wave number vector $\mathbf{m}$ which is oriented with the angle α to the horizontal direction as shown schematically in Figure 5.1. The total temperature field is composed of the basic state $\Theta(z)$ plus the wave perturbations $\theta(x,z,t)$. The resulting temperature field for an instantaneous time t_0 is shown in Figure 5.2.
The velocity components u, w and the pressure perturbations p are given by

$$w(x,z,t) = +w_0 \cos(kx + lz - \omega t), \tag{5.2}$$

$$u(x,z,t) = -u_0 \cos(kx + lz - \omega t), \tag{5.3}$$

$$p(x,z,t) = -p_0 \cos(kx + lz - \omega t). \tag{5.4}$$

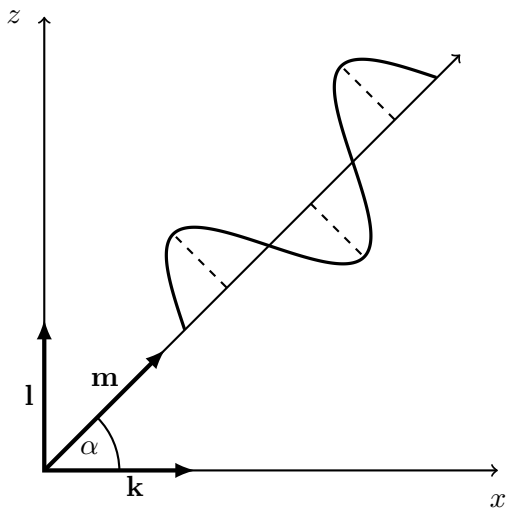

Fig. 5.1: Scheme of a wave propagating with an angle α to the horizontal (x) direction. Propagation wave number vector $\mathbf{m}$ and its components, $\mathbf{k}$ and $\mathbf{l}$ are shown as thick arrows. The phase lines are indicated by dashes.

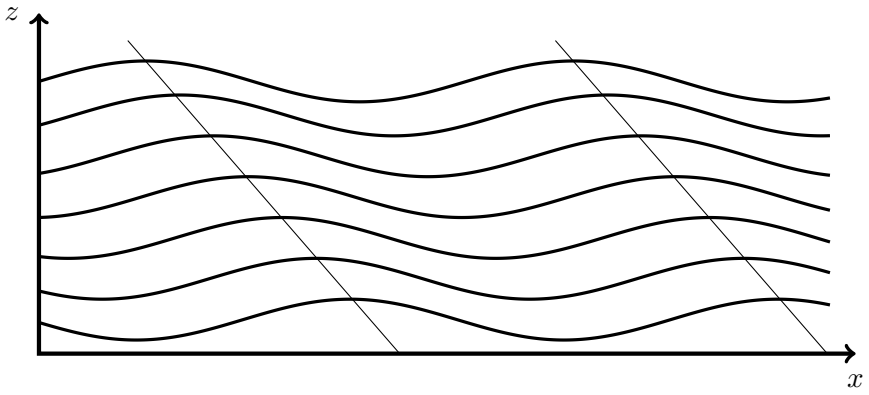

Fig. 5.2: Instantaneous field of potential temperature in a stably stratified atmosphere as induced by internal gravity waves with tilted phase lines as in Fig. 5.1.

The velocity amplitudes are related through

$$u_0 = \frac{l}{k} w_0 = \frac{L_x}{L_z} w_0. \tag{5.5}$$

The wave frequency ω is related to the Brunt-Vaisala frequency N by

$$\omega = N \frac{k}{\sqrt{k^2 + l^2}} = N \frac{k}{m} = N \cos \alpha. \tag{5.6}$$

The above relations show that the internal gravity waves can in principle be oriented at any angle to the horizontal axis or with respect to the direction of gravity. Due to relation 5.6, the wave frequency is always less than the Brunt-Vaisala frequency N. For $\alpha = 0$, the phase lines are vertical and the maximum frequency $\omega = N$ is obtained.

Now we may ask what is the motion of air parcels within the gravity waves? As can be seen from equations 5.2 and 5.3, vertical and horizontal velocity w and u are in phase but of opposite sign. Hence, if a particle is moving downward it is also moving forward and if it is moving upward, it also moves backward as illustrated in Figure 5.3. Consequently, air parcels are moving along the phase lines perpendicular to the direction of wave propagation. Hence, these kinds of idealized internal gravity waves in an unbounded domain with constant Brunt-Vaisala frequency are a type of transversal waves. For $\alpha = 0$, the phase lines are vertical and the vertical wave number l is zero. It follows from 5.5 that the horizontal wave velocity u is also zero, hence the fluid motion is purely in the vertical direction and all air columns are moving up and down in a synchronous manner with the frequency $\omega = N$ like single particles in a stratified environment as described in Section 3.4. This is a rather idealized situation which can occur only in a hypothetical fluid domain without boundaries and with constant stratification. Otherwise, the basic wave equations (see appendix) have solutions where the velocity amplitudes vary in the vertical direction, with horizontal particle motion even when the phase lines are purely vertical as will be illustrated in the next section.

In the atmosphere, the physical wave quantities like temperature, velocity and pressure can be obtained by measurements, but as we usually identify waves with the motion of visible objects

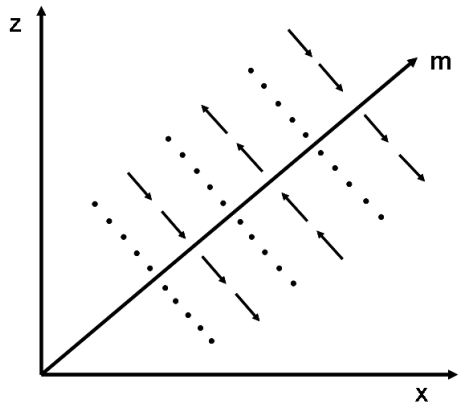

Fig. 5.3: Instantaneous field of particle motion in an internal gravity wave propagating in the **m**-direction. Dotted lines: no motion.

such as a water surface, it might be of interest to know the motion of fluid particles in gravity waves. As shown in Section 2.1, the trajectories of particles in fluid motion are directly related to the velocity components, u and w by $dx/dt = u$ and $dz/dt = w$. In order to obtain the locations of particles, one has to integrate the wave velocities in time. From equations 5.2 and 5.3, one obtains

$$x(t) = \frac{u_0}{\omega}\sin(kx + lz - \omega t) + c_1 \tag{5.7}$$

and

$$z(t) = -\frac{w_0}{\omega}\sin(kx + lz - \omega t) + c_2, \tag{5.8}$$

where c_1 and c_2 are integration constants. From these solutions, one can see that the particle coordinates, x and z are related by

$$z = -x\frac{w_0}{u_0} + c_3 = -x\frac{k}{l} + c_3, \tag{5.9}$$

where equation 5.5 has been used here. The variation of the vertical particle position as a function of its horizontal position is just a line with negative slope k/l. Hence, the particle motion is along a straight line inclined backward with angle α to the vertical axis as sketched in Fig. 5.4.

Now what is the maximum distance a particle would be shifted from its equilibrium position

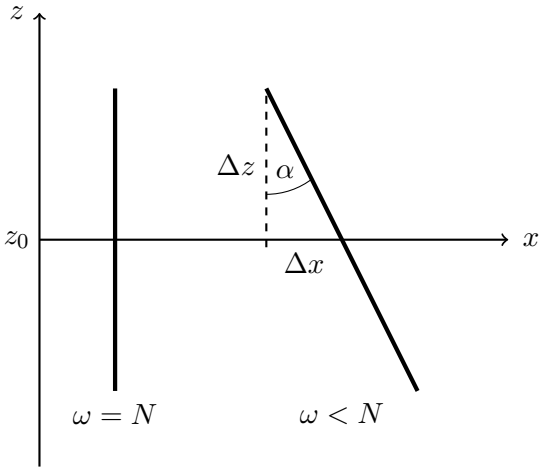

Fig. 5.4: Particle orbits due to gravity waves in unbounded domains with $\omega < N$.

at some position (x_0, z_0) due to the action of internal gravity waves? From 5.7 and 5.8, one gets

$$(z - z_0)_{\max} = \Delta z = \frac{w_0}{\omega}, \qquad (x - x_0)_{\max} = \Delta x = \frac{u_0}{\omega} = \Delta z \frac{l}{k}. \tag{5.10}$$

Let us for example consider the vertical amplitude of the particle motion:

$$\Delta z = \frac{w_0}{\omega} = \frac{w_0}{N \cos(\alpha)}, \tag{5.11}$$

where we have used the frequency relation 5.6. If we take the case with vertical phase lines ($\alpha = 0$) and hence pure vertical wave motion, then $\Delta z = w_0/N$. For typical values of $w_0 = 2\,\mathrm{m/s}$ and $N = 0.011$ as found in atmospheric gravity waves, the maximum vertical excursion is about $\Delta z = 220\,\mathrm{m}$, which would be a typical amplitude for vertical particle displacements. More details on this aspect are provided in Section 7.5.

Finally, we may provide the phase speed for free internal gravity waves for the case of vertical phase lines ($\alpha = 0$), where the maximum angular frequency $\omega = N$ is possible. As the phase speed c is related to frequency ω and wave number k by $c = \omega/k$, one obtains

$$c = \frac{N}{k} = \frac{NL}{2\pi}. \tag{5.12}$$

As the phase speed depends on the wavelength L, internal gravity waves are also-called dispersive waves just as in the case of deep water waves (see Section 4.4). For example, if we take as typical values for gravity waves in the atmosphere as $L = 10\,\mathrm{km}$ and $N = 0.012$, we get $c = 20\,\mathrm{m/s}$ or $36\,\mathrm{kn}$. As this is in the range of typical wind speeds, it is an important point with respect to stationary mountain waves to be discussed in Section 5.4.

5.2 Forced gravity waves

The simple plain waves described in the previous section are also called free gravity waves, as they can exist in a stratified fluid with constant Brunt-Vaisala frequency N without external forces. The only forces involved are the buoyancy force (3.24) and the pressure force (2.11). Under these conditions, the wave frequency ω is always less than N (see 5.6) and the fluid particles oscillate with this frequency once lifted from their equilibrium position. When we consider the case of single particle oscillation described in Section 3.4, this is like a free pendulum. But from physics we know that one could also force the pendulum with a frequency ω larger than its natural oscillation frequency (for a stratified fluid, the natural frequency is N). Then one speaks about forced oscillations and the phenomenon of resonance leading to larger oscillation amplitudes can occur.

Here we may ask if similar phenomena can happen for internal gravity waves, i.e. for waves with $\omega > N$? Let us assume that a plane of constant potential temperature at some height $z = z_0$ is perturbed by

$$\Theta(x, z_0, t) = \Theta_0(z_0) + \theta_0(z) \sin(kx - \omega t). \tag{5.13}$$

With this forcing and $\omega > N$, the wave equations (see Appendix AII) do not permit periodic (sine-like) solutions in the vertical direction as was for the case $\omega < N$ as described in Section 5.1. Instead, there must be a decrease in wave amplitude away from the position of wave forcing at the reference position, $z = z_0$. The solutions are now (see Nappo, 2012 or Sutherland, 2010):

$$\theta(x,z,t) = \theta_0 \exp(-m(z-z_0)) \sin(kx - \omega t) \qquad z > z_0, \tag{5.14}$$

$$\theta(x,z,t) = \theta_0 \exp(+m(z-z_0)) \sin(kx - \omega t) \qquad z < z_0. \tag{5.15}$$

The Brunt-Vaisala frequency N, wave frequency ω and horizontal wave number $k(= 2\pi/L)$ are now related through

$$m^2 = k^2 \left(1 - \frac{N^2}{\omega^2}\right), \tag{5.16}$$

where m is the amplitude decay factor. The resulting field of potential temperature (or density) including the background state $\Theta_0(z)$ is shown schematically in Fig. 5.5.

The related wave velocity components u and w and the dynamic pressure p are given for $z < z_0$

$$w(x,z,t) = w_0 \exp(m(z-z_0)) \cos(kx - \omega t), \tag{5.17}$$

$$u(x,z,t) = -u_0 \exp(m(z-z_0)) \sin(kx - \omega t), \tag{5.18}$$

$$p(x,z,t) = -p_0 \exp(m(z-z_0)) \sin(kx - \omega t). \tag{5.19}$$

If we compare these wave fields with the case for plane waves with $\omega < N$ presented in Section 5.1, there are two distinctions: the phase lines are now oriented in the vertical (z) direction and the amplitudes are decreasing with distance from the forcing height $z = z_0$. Hence, these waves are called damped or evanescent gravity waves. Also of interest is the fact that vertical and

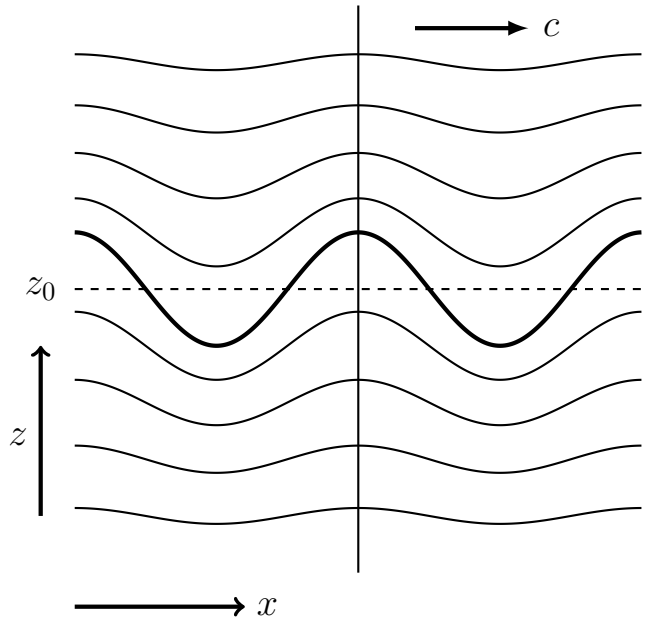

Fig. 5.5: Instantaneous field of potential temperature for the case of a damped gravity wave ($\omega < N$). The forcing wave at mid plane is shown as a solid line. A phase line is shown as a vertical straight line.

horizontal velocity components are now out of phase. Therefore, the pathways of fluid particles are not inclined lines like in Fig. 5.4.

Particle positions, x and z, for the case of damped gravity waves can be obtained from the wave velocities, u and w, as described in Section 5.1. The result for the lower part ($z < z_0$) is

$$x(t) = \frac{u_0}{\omega} \exp(+m(z - z_0)) \cos(kx - \omega t) + c_1, \tag{5.20}$$

$$z(t) = - \frac{w_0}{\omega} \exp(+m(z - z_0)) \sin(kx - \omega t) + c_2. \tag{5.21}$$

The temporal change of horizontal and vertical particle positions are now out of phase and the resulting orbits have the shape of ellipses as shown in Fig. 5.6 similar to water waves. As the phase lines are oriented in the vertical (z) direction (see Fig. 5.5) but the particles can also move in the direction of wave propagation (x-direction), these forced internal gravity waves are a mixture of transversal and longitudinal waves with respect to fluid particle motion. The maximum particle excursions are similar to the ones presented for plain gravity waves in Section 5.1:

$$\Delta z = \frac{w_0}{\omega}, \qquad \Delta x = \frac{u_0}{\omega} = \Delta z \frac{m}{k}. \tag{5.22}$$

These amplitudes can be regarded as the ellipse half axes of the particle orbits. They decay with distance from the forcing position z_0 with $\exp(m(z - z_0))$, $z < z_0$, as shown schematically in Fig. 5.6. By comparing these orbits with those in water waves shown in Fig. 4.6, one notices that the longer axis of the elliptical orbits is in the vertical direction for internal gravity waves and in the horizontal direction for water waves.

5.3 Gravity waves restricted by horizontal boundaries

The case of simple gravity waves in an unbounded fluid domain is of course not realistic concerning application to the atmosphere, as the earth's surface is a surface through which air

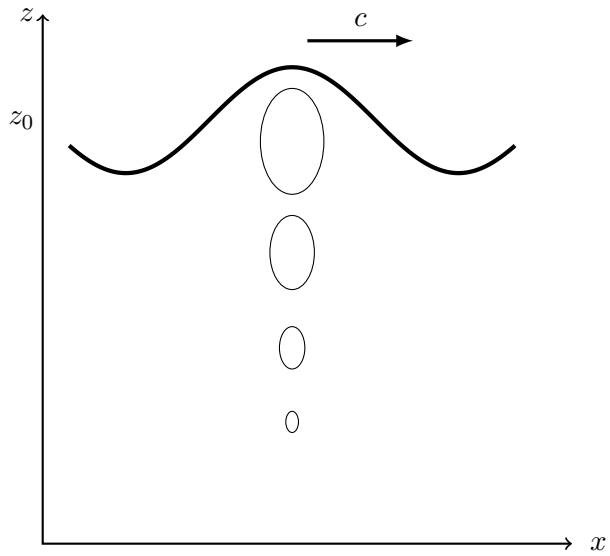

Fig. 5.6: Sketch of particle orbits in a damped gravity wave as shown in Fig. 5.5. The direction of wave propagation is indicated by the arrow.

parcels cannot penetrate. Hence, from a physical point of view, there can be no vertical particle motion at the surface. As a consequence, it is not possible for the whole air column to oscillate in the vertical direction with the same frequency and amplitude in the case described in the last section. Let us, for example, consider the case of a stratified fluid with constant Brunt-Vaisala frequency N bounded at top ($z = H$) and bottom ($z = 0$) by solid walls.
In this example, internal gravity waves are still possible, but these are now restricted by the influence of the upper and lower boundaries, where the vertical fluid velocity must be zero ($w = 0$). The solutions of the wave equations for temperature, velocity and pressure are now given by the following relations (e.g. Baines, 1995), where we have used the horizontal wavelength L instead of wave number k $(= 2\pi/L)$:

$$\theta(x,z,t) = +\theta_0(z)\cos\left(\frac{2\pi}{L}x - \omega t\right), \tag{5.23}$$

$$w(x,z,t) = +w_0(z)\sin\left(\frac{2\pi}{L}x - \omega t\right), \tag{5.24}$$

$$u(x,z,t) = -u_0(z)\cos\left(\frac{2\pi}{L}x - \omega t\right), \tag{5.25}$$

$$p(x,z,t) = -p_0(z)\cos\left(\frac{2\pi}{L}x - \omega t\right). \tag{5.26}$$

The phase lines are now oriented in the vertical (z) direction and the wave is moving in the horizontal (x) direction. In contrast to free gravity waves (Section 5.1), vertical and horizontal velocities w and u are now out of phase, which has a marked influence on the particle motion (Fig. 5.8) The wave amplitudes for temperature and velocity are not constant any more, but vary with height due to the presence of solid boundaries at $z = 0$ and $z = H$. The amplitude functions are given by:

$$\theta_0(z) = \theta_{\max}\sin\left(\frac{\pi z}{H}\right), \tag{5.27}$$

$$w_0(z) = w_{\max}\sin\left(\frac{\pi z}{H}\right), \tag{5.28}$$

$$u_0(z) = u_{\max}\cos\left(\frac{\pi z}{H}\right), \tag{5.29}$$

$$p_0(z) = p_{\max}\cos\left(\frac{\pi z}{H}\right), \tag{5.30}$$

where the maximum amplitudes for horizontal and vertical wave velocities are related through

$$u_{\max} = w_{\max}\frac{L}{2H}. \tag{5.31}$$

The wave field $\theta(x,z)$ superimposed on the basic state $\Theta(z)$ for temperature (or density) is shown in Figure 5.7 at time t_0. Particle orbits due to travelling waves are not along straight lines as in the case of pure gravity waves (see Figure 5.3), but take more complicated forms as sketched in Figure 5.8, which are similar to that in water waves (see Fig. 4.6).

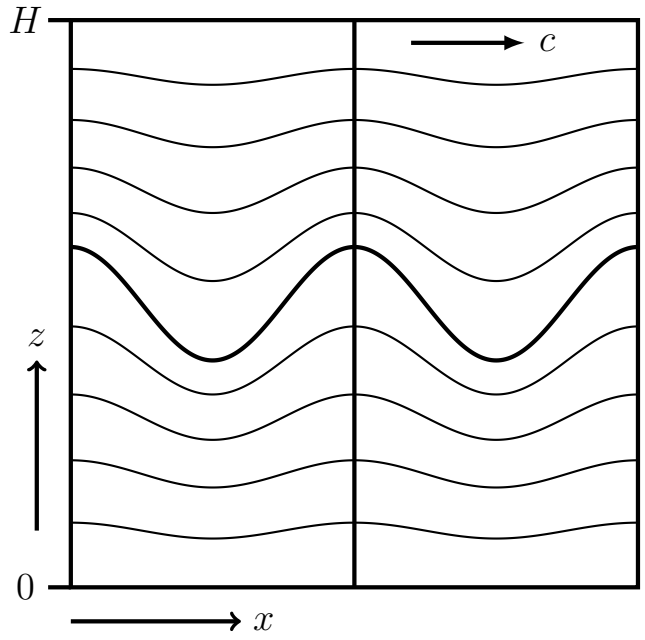

Fig. 5.7: Instantaneous field of potential temperature in a stably stratified fluid bounded by solid walls at $z = 0$ and $z = H$ as induced by an internal gravity wave. Phase lines are oriented in the vertical (z) direction.

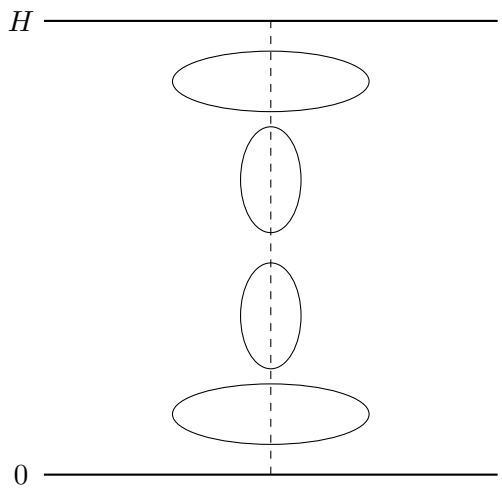

Fig. 5.8: Typical particle orbits as induced by the gravity wave shown in Figure 5.7.

5.4 Gravity waves with a background wind

So far we have considered wave motion in a fluid at rest. This is an idealized case which can be investigated, e.g., in laboratory experiments (see Figure 7.4). In geophysical applications however, the fluid of interest (air in the atmosphere or water in lakes and oceans) is usually moving (wind in the atmosphere, currents in the ocean). The background fluid motion has considerable influence on the properties of gravity waves, which leads to interesting consequences concerning waves usable for soaring flight and will be discussed later in Sections 6 and 7.

Let us here consider the most simple case of a background wind constant with height denoted by U. In this case, all properties of wave motion as discussed so far remain the same if observed from a coordinate system moving with the mean velocity U. If we fix the coordinate system with respect to the earth's surface (as is usually done), the wave is now moving with its absolute

phase speed (denoted by C_a) defined as

$$C_a = U \pm c. \tag{5.32}$$

The sign attached to the normal phase speed c (also called intrinsic phase speed) indicates whether the wave is moving in the direction of the mean flow (+) or against it (−). It is possible that the absolute phase speed C_a is zero so that the wave is stationary with respect to an observer at a fixed position x_0 as shown in Figure 5.9. In this case, the phase speed c is opposite to the direction of the background wind U but of the same magnitude ($c = U$). This kind of stationary wave can be found in the lee of mountain ridges and will be of most importance for soaring flight.

We might use the relation for stationary gravity waves to estimate the typical wavelength L for these waves. Let us consider the simple case of waves with vertical phase lines discussed at the end of Section 5.1. There we obtained for the intrinsic phase speed, $c = N/k$, where $k = 2\pi/L$. For stationary waves we have the condition $c = U$, hence we obtain

$$L_{\text{stat}} = \frac{2\pi U}{N}. \tag{5.33}$$

An example is if we take as typical atmospheric values, $N = 0.012$ and $U = 10\,\text{m/s}$, the wavelength of stationary gravity waves would be $L_{\text{stat}} \approx 5\,\text{km}$. If the wind speed is doubled to $20\,\text{m/s}$ (36 kn), the wavelength is also doubled to $\approx 10\,\text{km}$. This relation between wind speed and wavelength for stationary gravity waves will be of interest for the case of mountain lee waves as discussed in Section 7.1.

The idealized case of constant wind speed U will be rarely found in the atmosphere as the wind is usually varying with height $U(z)$, which leads to more complex wave properties including the reflection and suppression of waves. These aspects will be discussed in Sections 6 and 7.

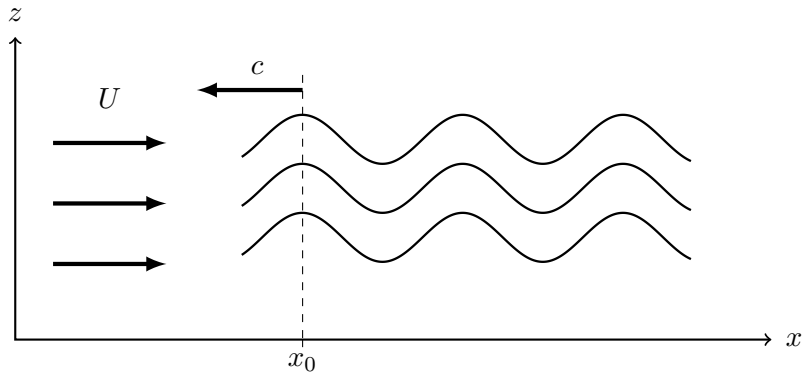

Fig. 5.9: Schematic of a stationary gravity wave with phase speed c opposite to the constant wind speed U. The ridges and troughs are fixed in space with respect to the surface (x-direction).

5.5 Triggering gravity waves

In the previous chapters, we have shown that gravity waves can exist in a stably stratified fluid. This was done by prescribing wave solutions to the equations of fluid motion. But the question of how these waves are initiated from a fluid state of rest was not discussed. In fact, in real flows, such as in in the atmosphere or the oceans, gravity waves do not exist a priori but have to be triggered by some mechanism. Let us take the following example well known to everybody. On a windless day, the water surface of a pond or a lake is very smooth with no surface waves to be observed. If we now throw a stone into the water, we observe the development of circular surface waves spreading outward from the point of impact as was already shown in Figure 4.3. The reason for wave development is the downward forcing of the water surface by the impact of the stone which creates a pressure disturbance leading to surface wave development.

A quite similar mechanism for triggering gravity waves can be observed in the atmosphere occuring in a convective boundary layer with a stably stratified layer above. The thermals impinging on the inversion at the top of the boundary layer (at a height of 1-2 km) deform this layer in the vertical direction and hence initiate oscillations in the stably stratified atmosphere above as shown schematically in Figure 5.10. The resulting gravity waves in the stably stratified atmosphere above are called "thermal waves" and have been treated in the book on thermals by Hertenstein (2005) to be discussed below in Section 10.2.

The second mechanism for triggering gravity waves is due to the mechanical forcing of the horizontal wind by mountain barriers and is the most important mechanism for gravity wave initiation of mountain waves suitable for soaring flight. The principle of topographic forcing can be illustrated by considering an air flow approaching a two-dimensional mountain ridge as sketched in Figure 5.11. As the air cannot penetrate the surface, the flow must follow the orography near the ground. Hence, the incoming flow with wind speed u is deflected from the horizontal and has now a vertical velocity component denoted by w in Figure 5.11. The vertical wind at the upwind side of the ridge is called ridge lift by soaring pilots and was traditionally the only source of lift for soaring before the detection of thermal lift. Details on ridge lift for

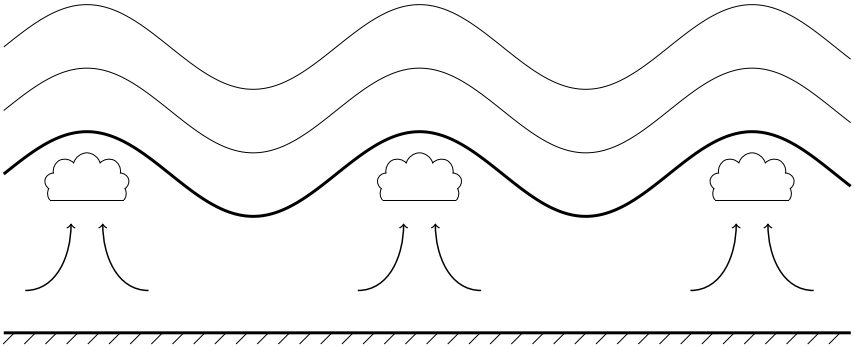

Fig. 5.10: Schematic of gravity waves triggered by thermals impinging on the boundary layer inversion (thick line).

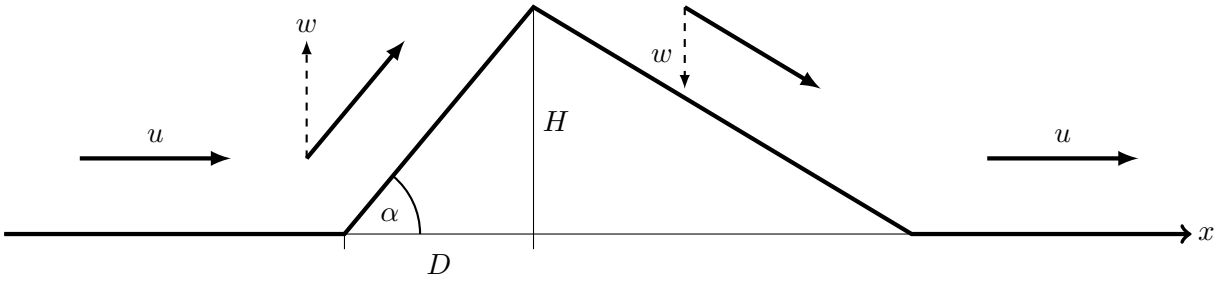

Fig. 5.11: Schematic of the vertical velocity w induced by deflection of a horizontal wind u by an asymmetric mountain barrier.

soaring flight is discussed in detail in Hertenstein (2011) and will not be treated here. We are more interested in the question of how gravity waves will be triggered by ridge lift in a stably stratified atmospheric environment as will be shown in the next chapter.

Here we just give some estimate of the strength of the ridge lift which will also be important for the amplitude of mountain waves in the lee of the ridge. In Figure 5.11, the mountain height is denoted by H and the mountain half-width by D. The angle of the mountain slope, denoted by α, is given through the relation

$$\tan(\alpha) = \frac{H}{D}. \tag{5.34}$$

If we assume for simplicity that the speed u of the oncoming air flow is not reduced when hitting the mountain but only follows the slope of the terrain, the vertical wind component w induced by the slope is related to the oncoming wind speed u by

$$w = u \sin(\alpha). \tag{5.35}$$

For small α (α less than 20°), calculus provides the approximation $\sin(\alpha) = \tan(\alpha)$ and hence we obtain for the vertical velocity induced by the mountain slope

$$w = u\frac{H}{D}. \tag{5.36}$$

Typical mountains of medium size have $H \approx 1000\,\mathrm{m}$ and $D \approx 10000\,\mathrm{m}$. Hence, $H/D = 0.1$ and $\alpha = 6°$, so the ridge lift w will be $u/10$. For a wind speed of $10\,\mathrm{m/s}$ ($18\,\mathrm{kn}$), we get a terrain-induced vertical velocity of $w = 1\,\mathrm{m/s}$. If the half width of the mountain is reduced to $D = 5000\,\mathrm{m}$, the slope increases to $H/D = 0.2$ ($\alpha = 11°$) and the ridge lift is doubled to $w = 2\,\mathrm{m/s}$. The dependence of w on mountain slope is shown schematically in Figure 5.11.

On the lee side of the mountain, one has just the opposite case: the air flow will follow the lee slope and produce a negative vertical velocity w making ridge soaring only possible above the upwind slope. The simple formula for ridge lift also tells us that steeper slopes produce stronger lift, but also stronger downward flow on the lee side. The latter is important for the triggering of mountain waves, where the mountain slope of the lee side is important for the wave strength as will be discussed later.

5.6 Forces driving internal gravity waves

In the preceding sections, we have presented internal gravity waves as possible solutions of equations describing fluid motion. These are the mathematical formulations (see appendix) of general conservation principles in physics, including the conservation of momentum, heat and mass. In this section, we will consider the forces driving gravity waves in some detail. In Section 3.4, we have described the oscillations of fluid particles in a stratified fluid due to the buoyancy force, which was defined as the difference between the gravity force acting directly on the mass particle and the vertical pressure force due to hydrostatic pressure of the fluid environment. This force is also one of the driving forces in gravity waves (see Section 5.1 and the appendix), but as it is only acting in the vertical direction, it produces only vertical motion. The organisation of horizontal waves in a fluid is only possible through pressure forces acting on all the fluid particles and from walls enclosing the fluid. Coupling between fluid particles is also possible by frictional forces, but these are not the primary drivers of gravity waves. These forces act more to damp wave amplitudes rather than as a source of wave motion. Hence, idealized wave motion is usually described without frictional forces (a so-called inviscid fluid) as is also done here.

In the following, we consider the interaction of the buoyancy force with the pressure force for the simple wave motion described in Sections 5.1 – 5.3. In these sections, the fields of the perturbation temperature $\theta(x, z, t)$ and the perturbation pressure $p(x, z, t)$ of gravity waves have been presented for various cases. The buoyancy force B and pressure forces, P_x and P_z, in the horizontal and vertical directions are related to these wave properties by

$$B = \frac{g}{\Theta_0}\theta, \tag{5.37}$$

$$P_x = -\frac{1}{\rho_0}\frac{dp}{dx} \tag{5.38}$$

and

$$P_z = -\frac{1}{\rho_0}\frac{dp}{dz}, \tag{5.39}$$

where Θ_0 and ρ_0 are constant reference values for the temperature and density of the fluid, respectively.

As outlined in Chapter 2, these forces drive fluid motion according to Newton's law by

$$\frac{du}{dt} = P_x \tag{5.40}$$

and

$$\frac{dw}{dt} = P_z + B, \tag{5.41}$$

where du/dt and dw/dt are the accelerations in the horizontal and vertical direction, respectively.

Concerning the buoyancy force B, it should be noted that the perturbation temperature θ of a fluid particle at positions, x and z at time t, is not defined as the difference between the

particle temperature and the temperature of its surrounding as in the derivation of the buoyancy of single particles lifted in a still environment in Sections 3.3 – 3.5, but with respect to the initial state $\Theta_0(z)$ of a stratified fluid (air or water) at rest:

$$\theta(x, z, t) = \Theta(x, z, t) - \Theta_0(z), \tag{5.42}$$

where $\Theta(x, z, t)$ is the particle temperature. This is necessary because in gravity waves, all fluid particles are moving up and down with respect to their initial equilibrium position at some height z_i where $\Theta(x, z_i, t) = \Theta_0(z_i)$ or $\theta(x, z_i, t) = 0$ (see Fig. 5.13). Hence, the buoyancy must be defined as an excess in temperature (or density) with respect to this equilibrium temperature (or density) and not with respect to the neighboring particle at the same height.

In the following, some examples of forces acting on a fluid particle in a gravity wave are presented.

(a) A popular explanation

As the full physics of internal gravity waves are not always easy to understand, more popular explanations of the formation of gravity waves exist based on single fluid parcels oscillating in a stably stratified flow. Considering the situation sketched in Fig. 5.12 showing an fluid parcel moving at a certain height $z = z_0$ with the wind in the horizontal direction. As there is no vertical motion, the forces acting on the parcel in the vertical direction, the gravity force per unit volume G $(= -g\rho_\mathrm{p})$ and the hydrostatic pressure force per unit volume P $(= -dp_\mathrm{h}/dz)$, must be in equilibrium. Concerning the vertical variation of these forces, the gravity force G remains constant as the parcel density ρ_p does not change. The hydrostatic pressure force P due to the environmental fluid mass is related to the environmental fluid density ρ by the hydrostatic pressure law (Section 2.4) as $P = g\rho$. As the density ρ decreases with height in a stably stratified fluid, the variation of pressure force P with height is given by

$$\frac{dP}{dz} = g\frac{d\rho}{dz} < 0. \tag{5.43}$$

Hence, in a stably stratified fluid, the hydrostatic pressure force decreases with height.

Now we consider what happens, if the fluid parcel is pushed upward instantaneously at some position $x = x_0$ as indicated by the green arrow in Fig. 5.12 (in practice, this could be due to a thermal impinging from below or by obstacle forcing as was discussed in Section 5.5). According to (5.43), the pressure force P above the equilibrium height z_0 is less than at $z = z_0$, but the gravity force G remains the same as indicated in Fig. 5.12. The resulting net force results in an downward acceleration of the parcel. If the parcel is below the height z_0, the pressure force P is larger than at z_0 as is also shown in Fig. 5.12. The resulting net force hence leads to an upward acceleration of the parcel. The difference between gravity force G and hydrostatic pressure force P is just the buoyancy force B as introduced in Chapter 3 and shown in the lower part of Fig. 5.12.

As discussed in Section 3.4, buoyancy forces will lead to vertical oscillations of fluid parcels lifted from their equilibrium position z_0. In Fig. 5.12, the parcel is oscillating up and down but at the same time is moving horizontally with the wind. The parcel trajectory will thus follow a sine-wave in the horizontal direction. If the forcing at position x_0 acts on the all fluid parcels moving originally at the height $z = z_0$, the result will be a stationary sine-wave as shown in Fig. 5.12. As only buoyancy forces are acting in this flow situation, the wave is indeed formed due to buoyancy as is often assumed for the formation of mountain lee waves. But in the situation sketched in Fig. 5.12, the parcels moving horizontally at their initial height z_0 do not interact among each other or with fluid parcels located above or below. In reality however, all fluid parcels in the x-z-plane will be affected by the forcing at position x_0 and the resulting gravity wave will be the result of buoyancy forces and pressure forces acting in the horizontal and vertical direction in order to fulfill the continuity principle outlined in Section 2.6.

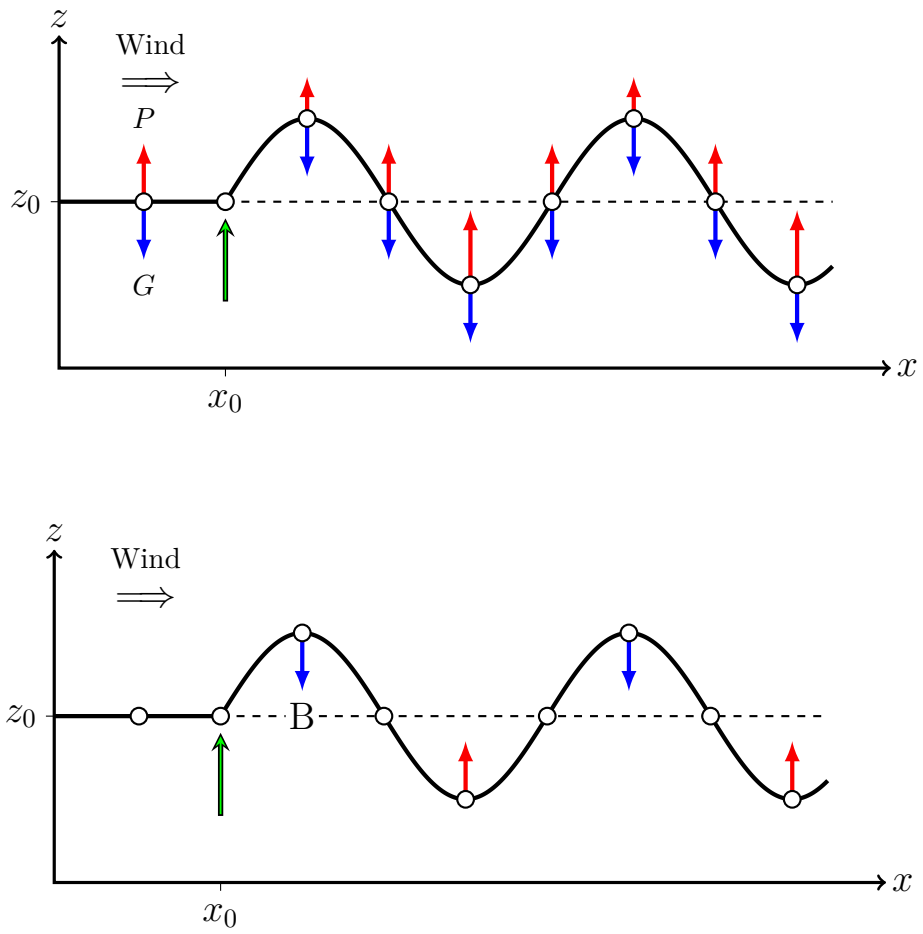

Fig. 5.12: Sketch of the forces acting on a fluid parcel (indicated by a circle) in a stably stratified fluid while moving in the horizontal direction. The parcel is pushed upward at position $x = x_0$ (green arrow). The trajectory of the parcel is indicated by the black line. Upper part: G = gravity force, P = hydrostatic pressure force. Lower part: B = buoyancy force.

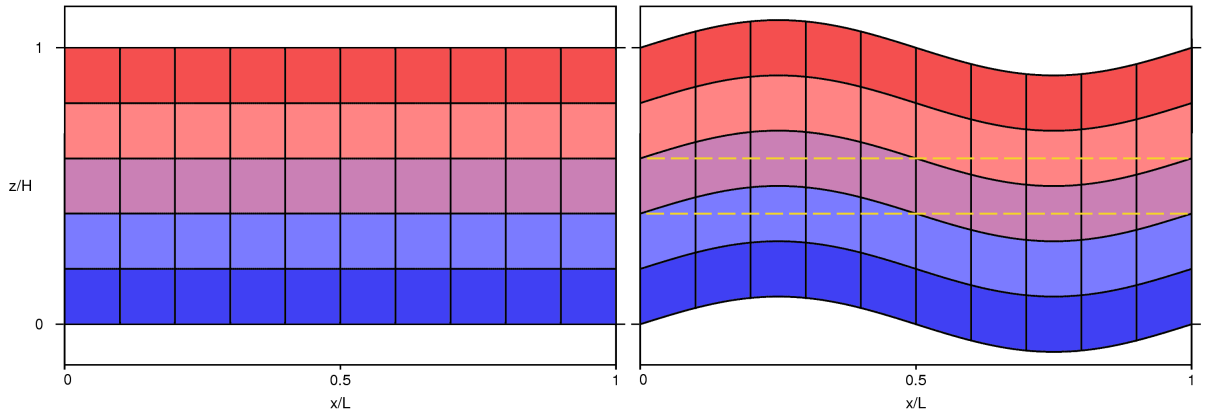

Fig. 5.13: Location of fluid parcels in a stably stratified fluid. Blue colors: heavy fluid parcels, red colors: light fluid parcels. Left: fluid at rest. Right: instantaneous situation in a free gravity wave with vertical phase lines as described in Section 5.1. Dashed yellow lines: location of fluid parcels in the middle layer at rest.

This situation is shown in Fig. 5.13, where the displacement of all fluid parcels from their initial equilibrium due to a gravity wave is sketched. Hence, although buoyancy forces are the main source of gravity wave formation, the interaction of all fluid parcels in the wave has to be due to pressure forces as will be shown in the examples described below.

(b) Free gravity waves in an unbounded domain

As presented in Section 5.1, the solutions for the pressure field (eq. 5.4) show that lines of constant pressure are oriented parallel with the phase lines. Hence, the total pressure force P (the sum of P_x and P_z) is acting at right angles to the phase lines. The buoyancy force B is always acting in the vertical direction but can change sign depending on the location of a fluid particle with respect to its equilibrium position where $B = 0$. As outlined in Section 5.1, fluid particles in this kind of gravity wave move along straight lines slanted backward with respect to the vertical coordinate z (see Fig. 5.4) with the forces acting on a fluid particle during its motion sketched in Fig. 5.14 . Without pressure forces, the particle would move only in the vertical direction due to buoyancy forces. Hence, in order to move along the inclined phase line, pressure forces must also push the particle in the horizontal direction as sketched in Fig. 5.14 . The magnitude of the pressure force P can be related to the magnitude of the buoyancy force B by $P \sim B \sin(\alpha)$. Hence, P is always less than B and vanishes for the case of $\alpha = 0$ (vertical phase lines).

(c) Free gravity waves in a bounded domain

This type of gravity wave has been discussed in Section 5.3 and might be regarded as the other extreme to the gravity waves in an unbounded domain discussed in Section 5.1 and in part (b) above, as the fluid is now bounded by solid surfaces at $z/H = 0$ and 1 as is shown in Fig. 5.15. These waves have been observed in laboratory experiments and have some similarities

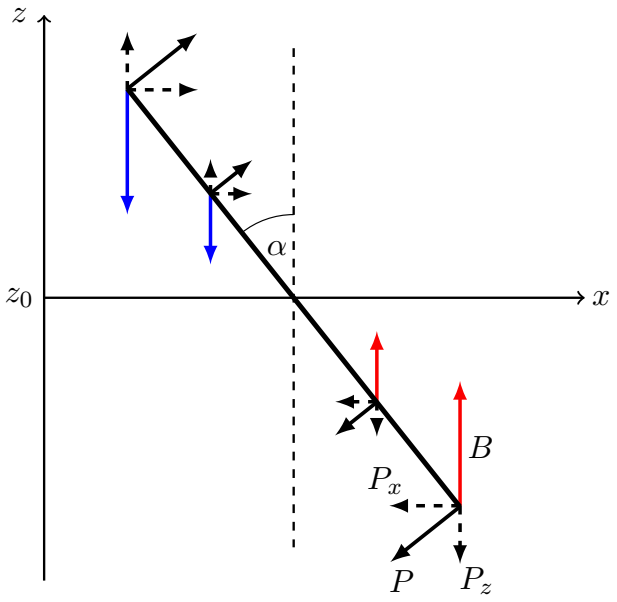

Fig. 5.14: Sketch of the forces acting on a fluid particle in an internal gravity wave. The particle is moving along the straight line inclined at an angle α to the vertical direction (dashed line). B: buoyancy force, red or blue arrows, P: pressure force, black arrows. The horizontal and vertical components of the pressure force, P_x and P_z are indicated by dashed arrows. Red: particle warmer than environment, blue: particle colder than environment.

with trapped gravity waves like mountain lee waves (see Chapter 7). The wave fields of potential temperature $\theta(x, z, t)$ and pressure $p(x, z, t)$ are provided by equations 5.23 and 5.26. The fields of buoyancy and pressure forces can be obtained from these by equations (5.37 - 5.39). For an instantaneous time $t = t_0$, the field of total potential temperature (base state $\Theta(z)$ + wave field $\theta(x, z, t_0)$) is shown in Fig. 5.15 and the corresponding fields of buoyancy and pressure forces are shown in Fig. 5.16.

By comparing the top and middle parts of Fig. 5.16, it can be seen that buoyancy and vertical pressure forces are exactly in phase but of opposite sign. Concerning the magnitude of both forces, it can be shown that for the special wave configuration discussed here, the buoyancy force B is always larger than the vertical pressure force P_z. Hence, the net vertical force has the direction of buoyancy force but is less than the buoyancy force alone. This is different from the simple case discussed in (a), where buoyancy is the only force acting on the air parcel (see Fig. 5.12). The relative magnitude of both forces shown in Fig. 5.16 is given by $B/P_z = 1+4(H/L)^2$. When the horizontal wavelength L is much larger than the vertical extent H, we have $B \approx P_z$ which means that the vertical pressure force is approximately in hydrostatic balance with the buoyancy force and the wave motion is mainly driven by horizontal pressure forces P_x (see also Section 5.7). In the opposite case, $L \ll H$, the vertical pressure force P_z is much smaller than the buoyancy force and the gravity wave is mainly driven by buoyancy forces acting in the vertical direction. In any case, pressure forces do not vanish completely as with the simple parcel argument provided in Section (a), but modify the buoyancy forces and are responsible for horizontal motion in gravity waves as manifested in the elliptical shape of particle trajectories shown in Figs. 5.6 and 5.8.

In summary, the interaction of buoyancy and pressure forces for this kind of gravity wave is much more complex than for the cases shown in Figs. 5.12 and 5.14. Also, one has to consider

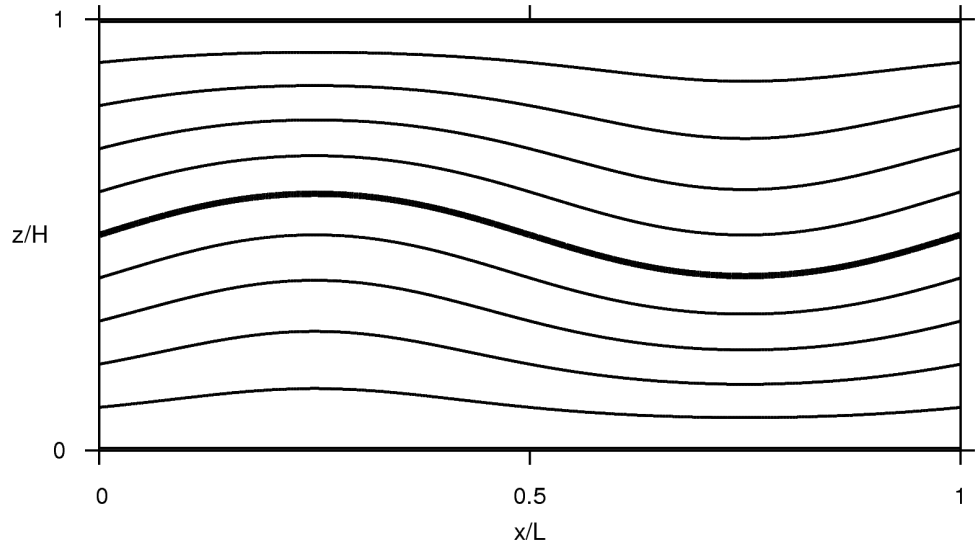

Fig. 5.15: Field of potential temperature (base state $\Theta(z)$ + wave field $\theta(x, z, t_0)$) for a an instantaneous time $t = t_0$ for a bounded gravity wave discussed in Section 5.3. The fluid layer with maximum amplitude is indicated by the thick line. The wave field is shown for one wavelength L. The height of the fluid layer is given by H.

that only a snapshot of a moving gravity wave is presented in Figs. 5.15 and 5.16 since forces are changing in magnitude, direction and time which makes it nearly impossible to draw a simple picture of the mechanisms driving gravity waves.

5.7 Gravity waves driven by hydrostatic pressure forces

The discussion of forces acting on internal gravity waves provided in the previous sections has shown that there is a complex interaction between buoyancy forces, acting always in the vertical direction and pressure forces acting in the horizontal and vertical directions. We take the last example of bounded gravity waves as an opportunity to discuss the nature of pressure forces in these type of waves. As defined in Sections 2.4 and 2.5, pressure can be divided into a hydrostatic part (say p_h) due to the fluid column weight and a dynamic part (say p_d) due to accelerations and decelerations of fluid particles in the wave field (Bernoulli's equation). This is of course somewhat artificial as instruments to measure pressure cannot distinguish between these parts a priori.

Through mathematical analysis of the gravity wave problem, it has turned out that gravity waves with horizontal wavelengths larger than their vertical extent (say the height of the troposphere, $H \approx 10\,\mathrm{km}$) are mainly driven by horizontal gradients of hydrostatic pressure (see Nappo (2012) and Sutherland (2010) for detailed discussions). These waves with wavelength larger than about 30 km are then termed *hydrostatic gravity waves* and they occur mainly over large mountain ranges like the rocky mountains or the Andes as will be discussed in Section 7.2.

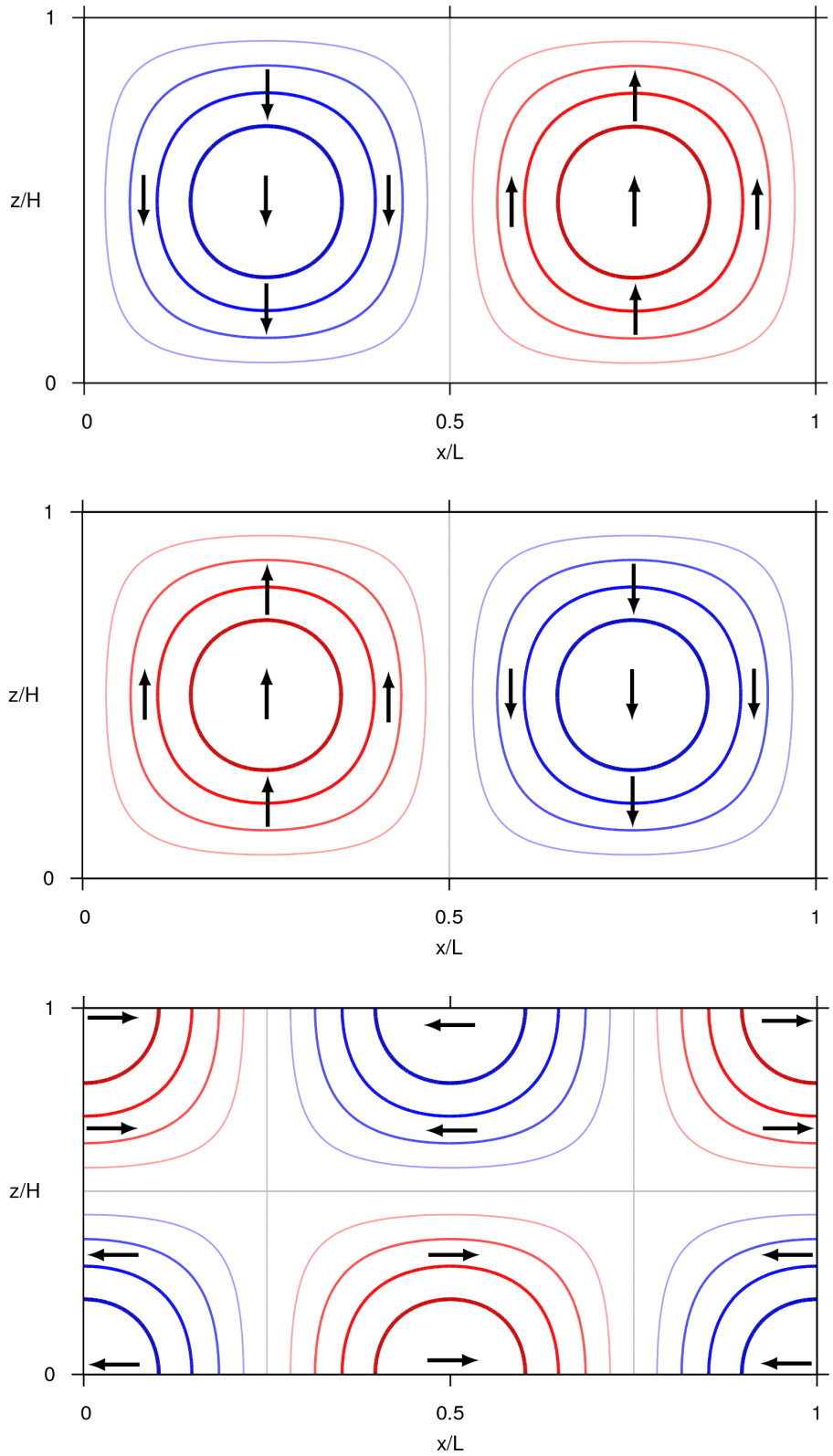

Fig. 5.16: Instantaneous fields of forces acting on the gravity wave shown in Fig. 5.15. Top: buoyancy force B; middle: vertical pressure force P_z; bottom: horizontal pressure force P_x. The non-dimensional magnitude of forces are indicated by the variable thickness of isolines: thick lines: strong, thin lines: weak. The direction in which forces are acting are indicated by arrows and the color code of isolines.

In contrast, gravity waves with smaller wavelengths discussed in Sections 5.1 – 5.3 are usually believed to be mainly forced by buoyancy forces. But here we may ask if this is really the case? The reason for this question comes from the limitation that Archimedes' principle and the related buoyancy force, as discussed in detail in Chapter 3, are defined for a single fluid particle not interacting with the surrounding fluid. This is rather idealized because the oscillating particle will interact with its environment by dynamic pressure forces. In fact, if a solid obstacle (say a sphere or cylinder) is shifted up and down periodically in a stratified fluid, it triggers gravity waves in the environment (examples can be found in Sutherland, 2010).

The hydrostatic pressure law has been introduced in Sections 2.4 and 3.2 and is repeated here for convenience:

$$\frac{dp_\mathrm{h}}{dz} = -g\rho. \tag{5.44}$$

It is strictly valid for a fluid at rest where no horizontal and vertical motion is present. In this case, the fluid density ρ can vary only in the vertical direction: $\rho = \rho(z)$. The resulting hydrostatic pressure $p_\mathrm{h}(z)$ can be obtained from (5.44) by integration:

$$p_\mathrm{h}(z) = p_\mathrm{h}(z=0) - \int g\rho\, dz, \tag{5.45}$$

where $p_\mathrm{h}(z=0)$ is the pressure at the ground.

This law is also valid for fluids in motion where the vertical accelerations and velocities are small compared with their horizontal counterparts. In this case, the density ρ and pressure p_h can also be a function of the horizontal coordinate x, i.e. $\rho(x,z)$ and $p_\mathrm{h}(x,z)$. As the horizontal pressure force P_x is related to the horizontal variation of pressure given in (5.38), horizontal variations in the hydrostatic p_h will lead to horizontal motion according to Newton's law (equation 2.11). In fact, all large scale atmospheric motion (e.g., the wind in cyclones and anticyclones) are driven by hydrostatic pressure forces.

The horizontal pressure gradient and hence the horizontal pressure force can be related to the density field $\rho(x,z)$ using the hydrostatic pressure law by

$$\frac{dp_\mathrm{h}(x,z)}{dx} \sim g \int \frac{d\rho(x,z)}{dx}\, dz, \tag{5.46}$$

which shows that horizontal variations in fluid density will lead to horizontal motion as illustrated by a simple example provided in Figure 5.17 where three columns of fluids with densities ρ_1 and ρ_2 ($\rho_1 < \rho_2$) are separated by vertical walls. The hydrostatic pressure in each volume is obtained from (5.45) as $p_\mathrm{h}(z) = g\rho(h-z)$. Hence, the pressure in the column with density ρ_2 will be always larger than in the columns with density ρ_1. If we remove the walls between the fluid layers at some time $t = 0$, the instantaneous hydrostatic pressure forces, as indicated by arrows in Fig. 5.17, will lead to horizontal motion in the same direction. As the fluid is contained in a box, it cannot escape and some vertical motion has to be induced by dynamic pressure forces in order to fulfill the continuity principle (see Sections 2.5 and 2.6). Possible later stages of the situation are sketched in the lower part of Fig. 5.17. In principle, this simple configuration can

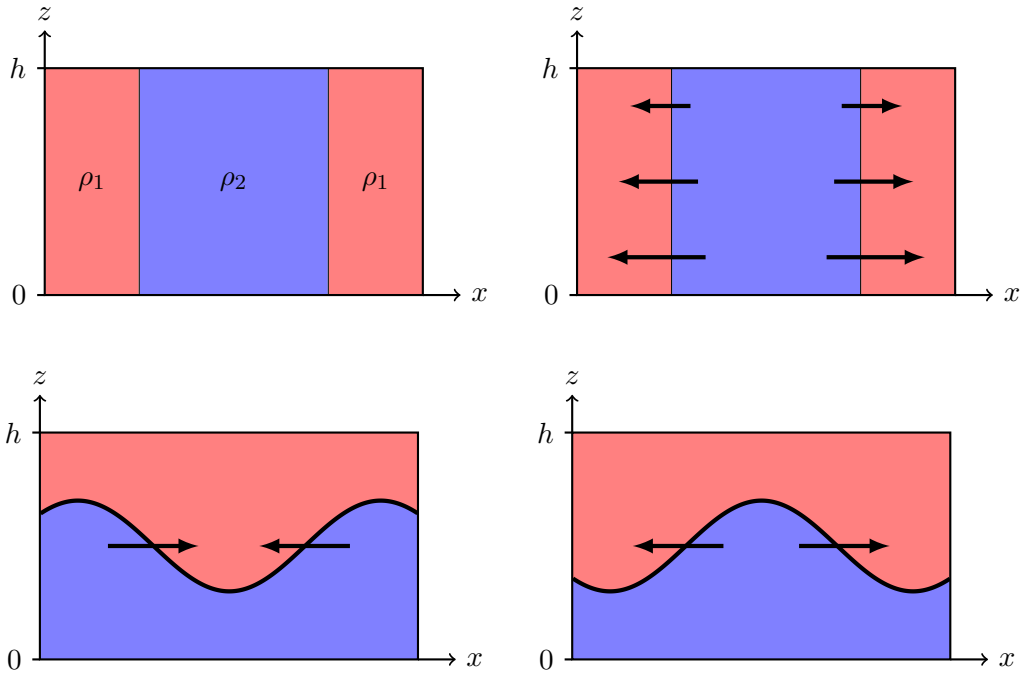

Fig. 5.17: Development of a two layer fluid with densities ρ_2 (heavy fluid, blue) and ρ_1 (light fluid, red) initially separated by vertical sidewalls (upper left). The hydrostatic pressure forces after the removal of the walls are indicated by arrows in the upper right. Later possible stages of fluid motion are shown in the lower part of the figure.

lead to standing waves at the interface of the two fluid layers. In practice however, frictional forces come into play and the final state will be a two layer configuration with the lighter fluid (ρ_1) located above the heavier fluid (ρ_2), so that finally the fluid becomes stably stratified.

The arguments presented above for flows driven by hydrostatic pressure forces can also be used to explain gravity waves. As was discussed in Section 5.6 (c), buoyancy forces and vertical pressure forces are in near hydrostatic balance for waves with wavelength L much larger than the vertical extent H of the wave field. In this case, the horizontal pressure forces are mainly due to hydrostatic pressure gradients and vertical waves, which are then usually weak and have to be driven by dynamic pressure forces.

For $L \sim H$ where the buoyancy force is larger than the vertical pressure force (see Section 5.6 (c)), vertical wave motion is driven by the sum of these forces and one can split the pressure into a hydrostatic part p_h and a dynamic part p_d. Here, the hydrostatic part is in balance with the buoyancy force and hence cannot drive vertical wave motion. Wave motion would instead have to be driven by pressure forces due to vertical gradients of dynamic pressure p_d, which would then of course show a different distribution to that in Fig. 5.16. However, vertical wave motion does not have to be small as for the pure hydrostatic case but may be of the same magnitude as the horizontal wave motion.

Formally, the equations for fluid accelerations in this interpretation of forces driving gravity waves are described by

$$\frac{du}{dt} = P_{\mathrm{h}x} + P_{\mathrm{d}x} \tag{5.47}$$

and

$$\frac{dw}{dt} = P_{\mathrm{d}z}, \tag{5.48}$$

where $P_{\mathrm{h}x}$ is the horizontal hydrostatic pressure force and $P_{\mathrm{d}x}$ and $P_{\mathrm{d}z}$ are the horizontal and vertical dynamic pressure forces, respectively. This has to be compared with the buoyancy view of wave forces given by equations 5.42 and 5.44. In any case, the resulting wave forms have to be the same (e.g., as provided in Section 5.3), with the difference being in the physical interpretation of the buoyancy force versus the hydrostatic pressure force as the main driving force for gravity waves.

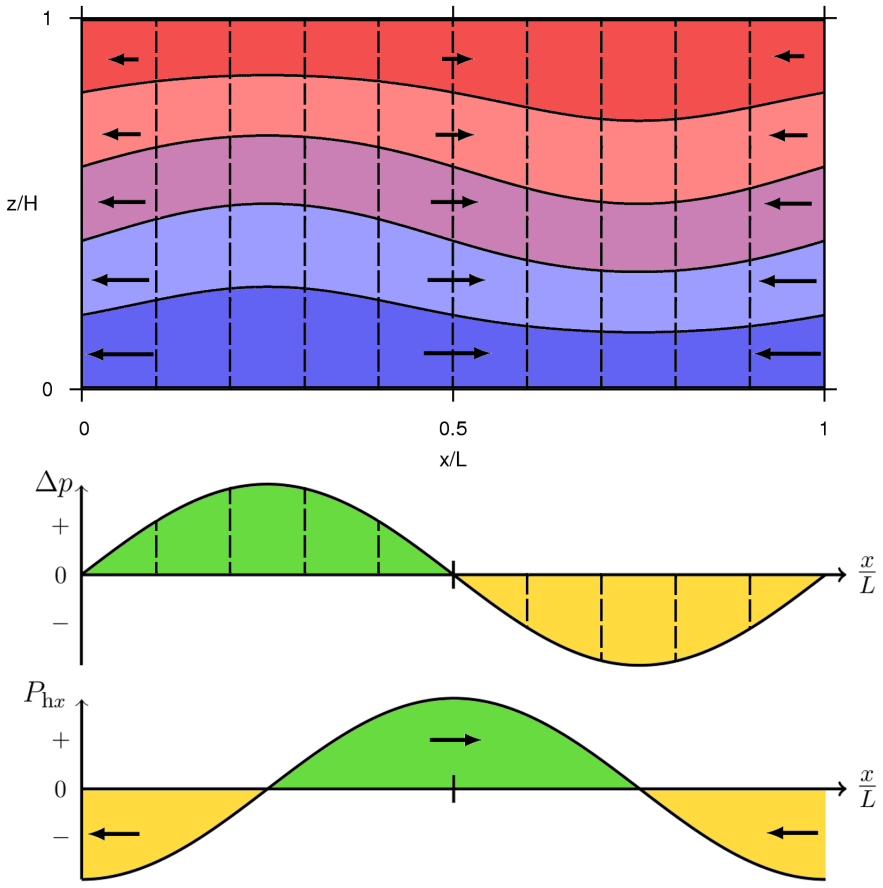

Fig. 5.18: Hydrostatic pressure forces acting in the gravity wave shown in Fig. 5.15. Top: strength and direction of pressure forces as indicated by arrows at some locations in the wave. The vertical dashed lines indicate columns with fluid parts of different density (blue: dense, red: less dense). Middle: hydrostatic pressure variations Δp at the surface ($z = 0$) as induced by the wave. Bottom: variation of the hydrostatic pressure force $P_{\mathrm{h}x}$ at the surface. Arrows indicate the direction of forces.

This aspect is illustrated in Fig. 5.18, where the hydrostatic parts of pressure are sketched for the wave discussed in Section 5.6c. The variation of hydrostatic pressure at the surface ($z = 0$) has been obtained by integration of the hydrostatic pressure law (eq. 5.45) over the fluid columns indicated by vertical dashed lines. The pressure deviation from the situation in the fluid at rest p_0 (see Fig. 5.13, top), $\Delta p = p(x) - p_0$, as induced by the gravity wave is shown in the middle part of Fig. 5.18. The high surface pressure to the left is due to the denser fluid (blue) in the fluid columns compared with the state at rest. The low surface pressure to the right is caused by lighter fluid (red) in the fluid columns. The resulting hydrostatic pressure force at the surface ($z = 0$) as obtained from eq. 5.46 is shown in the bottom of Fig. 5.18. The vertical variation of horizontal hydrostatic pressure forces $P_{\mathrm{h}x}$ in the wave is indicated at some locations by arrows. As hydrostatic pressure forces are acting only in the horizontal direction, vertical wave motion has to be induced by dynamic pressure forces P_{d} (not shown here) according to eq. 5.48.

6 Gravity waves forced by topography

6.1 The Scorer parameter

We now treat the case where gravity waves in the atmosphere are triggered by the topography of the earth's surface as discussed in Section 5.5. We assume that the background stratification and the oncoming wind speed do not change with time, hence the wave forcing is stationary. In practice, this means that the wave crests and the related updraft and downdraft areas as induced by the topography are fixed in space and time. This is the perfect situation for soaring flight, as the lift sources are known to the glider pilots once they are provided with a good wave forecast (see also Section 8). Before we come to the case of waves behind single mountain ridges, we first treat the seemingly academic case of periodic topography as sketched in Figure 6.1. Nonetheless, this case permits simple analytic solutions of the wave equations, allowing some discussion of the physical mechanism of mountain waves.

In order to calculate the wave forms triggered by periodic ridges from the wave equations as given in the appendix, one has to provide the vertical profiles of the atmospheric stability in terms of the Brunt-Vaisala frequency $N(z)$ and the wind speed $U(z)$. We have already assumed that the mountains are two-dimensional so that wind direction is always perpendicular to the mountain crests. In fact, these parameters appear as N/U within the wave equations (see appendix AII), leading to the so-called Scorer-parameter after the British mathematician and glider pilot R. S. Scorer and is denoted by S here:

$$S = \frac{N}{U} \qquad \text{(Scorer parameter).} \tag{6.1}$$

This parameter is essential in determining the wave behavior for stratified flow over orography as will be discussed in the following chapters. We may note that the Scorer parameter is mostly called "l" in the literature, but we will keep the notation S here. Also, the full Scorer parameter includes an additional term for curvature of the velocity profile which is usually neglected in practical applications. The Scorer parameter has the dimensions of an inverse length (1/m) or, in terms of wave physics, of a wave number. Hence, one can assign a wavelength to S defined by

$$L_\mathrm{s} = \frac{2\pi}{S} = \frac{2\pi U}{N} \qquad \text{(Scorer length).} \tag{6.2}$$

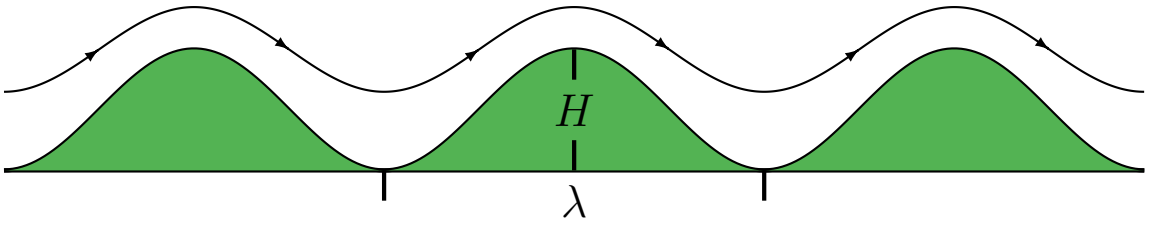

Fig. 6.1: Schematic of periodic terrain with height H and wavelength λ forcing gravity waves in the atmosphere above. The flow near the surface is indicated by the thin line.

Tab. 6.1: The Scorer length $\boldsymbol{L_s}$ in km for different combinations of wind speed U and temperature gradients, dT/dz and $d\theta/dz$. Note that the Scorer length can be also taken as an estimate for the wavelength of mountain lee waves.

dT/dz	$d\theta/dz$	U (m/s)		
(K/100 m)	(K/100 m)	10	20	30
- 0.65	0.35	**6.3**	**12.6**	**18.9**
0.0	1.0	**3.5**	**7.0**	**10.5**
2.0	3.0	**2.0**	**4.0**	**6.0**

As can be seen from this definition, the Scorer length corresponds to the wavelength of stationary gravity waves with intrinsic frequency $\omega = N$ in an airflow with constant wind speed U as shown in Section 5.4. Some values for the Scorer length as a function of wind speed U and temperature gradient dT/dz are given in Table 6.1. We will use the Scorer length in the following discussion of wave solutions for flow over periodic topography.

As sketched in Figure 6.1, the earth's surface is described by a periodic topography, $h(x)$ as

$$h(x) = h_0 \sin\left(\frac{2\pi}{\lambda}x\right), \tag{6.3}$$

where λ is the wavelength of the periodic "mountains" and $h_0 = H/2$. Before we present some solutions of the wave equations for a stably stratified flow over this specific lower boundary, we analyze the behavior of air parcels following the terrain surface. The time needed for an air parcel to move over one wavelength of the periodic surface is given by

$$\tau_\mathrm{f} = \frac{\lambda}{U} \qquad \text{(forcing time scale)} \tag{6.4}$$

which can be also expressed by a frequency

$$\omega_\mathrm{f} = \frac{2\pi}{\tau_\mathrm{f}} = \frac{2\pi U}{\lambda} \qquad \text{(forcing frequency)}. \tag{6.5}$$

As the parcel is following the surface terrain, it also moves up and down during this time. Hence, it is performing a forced vertical oscillation with period τ_f or frequency ω_f. This has to be compared with the "natural" oscillation frequency N or period $\tau_\mathrm{n} = 2\pi/N$ of air parcels in a stably stratified fluid. These frequencies can also be related to the mountain width λ and Scorer length L_s by

$$\frac{\omega_\mathrm{f}}{N} = \frac{L_\mathrm{s}}{\lambda}. \tag{6.6}$$

We will make use of this relation for the physical interpretation of the results given in the following section.

6.2 Gravity waves induced by periodic terrain

We consider the flow over a topography consisting of periodic ridges and troughs as sketched in Figure 6.1 and is described formally by a wave as given above. For simplicity, we assume that

stratification N and wind speed U are constant with height, hence also the Scorer parameter $S = N/U$ is constant. For this simple setup, analytical solutions for the wave equation (see appendix) are possible and can be found, e.g., in the monographs by Nappo (2012) and Sutherland (2010) or in the review article by Durran (1990). Here we will only present the final results.

The problem is characterized by two length scales, the wavelength of the topography λ and the Scorer length scale $L_s = 2\pi/S$ as defined in the previous section. It has been found that the possible waveforms from periodic surface forcing depend on the difference between these length scales. The corresponding wave solutions for the vertical velocity w are given for the cases $L_s \leq \lambda$ (a) and $L_s \geq \lambda$ (b) below.

$$\text{(a):} \quad L_s \leq \lambda \quad (\omega_f \leq N) \qquad \text{vertically propagating waves} \tag{6.7}$$

$$w(x, y) = w_0 \cos\left(\frac{2\pi x}{\lambda} + \mu z\right) \tag{6.8}$$

The wave amplitude at all heights corresponds to the amplitude forced at the periodic surface given by $w_0 = U 2\pi h_0/\lambda$, but the phase lines are tilted backward in the vertical by the phase μz, where μ is related to the Scorer length and the mountain length by $\mu = \sqrt{|k^2 - S^2|}$ with $k = 2\pi/\lambda$ and $S = 2\pi/L_s$.

The vertical velocity field and the resulting streamlines including the mean wind U, which can be also interpreted as lines of constant potential temperature, are shown in Figure 6.2. The

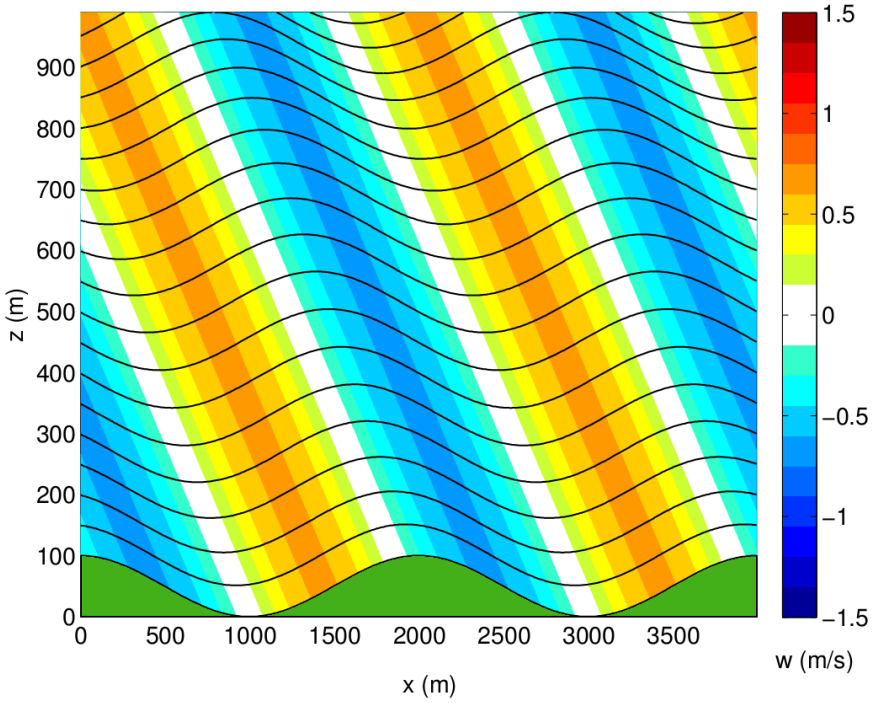

Fig. 6.2: Streamlines and field of vertical velocity (colored) for stratified flow over periodic terrain with wavelength λ for the case of constant Scorer length L_s. Propagating waves: $L_s \leq \lambda$. The wind U is directed from left to right.

waves extend without damping throughout the whole atmosphere and the phase lines are tilted backward against the oncoming wind U.

In this case, the forcing frequency ω_f of the parcel motion on the terrain surface is less than the natural frequency N of the stratified fluid. Hence, according to the results presented in Section 5.1, the phase lines should be tilted with an angle of α to the vertical, where α is determined by $\cos(\alpha) = \omega_f/N$. In fact, the solutions for forced gravity waves over periodic terrain correspond to the time dependent solutions of free gravity waves presented in Section 5.1.

$$\text{(b):} \qquad L_s \geq \lambda \quad (\omega_f \geq N) \qquad \text{vertically damped waves} \tag{6.9}$$

In this case, the solution is

$$w(x,z) = w_0(z) \cos\left(\frac{2\pi x}{\lambda}\right). \tag{6.10}$$

The wave amplitude is now variable with height, but the phase lines are oriented in the vertical. The amplitude $w_0(z)$ has its maximum value w_m at the surface and decays with height according to

$$w_0(z) = w_m \exp(-\mu z), \tag{6.11}$$

where the resulting streamlines are shown in Figure 6.3. The wave damping in the vertical direction is due to the fact that now the wave forcing frequency ω_f is larger than N. But as has been shown in Section 5.1, a stratified fluid cannot support vertical oscillations with frequencies larger than the Brunt-Vaisala frequency N.

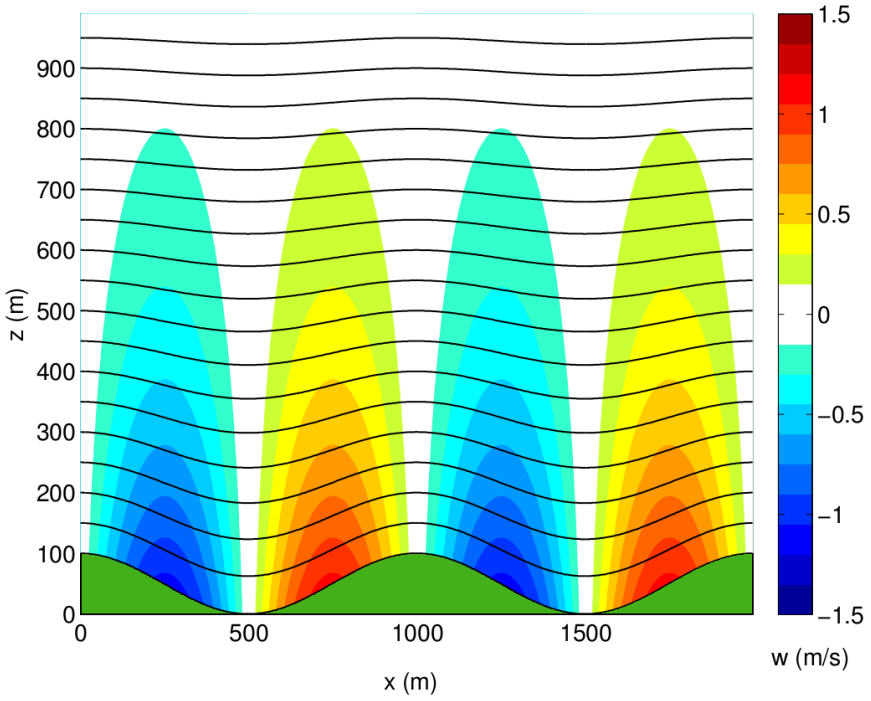

Fig. 6.3: As in Figure 6.2 but for damped gravity waves: $L_s \geq \lambda$.

6.3 Scorer parameter variable with height

The results in Section 6.2 showed the importance of the Scorer parameter (or the Scorer length) with respect to wave properties in a forced stratified flow even in the simple case of constant N and U. In the atmosphere however, the Brunt-Vaisala frequency and wind speed are usually varying with height, which leads also to a height dependent Scorer parameter $S(z)$. The effect of a variable Scorer parameter will be demonstrated by the following example.

In Figure 6.2, we have presented results for a flow over periodic surface where the Scorer length L_s is constant with height and smaller than the surface length λ (case a). For the specific case presented here, $\lambda = 2000\,\mathrm{m}$ and $L_s = 1700\,\mathrm{m}$. In a second case, we keep the Scorer parameter constant for the first 200 m with a sharp decrease to half of its value up to 500 m and constant above this level. This is achieved by a corresponding increase in wind speed $U(z)$. By this we have for the Scorer length scale: $L_s \leq \lambda$ for $z \leq 300\,\mathrm{m}$ and $L_s \geq \lambda$ for $z \geq 300\,\mathrm{m}$. The resulting streamlines and vertical velocities are shown in Figure 6.4. Here, the phase lines are oriented in the vertical and the wave amplitude is damped with increasing height as in case (b) in Section 6.2 (see Figure 6.3). The difference with this case is that the forcing frequency ω_f is smaller than the Brunt-Vaisala frequency N, thus permitting vertically propagating waves as in Figure 6.2. The resulting wave frequency now increases with height due to the increase in wind speed. Above the level where $L_s = \lambda$, this results in $\omega \geq N$ so that gravity waves can no longer be supported by the surface forcing. These kinds of gravity waves are called "trapped" gravity waves which will be discussed in the context on mountain lee waves in the next chapter.

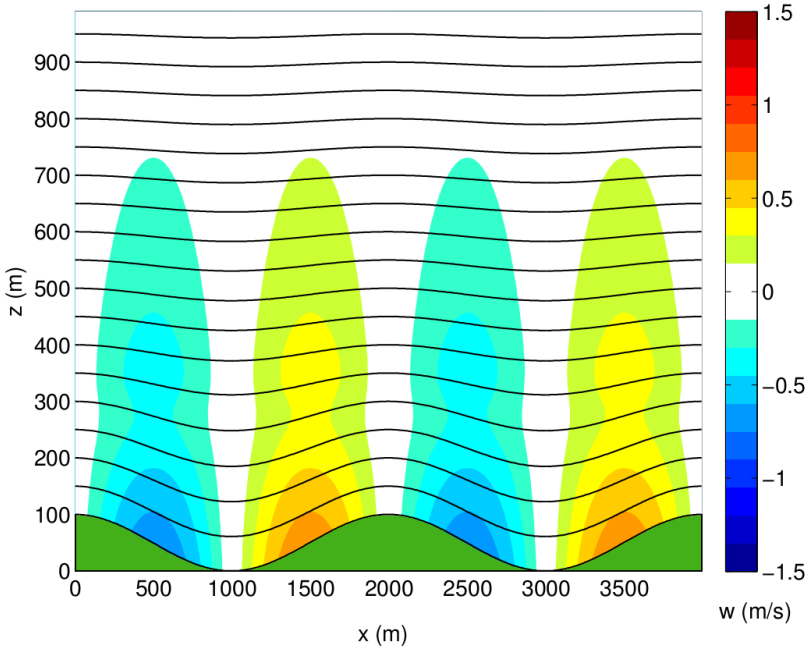

Fig. 6.4: As in Figure 6.2 but for trapped gravity waves. The Scorer length increases with height: $z \leq 300\,\mathrm{m}$: $L_s \leq \lambda$, $z \geq 300\,\mathrm{m}$: $L_s \geq \lambda$.

7 Mountain waves

7.1 Some general aspects

In the last chapter, we examined the more or less academic case of atmospheric gravity waves triggered by periodic surface topography. The reason was that some simple solutions of the wave equations can be found for this setup and the importance of the Scorer parameter $S = N/U$ for wave development could be shown. Real topography is of course not so simple, although some periodic terrain features can be found, e.g., in the form of longitudinal sand dunes. Mountain landscapes usually consist of several ridges of different horizontal sizes and heights that are not necessarily aligned parallel with respect to their crests. But even then, gravity waves can be organized in more or less a two-dimensional fashion perpendicular to the wind direction as shown in the satellite picture of the Adriatic Sea in Figure 7.1. These quasi two-dimensional mountain waves are ideal for wave soaring and will hence be the focus of this chapter. We might mention that gravity waves are also triggered by isolated three-dimensional mountains like vulcanoes or islands as shown in Figure 7.2 for the South Sandwich Islands in the Southern Atlantic.

To predict whether gravity waves will be triggered by a certain topography is not simple and can only be done by numerical models of the full nonlinear equations for atmospheric wave motion. Examples of those predictions are given in the next chapter. Here, we will only treat isolated two-dimensional mountain ridges, which are also rare in natural landscapes. Gravity waves triggered by these obstacles have been treated in a more mathematical fashion by Sutherland (2010) or Durran (1990, 2003). Some more popular treatments are provided by Whiteman (2000) and Barry (2008) and with application to soaring flight by Hertenstein (2011) and Mar-

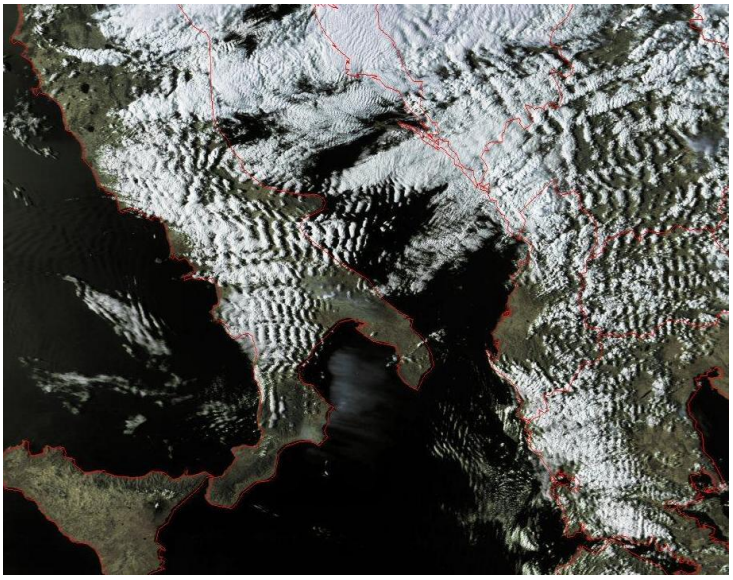

Fig. 7.1: Satellite picture of atmospheric cloud structures induced by gravity waves over Southern Italy and Serbia.
Source: NASA Visible Earth

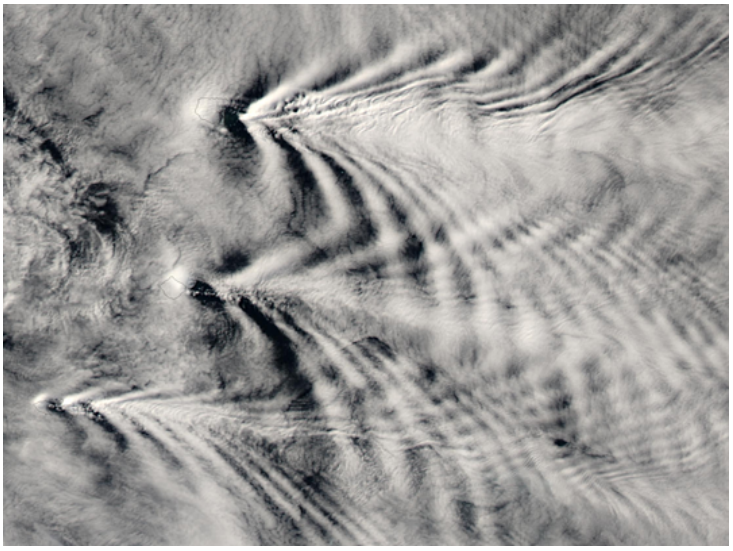

Fig. 7.2: Satellite picture of cloud structures over the South Sandwich Islands induced by three-dimensional gravity waves. These cloud forms are also called ship waves due to their similarity with surface water waves formed behind moving ships.
Source: NASA Modis Rapid Response Team

tinez (2012). To determine whether gravity waves will be formed in the lee of isolated mountain ridges depends on various factors as shown in Figure 7.3: the length λ, altitude H, the wind speed $U(z)$ and the temperature $T(z)$.

Due to these various factors, conducting laboratory experiments on the isolated mountain wave problem was quite popular in the early days of wave research (see, e.g., the monograph by Baines, 1995). An example of this kind of experiment is shown in Figure 7.4. The most simple way is to tow an obstacle (the red half cylinder in the figure) in a stratified fluid which is usually formed by layers of salt water of different density (colored in the figure). Although this arrangement is rather idealized, many features of mountain waves can be identified in laboratory experiments (see Baines, 1995). The interpretation of the experiment shown in Figure 7.4 in

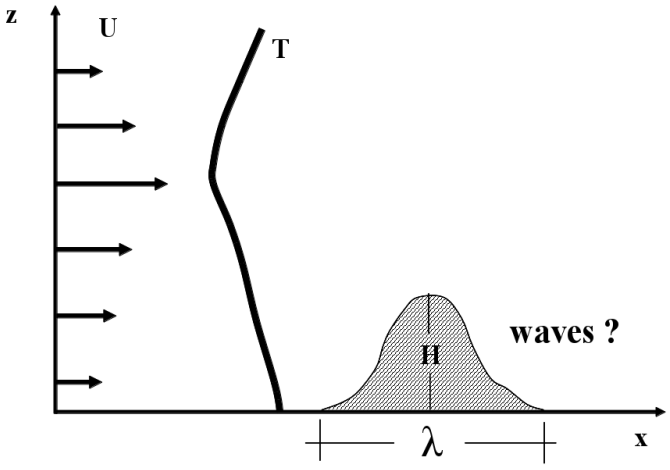

Fig. 7.3: Schematic setup for the problem of mountain waves. $U(z)$: vertical wind profile, $T(z)$: vertical temperature profile. λ: mountain width, H: mountain height.

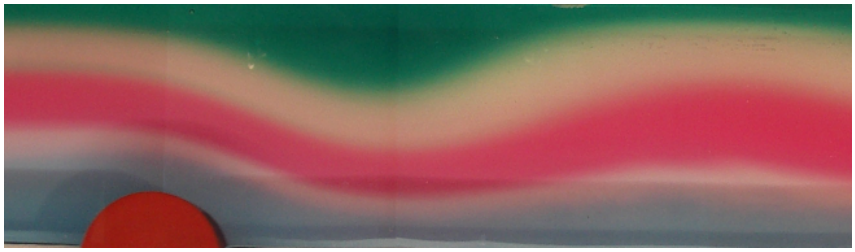

Fig. 7.4: Laboratory experiment on gravity waves in stratified flows over isolated obstacles. The obstacle (red) is towed from right to left through the stratified fluid (colored layers of salt water).

terms of atmospheric flow is given schematically in Figure 7.5. The isolated mountain induces gravity waves on the leeward side which extend horizontally and vertically. The phase lines (amplitude maxima) are tilted against the oncoming wind similar to the case of propagating gravity waves for flow over periodic terrain (see Section 6.2).

7.2 Vertically propagating mountain waves

In Section 6.2 on waves over periodic terrain, we discussed the case $L_s < \lambda$, where λ was the wavelength of the sinusoidal surface. In that case, the solutions of the wave equations gave vertically propagating waves with backward tilting phase lines (see Fig. 6.2). For single mountains, the base diameter of the mountain is denoted by λ in Fig. 7.3. In this section, we discuss the case $L_s < \lambda$. From Tab. 6.1, one can see that this condition will be found for larger mountain ranges like the Andes, the Alps or the Sierra Nevada. If the Scorer parameter S or the Scorer length L_s does not vary with height, the resulting wave formation is shown schematically in

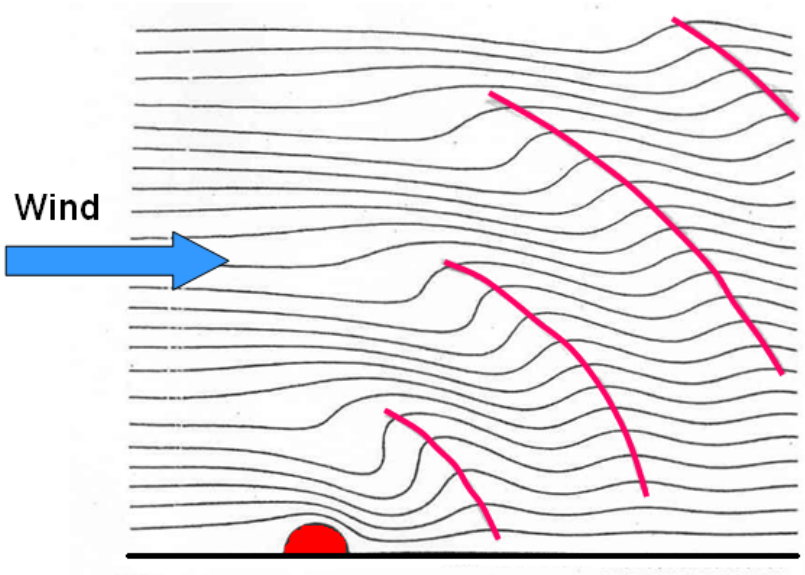

Fig. 7.5: Interpretation of the water tank experiment shown in Figure 7.4 with respect to the flow situation in the atmosphere. Wind is from left to right; air parcels follow the streamlines (black). Phase lines are indicated in red.

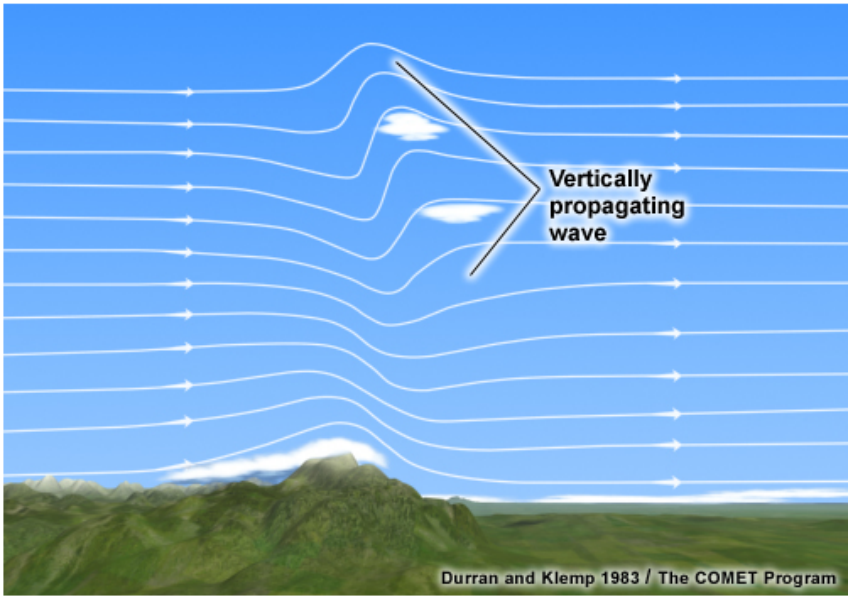

Fig. 7.6: Schematic of vertically propagating gravity waves induced by large mountains.
Source: UCAR/COMET

Figure 7.6. While in most cases only one wave crest is observed over the mountain, this wave can reach the upper troposphere (about 10 km), or even the lower stratosphere (about 15 km). This is just the situation where high altitudes can be reached by sailplanes. In fact, practically all wave flights up to more than 10 km have been performed over large mountain ranges like the Andes, the Alps (European and New Zealand) and the Sierra Nevada.

The structure of vertically propagating gravity waves over a mountain of height $H = 1\,\mathrm{km}$ and length $\lambda = 40\,\mathrm{km}$ as calculated with a linear wave model is shown in Figure 7.7. The areas of positive and negative vertical velocity (lift) are staggered in the vertical which demands a special tactic for wave soaring.

7.3 Trapped mountain waves (lee waves)

Now we consider the case where $L_\mathrm{s} \approx \lambda$, which means that the same length as the expected wavelength is about the mountain width λ. Considering typical values for L_s in Table 6.1, one can see that this condition will be met quite often for medium or small scale mountain areas like in Northern Germany or in the UK. If the Scorer parameter S does not change too much with height, which means that temperature and wind profiles of the oncoming flow vary only little in the vertical, the resulting wave system is similar to the one shown in Figure 7.5. The mountain waves propagate downstream in the vertical and horizontal direction and weaken with distance from the mountain. In most cases however, the wind speed is increasing with height due to general wind behaviour in the free atmosphere. Consequently in these cases, the Scorer parameter decreases with height (the Scorer length increases with height). This situation was already discussed for the case of periodic surface terrain in Section 6.3 (see also Figure 6.4).

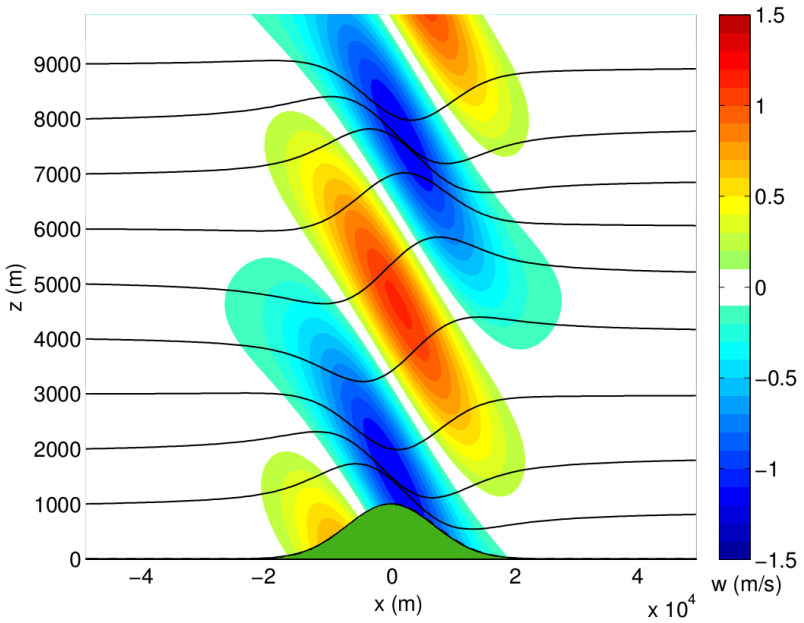

Fig. 7.7: Streamlines (black) and the field of vertical velocity (coloured) for the case $L_s < \lambda$ and Scorer parameter S constant with height as obtained by a linear wave model. The size of the mountain is $H = 1\,\text{km}$ and $\lambda = 40\,\text{km}$. Positive lift: red; negative lift: blue.

For the case of a single mountain, the resulting wave system is shown in Figure 7.8. The waves are now damped in the vertical and reach only altitudes of 6-8 km in practice, but the waves extend now for many wavelengths downstream in the horizontal direction. These waves are called trapped mountain waves or lee waves in the literature. In fact, periodic wave clouds as seen often in satellite pictures like in Figure 7.1 are due to these kinds of trapped gravity waves. The rotors under the wave crests as indicated in the lower layer of Figure 7.8 are treated separately in Section 8.

The structure of trapped gravity waves for a moderately sized mountain with $H = 640\,\text{m}$ and $\lambda = 16\,\text{km}$ as obtained with a linear wave model is shown in Figure 7.9. The resulting lee waves are most favourable for wave soaring over these mountains as the areas of upward velocity (positive lift) extend throughout the depth of the wave system without any vertical inclination.

7.4 Wave properties of interest for soaring flight

Once mountain waves do occur or are forecasted (see Chapter 8), some basic properties of these waves are of interest for glider pilots. These are wavelength, wave amplitude (vertical displacement) and wave lift (vertical velocity). From observations taken during soaring flight and model simulations like those presented in Chapter 8, it has been found that these wave properties depend on the height, width and shape of the mountain and on the vertical wind- and temperature profiles as was sketched already in Figure 7.3. Here, we will give only some simple estimates for the length, amplitude and lift of mountain waves.

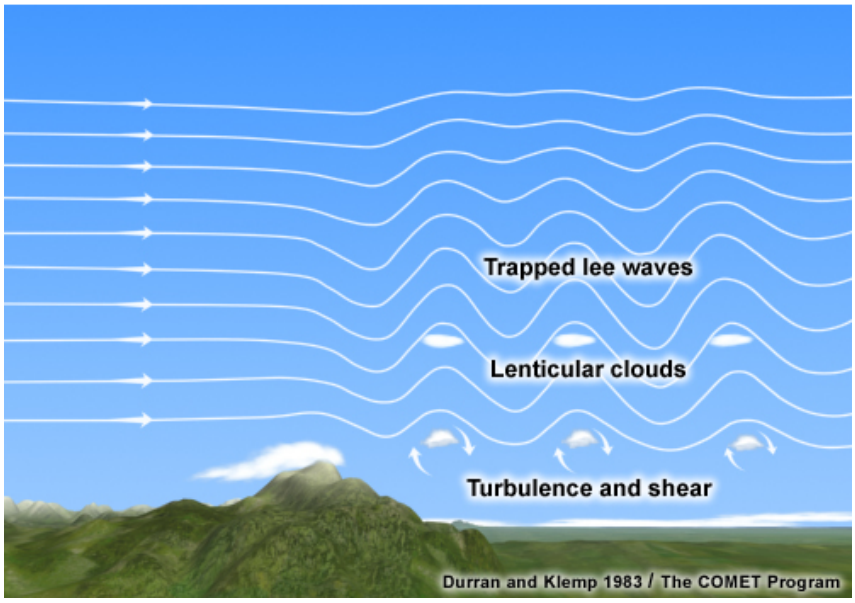

Fig. 7.8: Schematic of trapped mountain waves (lee waves) induced by moderately sized mountains. The lowest layer is characterized by turbulence and wind shear induced by rotors.
Source: UCAR/COMET

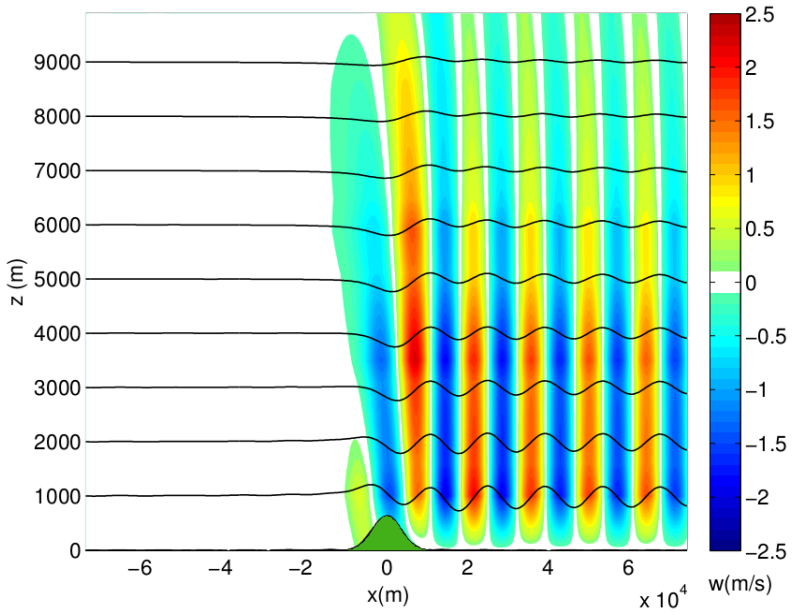

Fig. 7.9: Streamlines and vertical velocity for the case $L_s \approx \lambda$ and Scorer parameter decreasing with height as obtained by a linear wave model. Mountain size is $H = 640\,\mathrm{m}$, $\lambda = 16\,\mathrm{km}$. Coloring for the wave lift as in Figure 7.7.

A. Wavelength

The natural wavelength L of stationary gravity waves like mountain waves is given by the Scorer length L_s as defined by equation 6.2 in Section 6.1. We repeat this relation here for the benefit of further discussion below

$$L = 2\pi \frac{U}{N}, \tag{7.1}$$

where U is the wind speed and N is the Brunt-Vaisala frequency as defined in equation 3.29 in Section 3.5. Typical wavelengths for combinations of U and N were given in Table 6.1, Section 6.1. For the formation of mountain lee waves (see Section 6.3) that are most favorable for wave soaring, the condition is that the Scorer length increases with height. That would mean one would get a smaller wavelength near the mountain top and a larger wavelength in the upper part of the wave system. But as the phase lines of lee waves are not tilted against the vertical direction (see Figs. 7.9 and 7.10), the flow system must select a wavelength between the minimum and maximum Scorer length. To a first approximation, we might assume that the stratification is given by the ICAO standard atmosphere, where $N = 0.011\,1/\mathrm{s}$. Then the wavelength is proportional to the wind speed U and we may approximate 7.1 by:

$$L(\mathrm{km}) \approx 0.57\, U_\mathrm{m}(\mathrm{m/s}), \tag{7.2}$$

where U_m is the mean wind speed in the layer of the lee wave system. If the wind speed is measured in kilometres/hour (km/h) or in knots (kn), then

$$L(\mathrm{km}) \approx 0.16\, U_\mathrm{m}(\mathrm{km/h}); \qquad L(\mathrm{km}) \approx 0.29\, U_\mathrm{m}(\mathrm{kn}). \tag{7.3}$$

Formula 7.2 is quite similar to the estimation $L(\mathrm{km}) = 0.6\, U(\mathrm{m/s}) - 3$, as found in the soaring literature. Hence, the wavelength based on equation 7.2 or 7.3 is larger than observed in practice, but can still serve as guideline.

One may ask why the knowledge of wavelength is of interest for soaring flight as pilots would usually fly parallel to the wave crests in order to use the positive lift associated with the wave as

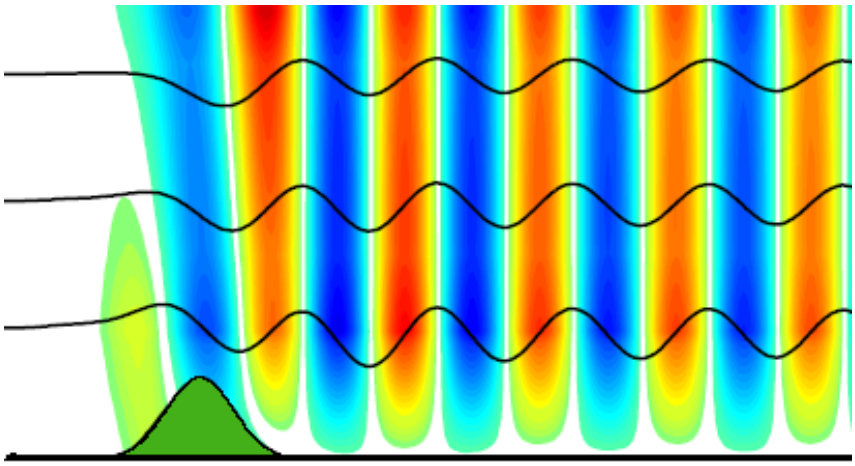

Fig. 7.10: Close up of streamlines (black lines) and vertical velocity (colored) in a lee wave shown in Fig. 7.9. Blue colors: downward motion, red colors: upward motion.

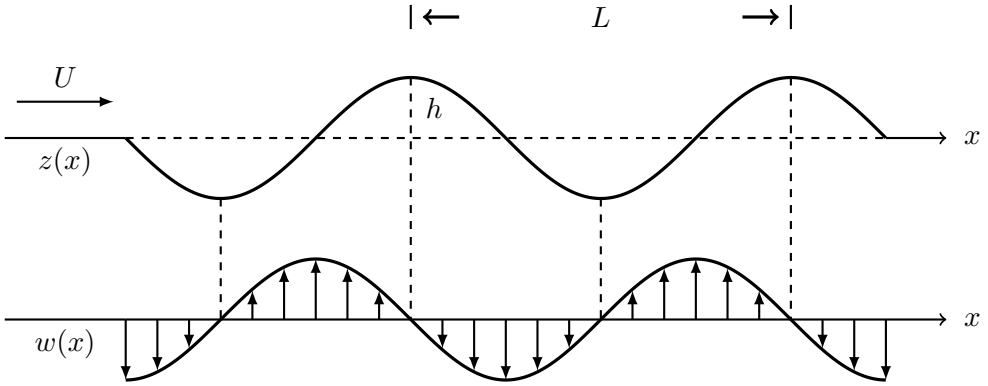

Fig. 7.11: Vertical displacement $z(x)$ of an air parcel due to a mountain wave with vertical velocity $w(x)$. U: upstream wind speed, L: wavelength, h: amplitude.

long as possible? One reason is that the horizontal extension of the updraft (but also downdraft) areas is directly related to the wavelength, as is shown in Fig. 7.11.

B. Wave amplitude

Unless we are dealing with surface water waves, we cannot see mountain waves (lee waves) directly, hence we usually have no idea about their amplitude. Before we give an estimate of wave amplitude as related to the horizontal and vertical wind speed, we first provide a simple estimate of the vertical excursion of air parcels in a stably stratified atmosphere. In Section 3.4, it was shown that a fluid parcel can undergo vertical oscillations due to buoyancy forces. The temporal variation of the particle position (equation 3.17) was obtained for a parcel lifted a small height h from its equilibrium position. One can also initiate the oscillations by pushing the particle from its equilibrium position by a prescribed vertical impulse (initial vertical velocity) denoted by w_0 as sketched in Fig. 7.12 (this is like kicking a soccer ball). The solution of the oscillation equation 3.15 is then given by

$$z(t) = \frac{w_0}{N} \sin(Nt) \tag{7.4}$$

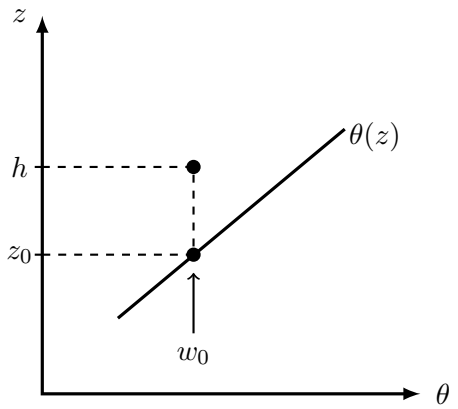

Fig. 7.12: Air parcel in a stably stratified environment (potential temperature θ increasing with height z) pushed upward from its equilibrium position z_0 by an initial impulse w_0.

Tab. 7.1: Height amplitudes $\boldsymbol{h}$ (in m) for air parcels pushed in the vertical direction by an initial impulse w_0 for different stratification $d\theta/dz$.

$d\theta/dz$	N	w_0 (m/s)		
(K/100 m)	(1/s)	3	6	9
0.35	0.011	**270**	**540**	**810**
1.0	0.018	**170**	**340**	**510**
3.0	0.031	**100**	**200**	**300**

and the amplitude is determined through

$$h = \frac{w_0}{N}. \tag{7.5}$$

The amplitude is larger for a larger impulse w_0 and for a smaller Brunt-Vaisala frequency N (weaker stratification). Some examples are given in Table 7.1. The total height difference an air parcel is experiencing during one oscillation period is twice the amplitude h given in Tab. 7.1. Sometimes, this value is denoted as the wave amplitude in the literature.

The amplitude of mountain waves is quite closely connected with the free amplitude of air parcels oscillating in a stratified atmosphere as described by equations 7.4 and 7.5 as will now be discussed. Let us consider the situation of the simple lee waves sketched in Fig. 7.11. An air flow with wind speed U approaching a mountain ridge is forced to oscillate around its initial height level z_0 due to a wave with vertical velocity w described by

$$w(x) = w_0 \sin\left(\frac{2\pi x}{L}\right). \tag{7.6}$$

The vertical displacement is then given by

$$z(x) - z_0 = -h \cos\left(\frac{2\pi x}{L}\right). \tag{7.7}$$

The amplitude h is related to the vertical velocity amplitude w_0 through

$$h = w_0 \frac{L}{2\pi U}. \tag{7.8}$$

At first, one gets the impression that the longest waves have the largest wave amplitudes for a fixed combination of vertical velocity w_0 and horizontal wind speed U. But the wavelength L is also related to wind speed U by equation 7.1. By combining 7.8 with 7.1, the amplitude h can be written as $h = w_0/N$, which is just the same as for the vertical oscillations of a single air parcel according to equation 7.5.

The trajectory of air parcels within lee waves are obtained by a combination of the horizontal distance x and vertical displacement $z(x) - z_0$ as shown in Fig. 7.11 indicating the areas with upward and downward vertical wind components. One can see that these span half a wavelength each and that the maximum velocities can be found in the middle of updraft and downdraft

areas. This is of importance for practical wave soaring, especially when soaring in the direction of the waves will encounter periodic positive and negative lift.

C. Vertical velocity (lift)

The amplitude h of mountain waves depends to a first approximation on the Brunt-Vaisala frequency N and the maximum vertical velocity w_0 as given in equation 7.5 and Table 7.1. Then the question remains, which factors determine the vertical velocity in mountain waves? From all wave properties, this is the most important for wave soaring. The reason is simple: the lift a glider pilot can achieve is the difference between the vertical velocity of the air stream minus the sinking rate of the airplane. If we assume a typical sinking rate of 1 m/s, the surrounding air must rise with a speed of at least 1 m/s in order to stay airborne. When the air rises with say 4 m/s, the lift with respect to ground level would be 3 m/s.

The magnitude of vertical velocity within mountain wave systems depends, as with the wavelength, on the mountain properties (height, base diameter, shape) and the meteorological conditions (wind speed, stratification). These dependencies have been investigated by field observations, reports from glider pilots and numerical simulations (like those described in Chapter 8). Here we will present some principal rules derived from these investigations below:

1. The largest wave amplitudes are obtained when the natural wavelength L (see equation 7.1) matches the horizontal extension (base diameter λ) of the mountain ridge, i.e. $L \approx \lambda$.

2. The wave amplitude is mainly determined by the strength of the downward flow on the leeward mountain slope.

3. Asymmetric mountains with steeper lee-side slopes produce stronger waves.

4. Higher mountains produce larger wave amplitudes.

5. Stronger upstream winds lead to larger amplitudes.

Rule 1 is related to the fact that for $L \approx \lambda$, the forcing length scale of the mountain (λ) is in resonance with the resulting length scale of the mountain wave (L). That does not mean that waves do not form if $L > \lambda$ or $L < \lambda$, but in these cases the wave amplitude (vertical displacement and vertical velocity) is weaker than in the resonance case.

Rule 2 is due to the internal dynamics of stratified flows over obstacles and is not easily explained. One could loosely compare the behaviour of airflow over mountains with the situation of a river flowing over a weir, where the largest acceleration occurs on the weir slope. Indeed, this comparison holds for so-called downslope wind storms occurring occasionally on the leeward slope of large mountain ranges like the Rocky Mountains. These winds are closely related to the gravity wave system formed above the mountain (see, e.g., Durran, 1990). For the case of lee waves, we might consider Fig. 7.10, where the upward flow at the luff slope is much weaker than the downward flow on the lee side of the mountain. As illustrated in Fig. 7.10, mountain lee

waves usually start with sinking air above the mountain and the rising air usable for soaring flight will be found about half a wavelength downstream from the mountain top.

Rules 3 – 5 are related to the forcing of the oncoming airstream by the mountain ridges as will be discussed now. Vertical wind components (updraft or downdraft) in mountain wave systems are mechanically induced by deflection of the horizontal approach flow (denoted by U) by the mountain. The flow near the ground has to follow the shape of the mountain surface as the air cannot penetrate the surface as sketched in Fig. 5.11, Section 5.5. Let us denote the topography of the mountain ridge by $h(x)$ and the undisturbed wind speed by U. If the air stream follows the mountain topography, the vertical wind component $w(x)$ is given by

$$w(x) = U\frac{dh(x)}{dx}, \tag{7.9}$$

where $dh(x)/dx$ is the mountain slope. For a simple estimation of the vertical velocity induced by mountain ridges, we consider a mountain of triangular shape depicted in Fig. 5.11, where the height is denoted by H and the *half base diameter* by D. For this case, the slope is constant and is given as $dh(x)/dx = H/D$. Hence, the vertical velocity on the slope is also constant and is given by:

$$w_0 = U\frac{H}{D}. \tag{7.10}$$

Some values for w_0 for different mountain slopes and wind speeds are given in Table 7.2. The vertical velocity over mountain slopes provided by equation 7.10 is not exactly the same as can be expected in the lee waves forced by the mountain except for the more academic case of periodic mountains treated in Section 6.2 (see, e.g., Fig. 6.2). But as the amplitude of the forced lee waves depends on the amplitude of the forcing by the mountain, it might provide some estimates for the expected wave lift.

Consulting equation 7.10 and Table 7.2, we can provide some support for rules 3 – 5 concerning vertical velocities and amplitudes as found in mountain waves. Rule (3) is directly stated in equation 7.10 as w_0 is proportional to the mountain slope. Rule (5) also follows directly from equation 7.10 as w_0 increases linearly with the wind speed U. Rule (4) will hold for mountains with the same half base diameter D. But as higher mountains usually have larger base diameters, these mountains may be less steep compared with smaller ones. The observation that stronger waves can be found behind higher mountains is more often related to the fact that the

Tab. 7.2: Vertical velocity $\boldsymbol{w_0}$ (in m/s) induced by a mountain slope H/D for different horizontal wind speeds U.

	U (m/s)		
H/D	10	20	30
0.1	**1**	**2**	**3**
0.2	**2**	**4**	**6**

wind speed U usually increases with height. Therefore, higher mountains experience larger wind speeds and hence rule (5) applies.

The simple rules formulated above have been validated by many glider pilots soaring mountain waves. For moderately sized mountains like in Northern Germany, vertical velocities w of the order of 2 - 4 m/s have been reported (see flight reports under `www.schwerewelle.de`). For larger mountains like the European Alps or the Southern Alps of New Zealand, vertical winds of 6 - 9 m/s are not uncommon (see `www.mountain-wave-project.com`). Extreme upward and downward air motion of 12 m/s and more has been occasionally experienced by glider pilots over the Andes region (see also `www.mountain-wave-project.com`) and the Sierra Nevada (see Whelan, 2000).

In any case, wave properties like wavelength, wave amplitude (vertical excursion of air parcels) and vertical velocity (updrafts or downdrafts) vary from location to location and for the same location from day-to-day depending on the meteorological conditions found on the upstream side of the mountains. The simple formulas 7.2, 7.5 and 7.10 and the Tables 7.1 and 7.2 provide some rules of thumb for these wave properties.

7.5 Mountain waves as hazards to aviation

So far we have treated mountain waves as a possible source of lift for soaring flight. At the end of this chapter, we might mention that the mountain wave system is also hazardous for general aviation as illustrated in Figure 7.13. In this figure, two potential hazards are shown:

1. breaking gravity waves at high altitudes

2. turbulent rotors at low altitudes

It should be noted that these two phenomena do not occur at the same time for a given situation as suggested in Fig. 7.13, but separately according to the conditions outlined in Sections 7.2 and 7.3.

Breaking gravity waves as sketched in the upper part of Fig. 7.13 occur mainly over large mountain areas like the Alps or the Rocky Mountains when there is some decrease in wind speed (increase of the Scorer parameter) at high altitudes. Then, the mountain waves behave literally like breaking water waves on the beach. Wave breaking is accompanied by moderate to strong turbulence, hence this phenomenon falls into the category of Clear Air Turbulence (CAT). In fact, various reports of aircraft encounters with breaking gravity waves, sometimes with damage to the aircraft and injuries to passengers, can be found in the literature. Here, we mention only investigations of upper layer turbulence due to breaking waves over the contiguous USA by Wolff and Sharman (2008, Journal of Applied Meteorology and Climatology, p. 2198-2214) or the European Alps by Jiang and Doyle (2004, Journal of the Atmospheric Sciences, p. 2249-2266). One might also consider accident reports by the US National Transport Safety Board (NTSB) for cases of aircraft encounters with breaking gravity waves.

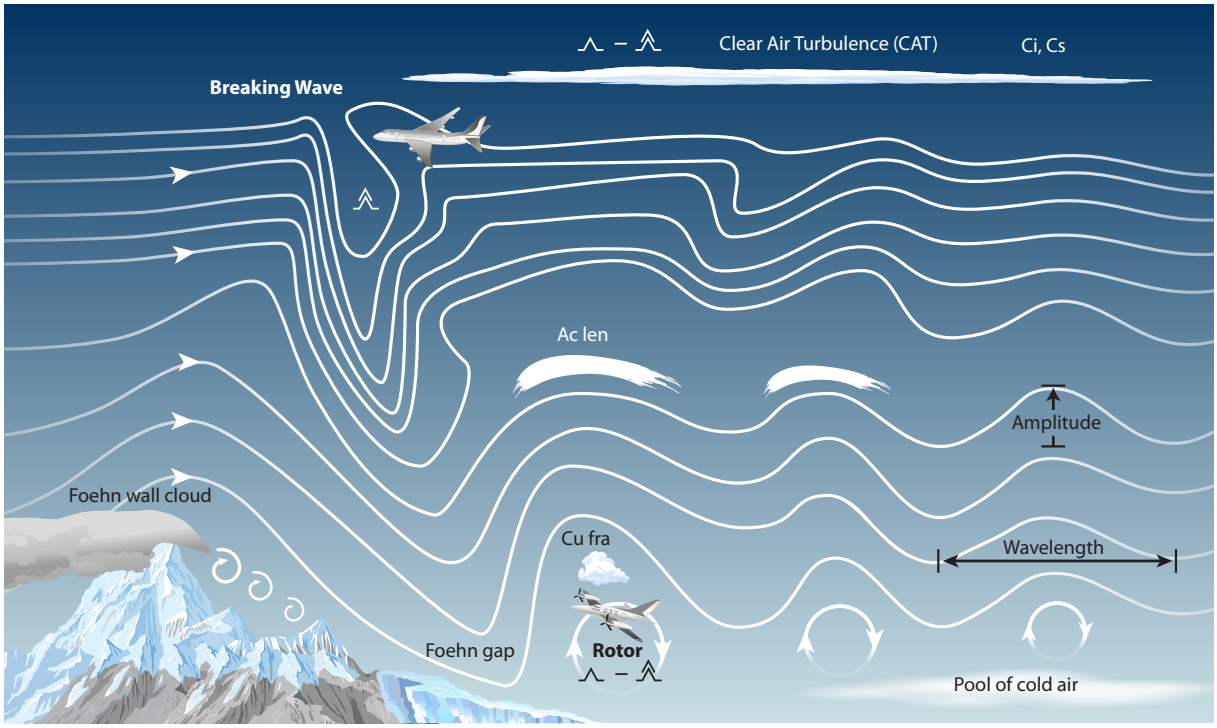

Fig. 7.13: Sketch of potential hazards for aviation in mountain wave systems. Upper part: breaking gravity waves; lower part: rotors.
Source: Mountain-Wave-Project

Concerning soaring flight, moderate to severe turbulence has been reported during some high altitude flights of the Sierra Wave Project (Whelan, 2000) or flights performed by the Mountain Wave Project over the Andes (`www.mountain-wave-project.com`) which might be attributed to breaking wave events.

The other potential hazard in mountain wave systems is the rotor flow connected with lee waves in the lower atmosphere. As illustrated in Fig. 7.13, rotors form approximately in the layer between the surface and the mountain top. This phenomenon is much more frequent than breaking mountain waves and has been experienced by most glider pilots practicing wave soaring. Some quite dramatic encounters with rotors by glider pilots have been documented in Whelan (2000). As moderate to severe turbulence is usually found in rotor flows, this part of the mountain wave system is not only dangerous for soaring flight but also for general aviation at lower flight levels. A more detailed description of rotors is provided in Chapter 9.

8 Forecasting mountain waves

8.1 General considerations

Weather forecasts on the radio, television and newspaper are part of our daily media consumption. The type and details of the weather forecast depend on the needs of the customer. This is especially true for soaring flight, where the forecast of upward atmospheric motion is essential. This includes the forecasts of convective weather conditions for thermal flight and of stably stratified atmospheric conditions for wave flights. Weather forecasts for soaring flight are usually treated in any book on soaring, e.g., the monographs by Eckey (2012) or Hertenstein (2005, 2011). A special publication entitled "Weather forecasting for soaring flight" has been published by the OSTIV (2009).

In the following, we give some examples of forecasts of mountain waves. They range from some empirical approaches, to model output from routine numerical weather prediction (NWP) models provided by weather services. With respect to the latter, we might remark that these models are based on the physical laws for fluid motion, which were given in simplified forms in Section 2 and in the appendix. As no analytic solutions of these equations can be found for the complicated forms of atmospheric motion, the equations have to be solved numerically. This is called "Numerical Weather Prediction (NWP)" and is the basis of all weather forecasts provided for the public in the media.

One limitation of these models is the spatial resolution necessary for solving the flow equations by numerical methods on powerful computers. Let us denote the resolution in the horizontal plane (also called the grid-size) with Δx, which means that all phenomena with horizontal extension L smaller than Δx cannot be represented by the numerical model and can therefore not be forecasted. In practice, atmospheric phenomena can be resolved by numerical weather prediction models if they are larger than 4 times Δx.

As a consequence of these restrictions, the following rules apply for atmospheric gravity waves, including mountain waves: If the wavelength is $L = 10\,\mathrm{km}$, the resolution should be at least $\Delta x = 2.5\,\mathrm{km}$. If the wavelength is $L = 40\,\mathrm{km}$, a resolution of $\Delta x = 10\,\mathrm{km}$ is sufficient. Hence, depending on the model available for the weather forecast, mountain waves may either be resolved (and forecasted) or not. Some examples of wave forecasts obtained by these models are given in the following sections.

8.2 Empirical methods

The basis for all wave forecasts is the knowledge of the vertical structure of the atmosphere upstream of the mountain range of interest, including the vertical temperature profile for calculating the stability parameter (Brunt-Vaisala frequency) N, the wind speed profile of magnitude U and the direction of the horizontal wind. From this information, we can calculate the Scorer parameter $S(z) = N(z)/U(z)$, which was explained in Section 6.1. Information about the ver-

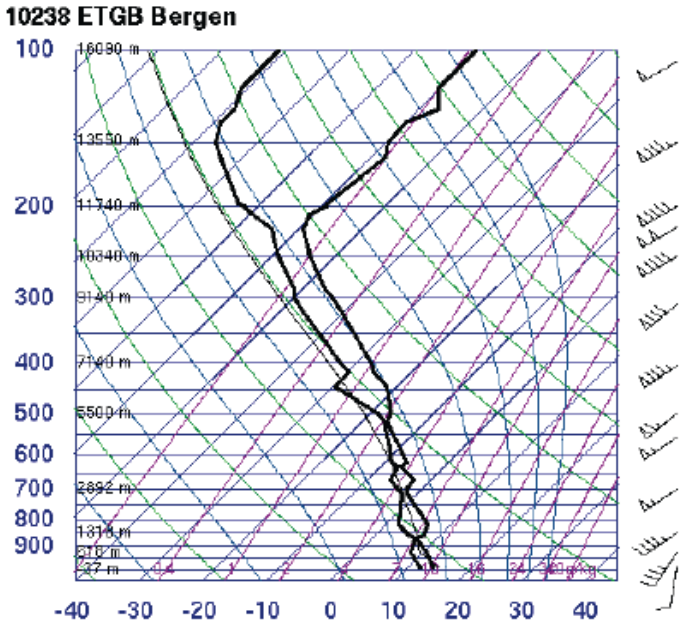

Fig. 8.1: Radiosonde observation at Bergen, Germany, for 14 November 2010, 12 UTC.
Source: University of Wyoming

tical structure of the atmospheric flow upstream of the mountain of interest can be obtained by so-called radiosonde observations, or shortly called "temp", which are provided through the world wide observational network run by the local weather services, freely available from the University of Wyoming at `http://weather.uwyo.edu/upperair/sounding.html`. An example

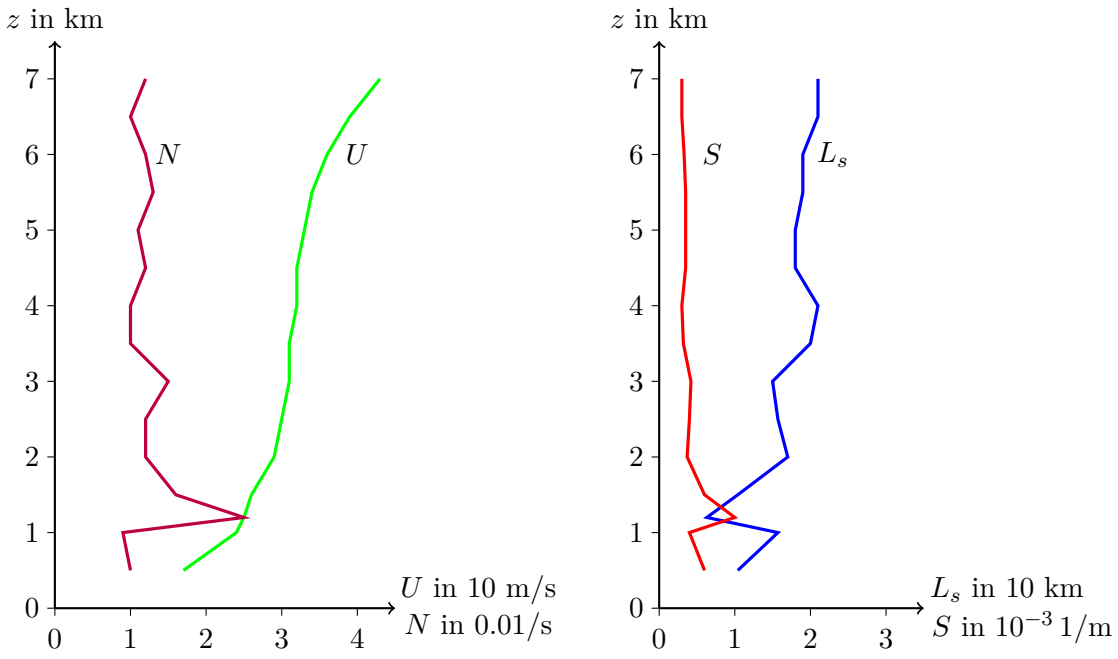

Fig. 8.2: Vertical profiles of wind speed U, Brunt-Vaisala frequency N, Scorer parameter S and Scorer lenght L_s for the radiosonde observations shown in Figure 8.1.

of a sounding from the radiosonde station Bergen in Northern Germany is shown in Figure 8.1. From these observations, profiles of Brunt-Vaisala frequency N and Scorer parameter S have been derived and are shown in Figure 8.2.

Some rules of the thumb concerning the occurrence of mountain waves at a particular location have been obtained through many observations and numerical simulations of mountain waves and can be summarized as follows:

1. The atmosphere has to be stably stratified from at least the mountain top upward.

   Reason: only in a stably stratified fluid can vertical oscillations and gravity waves develop. A neutral or unstable stratification below the mountain top (e.g., day time convective boundary layer) does not exclude gravity wave development above the inversion.

2. The approaching wind direction has to be within about $\pm 30°$ deviation from the direction perpendicular to the mountain ridge.

   Reason: as mountains are only approximately two-dimensional, wind direction more parallel to the ridge leads to three-dimensional effects unfavorable for wave development.

3. The variation of wind direction with height should be less than $\pm 20°$ from the wind direction at mountain top.

   Reason: a strong change in wind direction will damp out mountain waves.

4. The minimum wind speed at mountain top should be 15 - 25 kn (8 - 14 m/s).

   Reason: the lifting of air parcels in a stably stratified environment requires a minimum wind speed, otherwise the air cannot flow over the mountain to trigger mountain waves.

5. For the variation of wind speed with height (wind shear), it has been found:

   (a) vertically propagating (to high altitudes) mountain waves require a moderate increase in wind speed with height (low wind shear),

   (b) trapped mountain waves (lee waves) require a strong increase in wind speed with height (strong wind shear).

6. Conditions (1) and (5) can be related to rules for the Scorer parameter S:

   (a) vertically propagating mountain waves require S to be nearly constant with height,

   (b) trapped mountain waves require S to decrease rapidly with height.

We may, as an example, consider the wind and temperature profiles provided in Figures 8.1 and 8.2. These are applied to mountain wave forecasts in Sections 8.3 - 8.5 as they meet all the simple rules for mountain wave development. Trapped mountain waves (lee waves) can especially be expected since the Scorer parameter decreases with height (rule 6b). As will be seen in Sections 8.3 - 8.5, trapped mountain waves indeed occurred over parts of Germany on this day.

8.3 Linear wave models

If one wants to know not only whether mountain waves will occur, but in addition, the wavelength, amplitude and vertical extension of mountain waves, one has to use a model based on the physical laws for internal gravity waves as presented in the appendix. The most simplest case is a linear model (see Appendix AI, AII) in which the waves do not interact with the approaching flow. Some analytic solutions of the linear model equations were presented in Chapter 5 for very simple configurations. If the mountain shapes and/or the vertical wind and temperature profiles of the upwind atmospheric flow are more complicated, only numerical solutions are possible. Such solutions are provided, e.g., in the monograph by Nappo (2012) and an example is given in Figure 8.3. Here, the linear model has been applied to a real wave situation over the Thueringer Wald (Thuringian Forest) in Germany for the upstream wind and temperature profiles given in Figure 8.1 (Kubitschke, 2011).

In this case, the mountain is assumed to be two-dimensional in the crosswind direction, which is of course very idealized. But with this simple approach, one can nonetheless forecast wavelength and wave amplitude for mountain waves. A comparison between this linear model prediction and more complex nonlinear models for the same situation can be found in Figures 8.4 and 8.8. More realistic linear wave models calculate the wave field in three dimensions and include realistic topography of the mountainous terrain of interest. An example is the 3dVOM (3 dimensional Winds Over Mountains) model run by the UK Met Office.

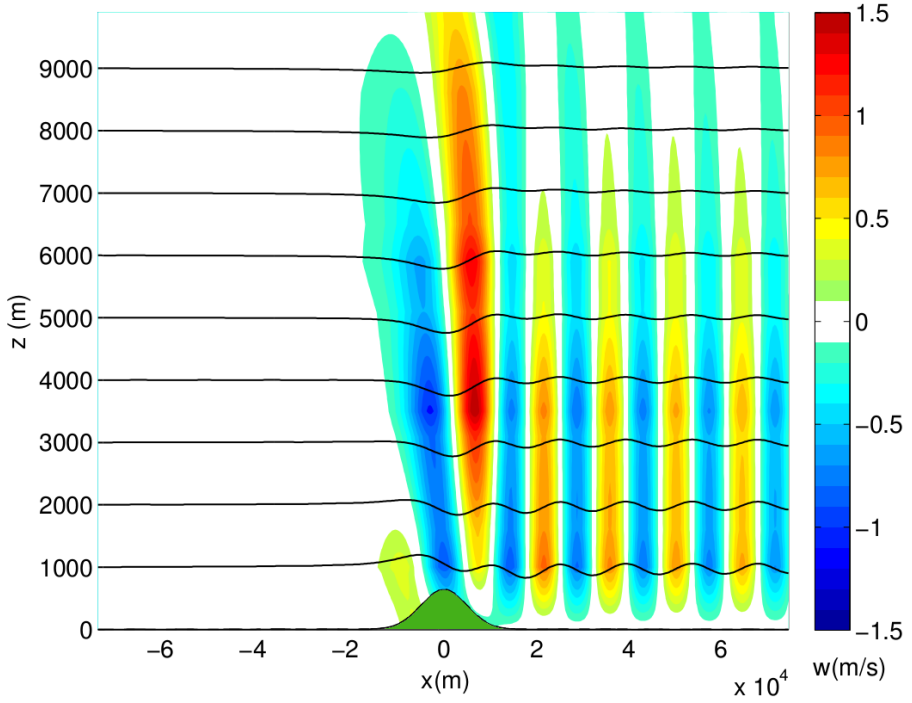

Fig. 8.3: Vertical velocity (colored) and streamlines (black) of mountain waves predicted with a linear wave model for an idealized topography of the Thueringer Wald (Thuringian Forest) for the observed radiosonde profiles shown in Figures 8.1 and 8.2

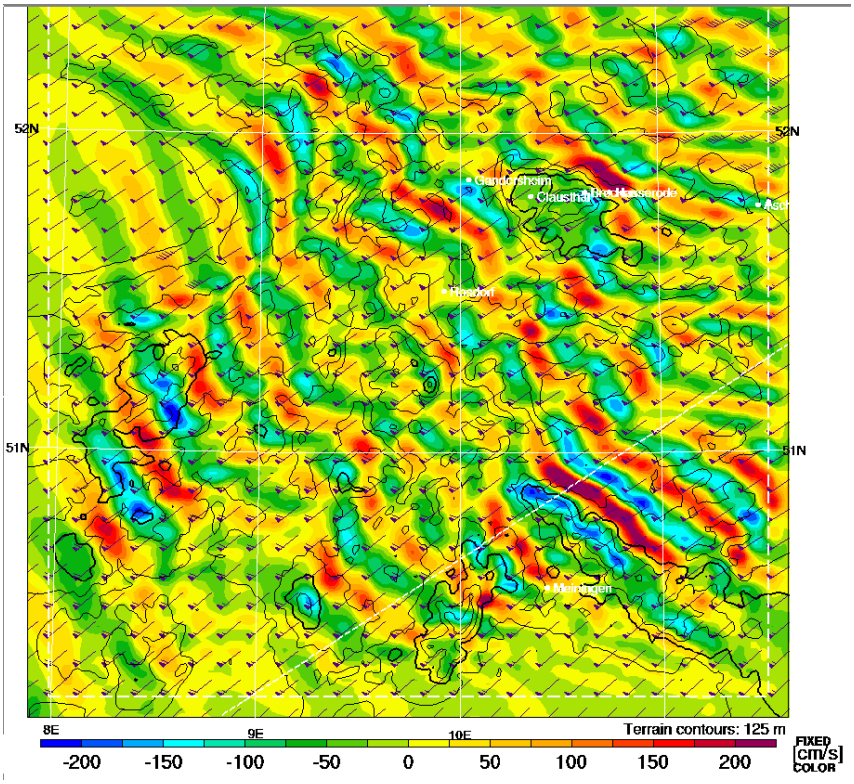

Fig. 8.4: Vertical velocity at the 700 hPa (∼ 3 km) pressure level over the Harz/Thueringer Wald region in Germany for 14 November 2010 as obtained with the RASP model.
Source: Hendrik Hoeth.

8.4 Nonlinear numerical models

Nonlinear atmospheric models make use of the full equations of fluid physics given in the appendix. One such model is the well known RASP (Regional Atmospheric Soaring Prediction) model developed by Dr. J.W. (Jack) Glendening (see: `www.drjack.info/RASP`), which is based on the widely used WRF (Weather Research and Forecast) model. Although this model is mostly used for predictions related to thermal flight, wave forecasts can also be performed as the horizontal model resolution can be reduced to 1 - 4 km. The model is also run by various soaring-weather enthusiasts throughout the world for their local soaring area. A list of these regional forecasts can be found under `www.drjack.info/RASP`. One of these forecasts is provided by Hendrik Hoeth, who runs the model for thermal flight and wave forecasts above the low mountain ranges of Central Europe, especially Germany (see `http://rasp.linta.de`).

An example of a wave forecast with the RASP model for 14 November 2010 in Northern Germany at a very high horizontal resolution of 1.4 km is shown in Figure 8.4. This is the same situation as simulated with the COSMO-DE model described in Section 8.6. A vertical cross section across the Thueringer Wald is shown in Figure 8.5, where the waves reach altitudes of about 7 km, and has been verified by glider pilots as described in Section 8.6. This wave forecast can also be compared with the results from the linear model provided in Figure 8.3.

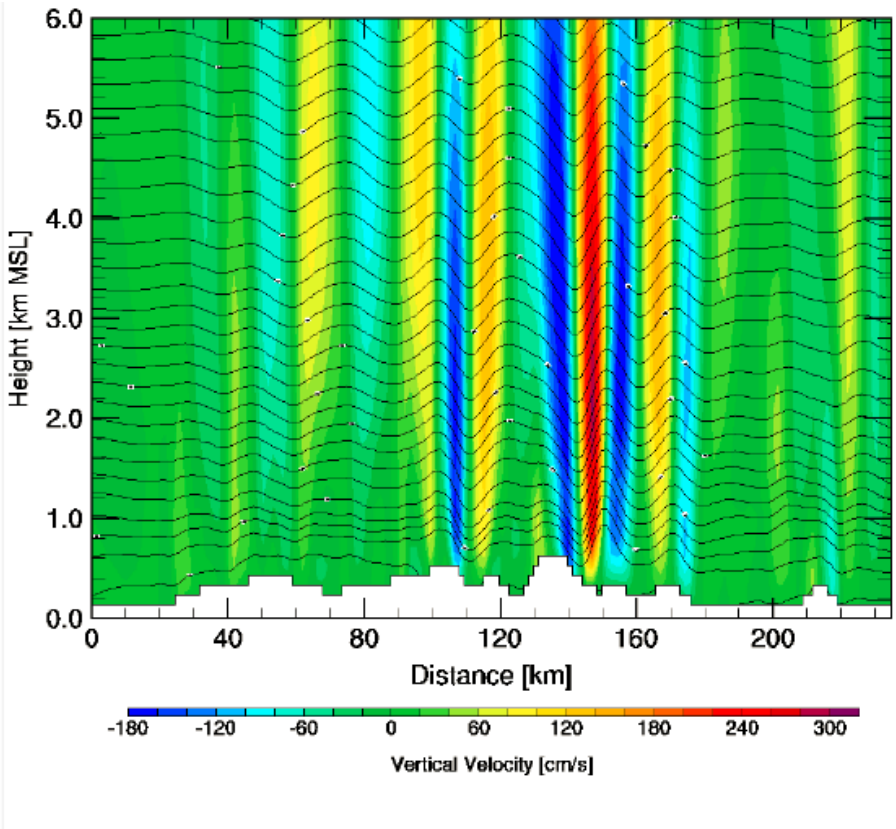

Fig. 8.5: Vertical cross section of vertical velocity along a line bisecting the Thueringer Wald (lower right in Figure 8.4) as obtained by the RASP model.
Source: Hendrik Hoeth.

8.5 Operational weather prediction models

As already mentioned, the horizontal grid resolution for numerical weather prediction (NWP) models has to be less than 4 km or so in order to capture atmospheric gravity waves with wavelengths of less than 15 km. Until recently, very few regional NWP models had such low resolution. One such model is the so-called COSMO-DE model run operationally for the area of central Europe by the German Weather Service (DWD). From the routine forecasts, some special model outputs for soaring flight are provided through the aviation tool PC_MET (see `www.flugwetter.de`). Among these are the fields of vertical velocity for flight levels 50, 100 and 180 over central Europe. An example for 11 December 2010 is given in Figure 8.6 where a large amplitude mountain wave is predicted in the lee of the Erzgebirge (Ore Mountains) with a wavelength of about 24 km and wave updrafts of about 3 m/s. Waves in other areas of Northern Germany are also predicted on this day as can be seen in the figure. A verification of this wave prediction can be made by comparing the satellite image for the same day as shown in Figure 8.7. Clearly, the strong wave event in the lee of the Erzgebirge can be identified in the lower right part. Other wave systems can also be identified over Germany as predicted by the COSMO-DE model.

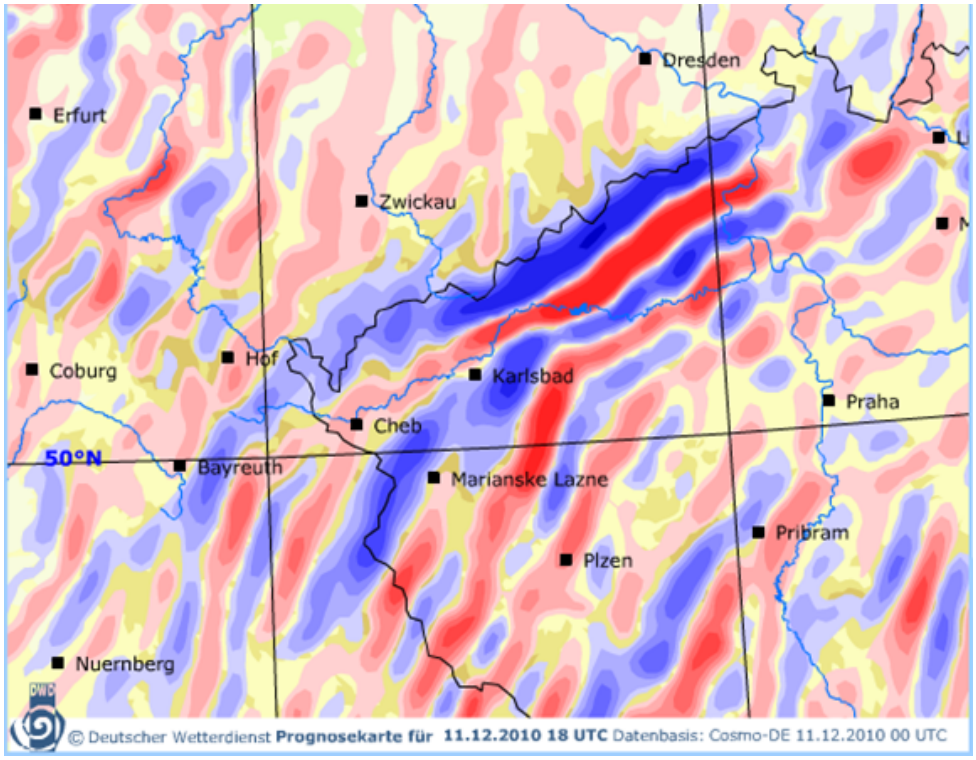

Fig. 8.6: Vertical velocity at flight level 100 (~ 3 km) in the area of Erzgebirge, Germany, for 11 December 2010, 12 UTC, as obtained by the COSMO-DE model.
Source: German Weather Service (DWD).

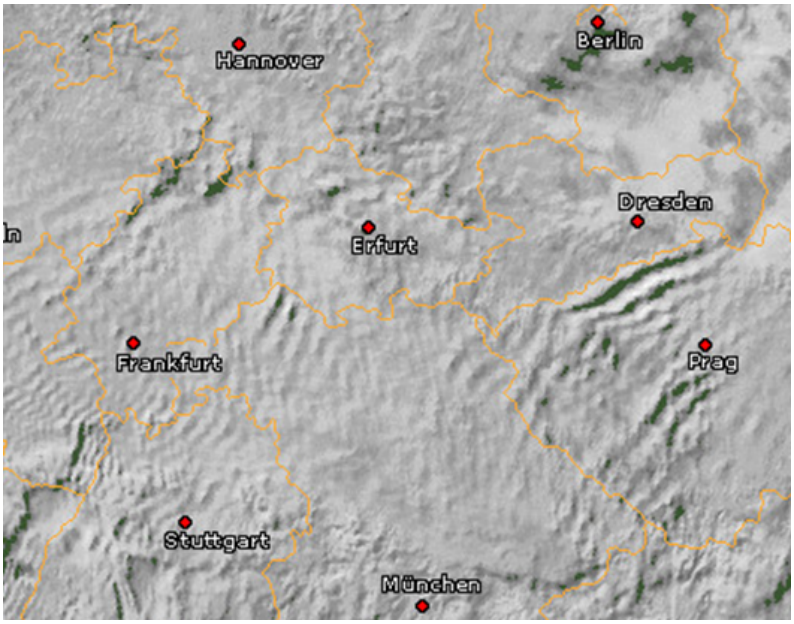

Fig. 8.7: Satellite picture of wave clouds over Germany on 11 December 2010, 12 UTC. The lee waves induced by the Erzgebirge (Ore Mountains) are seen along the path between Dresden and Prag (Prague).
Source: Wetteronline/Eumetsat.

8.6 Verification of mountain wave forecasts

Verification of weather forecasts is something we more or less automatically do when we compare the predicted with the actual weather. When the weather forecast promises sunshine for tomorrow, but then it rains for several hours, we tend to regard this as a false forecast. The verification of mountain wave forecasts is however not so simple. First, only a few people are provided with these special forecasts and second, the verification itself is not trivial. One could of course look at satellite images as shown in, e.g., Figure 8.7 or even to look to the sky to see if we can detect cloud bands in the lee of mountain ridges. On many occasions though there are no suitable clouds to be seen due to unsuitable atmospheric conditions so that the only way to verify is to believe the forecast and to try and catch the waves with our sailplanes.

This is practiced by, among others, a group of soaring pilots in Northern Germany who are provided with a mountain wave alert based on the forecast of the German Weather Service (DWD). In response, they are asked to provide a flight report to the soaring community which is then published on the website `www.schwerewelle.de`. In a thesis on mountain waves and soaring flight, Kubitschke (2011) has evaluated one of these forecasts for the mountain areas of Harz and the Thueringer Wald based on various flight reports. The wave prediction from the COSMO-DE model for 14 November 2010 is shown in Figure 8.8. This prediction can also be compared with the forecast of the RASP model for the same situation in Figure 8.4. The wavelength is about 24 km for Harz and about 20 km for the Thueringer Wald corresponding approximately with the Scorer length shown in Fig. 8.2, while wave updrafts have maxima of 2.5 - 3.0 m/s.

As an example for the comparison with flight reports, the wave flights in the Harz area performed on this day are shown in Figure 8.9. There, the field of vertical wind velocity provided from the model is overlaid with the flight tracks. In total, 8 flight reports were available for this day. From these reports (also published on the website mentioned above), the vertical wind velocity in the waves was reported to be about 3 m/s which is similar to the wave forecast shown in Figure 8.8. While some pilots reached altitudes of more than 6000 m MSL, higher flights were not possible due to air traffic control restrictions. These reports also verify the vertical extent of the mountain waves as predicted by the RASP model which can be seen in a cross section above the Thueringer Wald provided in Figure 8.5.

In summary, it can be stated that mountain wave forecasts by operational weather prediction models or by special soaring weather models like RASP are now possible. The reason for the good performance, e.g., compared with forecasts of rain showers, is because mountain waves are a (more or less) stationary atmospheric phenomenon fixed to the mountain range of interest. Hence, when the vertical structure of the atmosphere is favorable for wave development (see the rules in Section 8.2), it is likely that mountain waves will occur. As current weather forecast models include the physics of atmospheric gravity wave development, these waves should show

up in the forecast automatically, provided the horizontal grid resolution is fine enough (say below 4 km). It is more a problem of providing the wave forecast to the customers (glider pilots), as the model output requires specific processing.

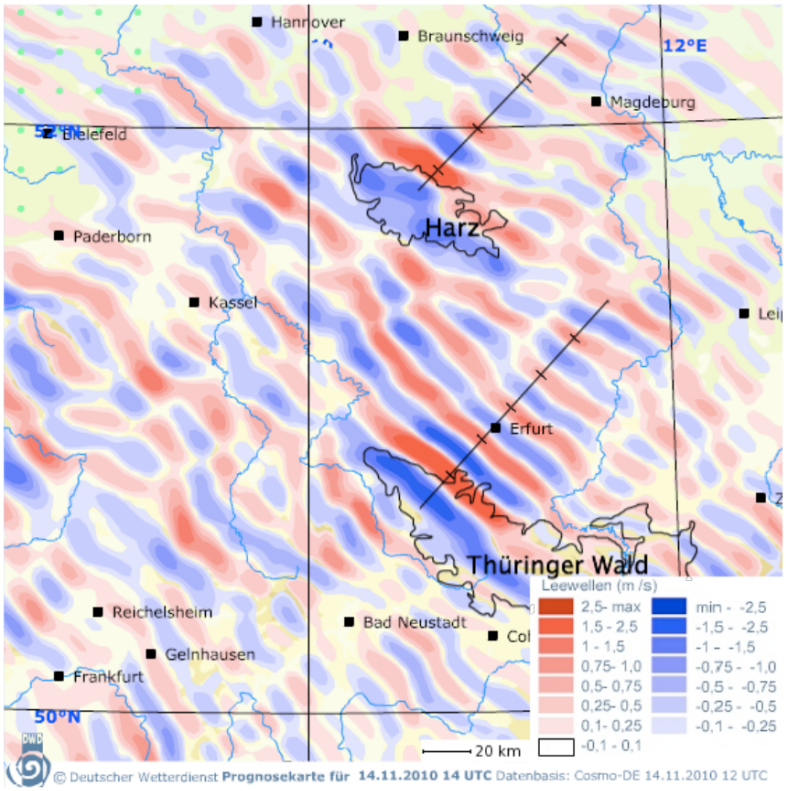

Fig. 8.8: Vertical velocity at flight level 100 (∼ 3 km) for day 14 November 2010, 14 UTC, in the area Harz/Thueringer Wald as obtained by the COSMO-DE model.
Source: German Weather Service (DWD).

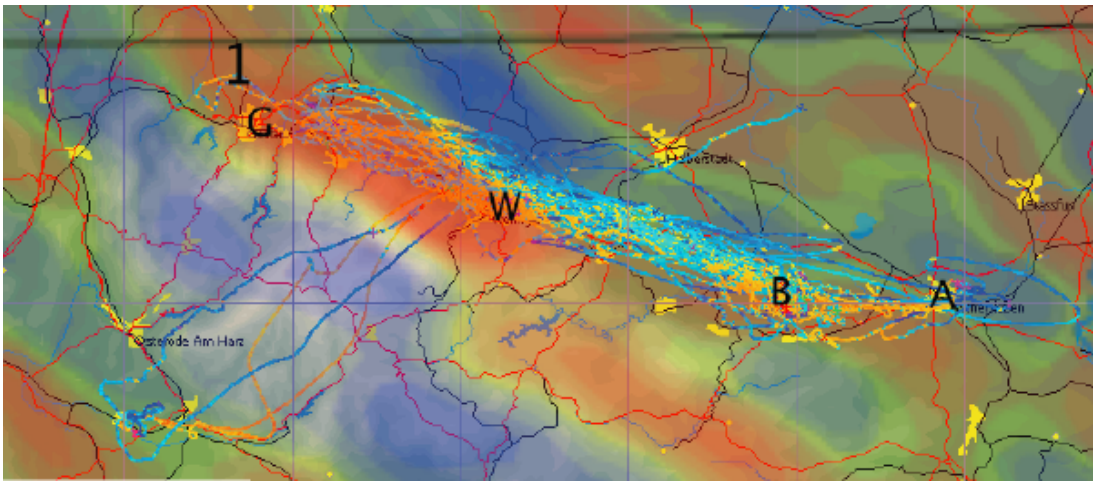

Fig. 8.9: Composite of mountain wave prediction (from Figure 8.8) and flight tracks reported by glider pilots in the lee of Harz for 14 November 2010. Flight track colors: orange: climbing, blue: descending.
Source: Kubitschke (2011).

9 Rotors

9.1 General aspects

A paper on mountain waves and soaring flight is not complete without a section on rotors. As already indicated in Figures 1.3 and 7.8, rotors can be found in the layer between the earth's surface and the first mountain wave crests. As the name "rotor" indicates, the airflow within a rotor is not consistently directed downstream, but can have surface winds opposing the flow approaching the mountain as shown schematically in Figure 9.1. It is not the reversed flow that is the main problem for gliders or any aviation vehicle, but rather the strong turbulence encountered in the upper part of the rotor which makes flight within the rotor dangerous. The strong turbulence can be accompanied by cumulus clouds at the rotor top in contrast to the smooth lenticularis clouds found at the wave crests at higher altitudes. An example of a rotor cloud is shown in Figure 9.2. In fact, glider pilots have traditionally used the rotor cloud as an indicator of the rotor location.

As rotor turbulence is not only dangerous for soaring flight but also for general aviation, several large field experiments have been performed in the last 50 years. Figure 9.1 shows the setup for the recent Terrain-induced Rotor Experiment (T-REX), which took place in 2006 in the Owens valley at the flanks of the Sierra Nevada in the USA (see Grubisic et al., 2008). This area was also used for the first large field experiment on mountain waves and rotors performed in 1955 named the Sierra Wave Project (see Grubisic and Lewis (2004) for a retrospect). The flanks of the Sierra Nevada are well known for inducing large amplitude mountain waves which can reach into the lower Stratosphere (12 - 15 km) so that during the 1955 field experiment, glider pilots were able to climb up to 13 km altitude by using the mountain wave lift. The wave system induced by moderately sized mountains is also usually accompanied by rotors in the lower layer as indicated in Figures 1.3 and 7.8. Some rotor observations behind a small mountain ridge on the Falkland Islands are described in Mobbs et al. (2005).

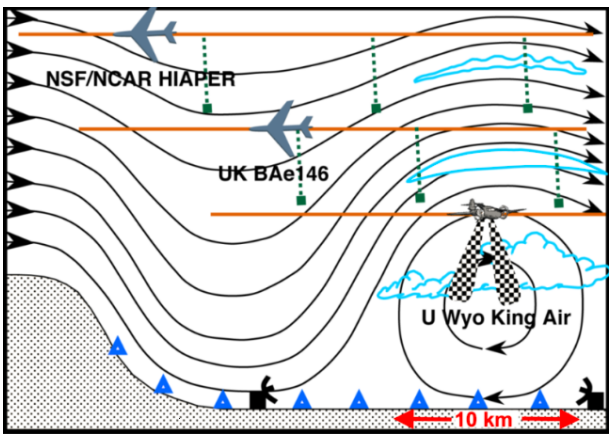

Fig. 9.1: Schematic of the setup for the T-REX field experiment in the Owens Valley, Sierra Nevada. Shown are streamlines of the mountain waves and the anticipated location and size of the rotor. Source: EOL NCAR.

Fig. 9.2: Rotor clouds in the lee of Mount Mitchell, North Carolina.
Photograph by Malosse, posted at Wikimedia Commons.

9.2 Rotor structure

Despite the field experiments mentioned in Section 9.1, most information about the velocity field within mountain induced rotors have been obtained from numerical simulations in recent years (see, e.g., Dale and Durran, 2002; Vosper, 2004). It has been found that an elevated temperature inversion as sketched in Figure 9.3 is favorable for rotor formation. Instead of presenting results from numerical simulations, we will show the typical rotor structure obtained by recent laboratory experiments that towed a mountain-shaped obstacle through a stratified water tank (Knigge et al. 2010; Knigge 2012). The setup was quite similar as the one used for numerical simulations shown in Figure 9.3. The rotor flow was visualized by particles submerged in the fluid as shown in Figure 9.4. The inversion is marked by streaks with dense particle concentration and the mountain wave is seen above the inversion. The rotor itself is indicated by the irregular particle paths due to rotor turbulence below the first wave crest. The resulting streamlines and the velocity field obtained from particle motion by means of PIV (Particle Image Velocimetry) are shown in Figure 9.5.

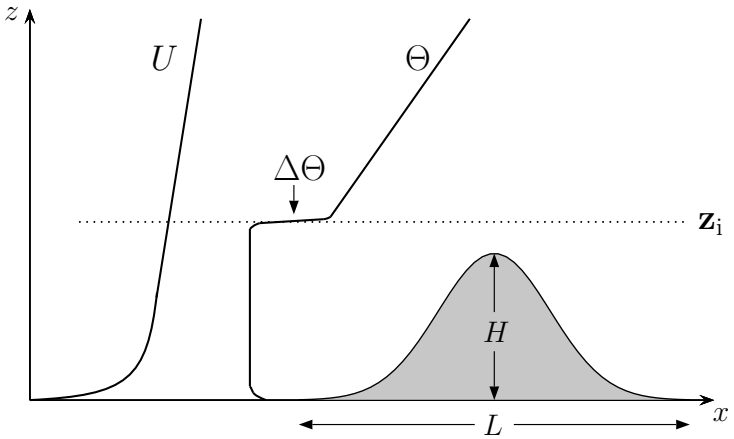

Fig. 9.3: temperature and wind conditions favorable for rotor formation in the lee of isolated mountains. The height of the temperature inversion $\Delta\Theta$ is denoted by z_i. These types of idealized profiles for wind speed U and potential temperature Θ have been used for numerical simulations and laboratory experiments of rotors.

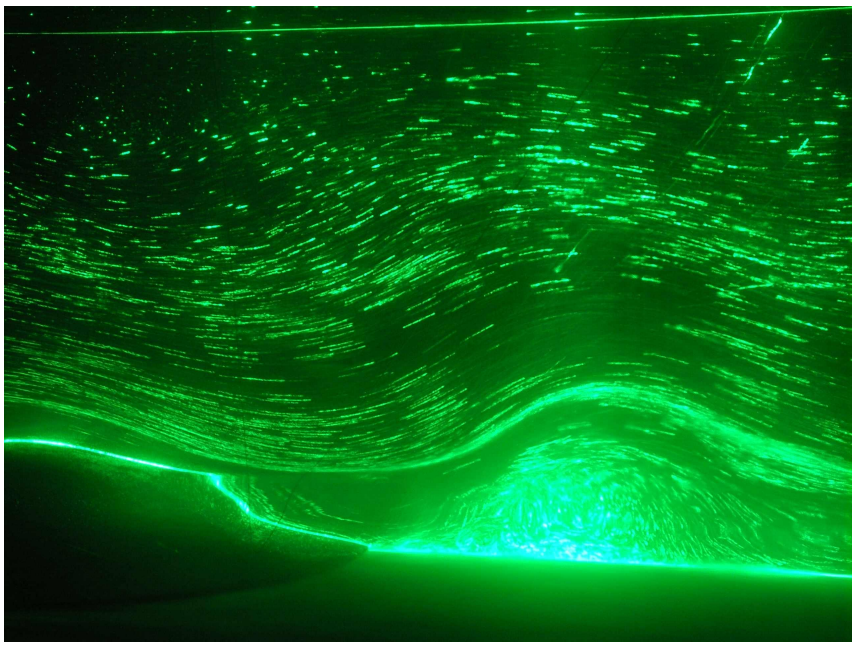

Fig. 9.4: Streaklines of wave and rotor in the lee of a mountain-shaped obstacle towed through a stratified fluid. The rotor is indicated by irregular streaks below the wave-like inversion layer.
From Knigge (2012).

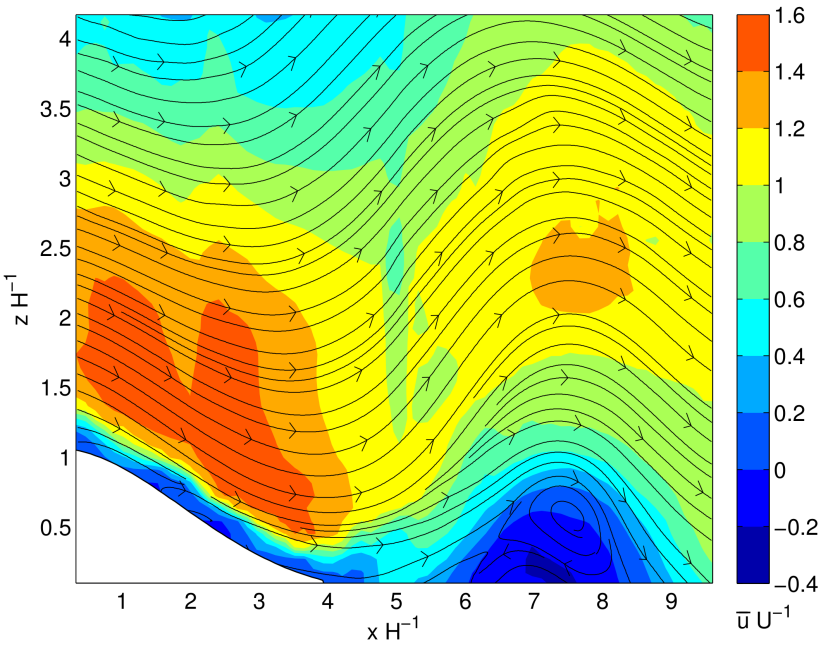

Fig. 9.5: Streamlines (black) and the velocity field (colored) for the rotor case shown in Figure 9.4 as obtained by PIV methods. Distances are normalized by the obstacle height H. Velocity is normalized by the undisturbed flow velocity U.
From Knigge (2012).

9.3 Rotor formation

In contrast to the physics of gravity waves, which has been understood in principle for 80 years or so, the formation of rotors is still a subject of investigation. Aside from field work like the large T-REX campaign mentioned in Section 9.1, most research on rotor physics has been done by numerical simulations (see the references in Section 9.2). The reason for the relatively slow progress in rotor research is that gravity wave research has been aided by linear theory, which allows analytical solutions for simple cases (see Section 5). The rotor however is a non-linear phenomenon also including turbulence which is a complex and difficult fluid problem in its own right. In order to give some impression of the underlying rotor physics, we mention two basic conditions for rotor formation as found by recent research aided by numerical simulations:

1. The reversed flow in the lower part of the rotor is induced by an adverse pressure gradient imposed by the lee wave system above the rotor.

2. Friction in the atmospheric boundary layer reduces the wind speed of the approaching flow near the ground and hence favours the development of a wind component flowing back toward the mountain in the direction of the wave-induced pressure gradient.

The first condition is illustrated schematically in Figure 9.6. The lee waves induce periodic pressure variations Δp in the boundary layer with amplitudes of about 10 Pa (or 0.1 mb). Under the wave crests, one finds increased pressure (denoted by + in Fig. 9.6) and under the troughs, decreased pressure (−). The direction of the pressure gradients in the rotor layer are also indicated. The adverse pressure gradient is directed toward the mountain and hence opposing the approaching flow. This does not necessarily mean that the wind speed in the rotor near the ground is also directed toward the mountain, but that it is reduced with respect to its value in

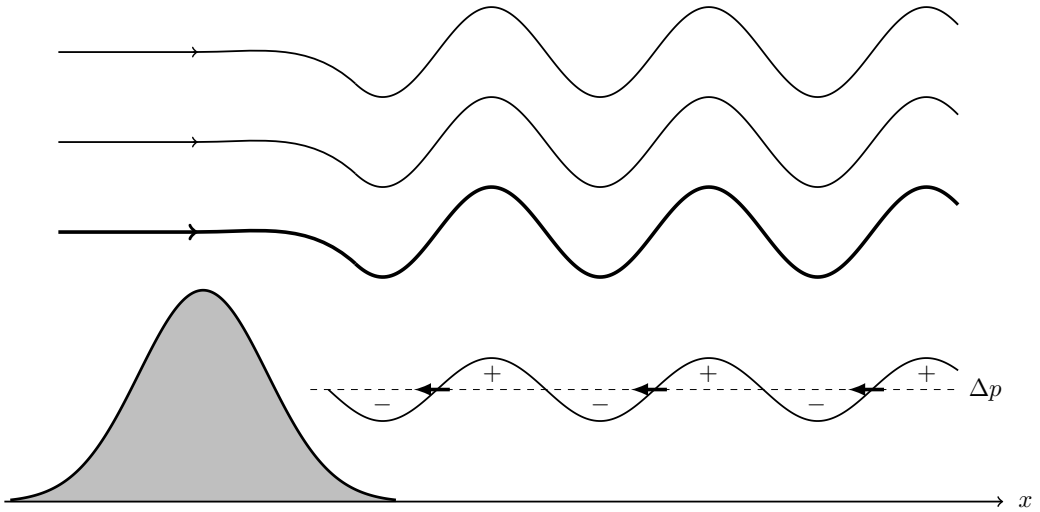

Fig. 9.6: Schematic of near surface pressure variations Δp as observed below mountain lee waves. Typical pressure amplitudes are about $\Delta p \approx 10$ Pa. The direction of adverse pressure gradients favorable for rotor formation are indicated by arrows.

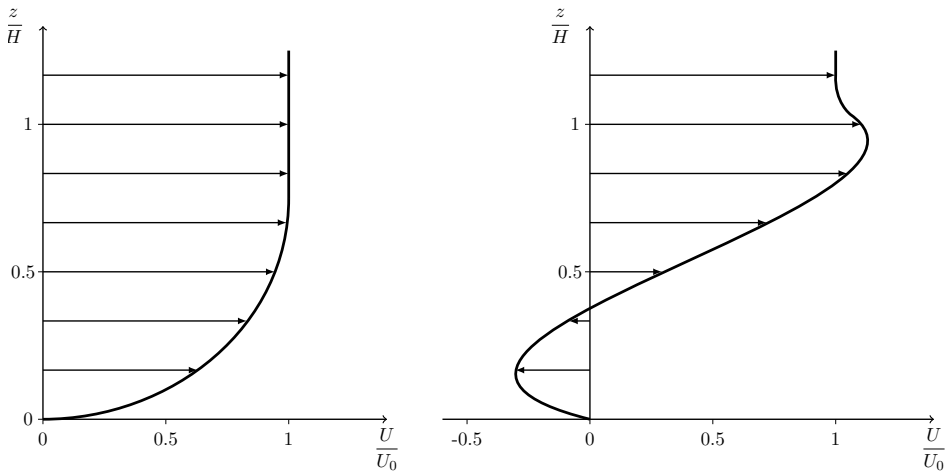

Fig. 9.7: Typical profiles of horizontal wind speed U as function of height z in the undisturbed boundary layer approach flow (left) and in the middle of a rotor (right). The vertical coordinate is normalized by the mountain height H, wind speed is normalized by the velocity U_0 above the mountain height. Wind profiles are based on field measurements and numerical simulations of rotors.

the approaching flow. As shown in Fig. 9.7, the wind speed in the approaching flow decreases near the ground due to frictional forces. If the wave-induced adverse pressure gradient is strong enough, the velocity induced by this force can exceed the wind speed of the approach flow resulting in a net flow backward to the mountain as is shown in Fig. 9.7 and happens in the fully developed rotor illustrated in Fig. 9.8.

This simple explanation for the rotor development underneath mountain lee waves is quite similar to the phenomena of boundary layer separation from airfoils leading to stall. In the latter, an adverse pressure gradient is induced by dynamic pressure differences over the wing system following Bernoulli's equation (see discussion in Section 2.5), a well known phenomenon in the field of aviation.

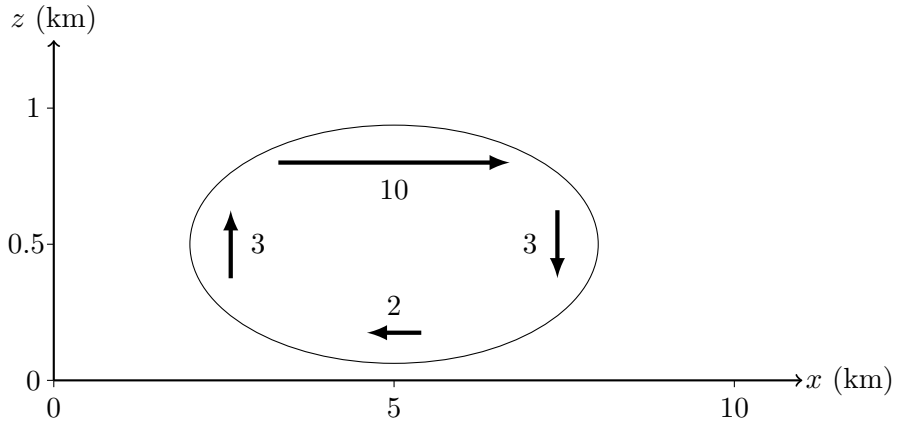

Fig. 9.8: Typical size of the rotor behind a mountain of moderate height ($H \approx 1\,\text{km}$). Typical horizontal and vertical wind speeds (in m/s) are indicated by arrows. Note that the scale of the vertical coordinate z is enlarged compared with the horizontal coordinate x.

The typical vortex size and wind velocities in rotors behind mountain ridges of moderate height ($H \approx 1\,\mathrm{km}$) are given in Fig. 9.8. The vertical extension of the rotor is of the order of the mountain height H, the horizontal size is about $6H$. Hence, the rotor is not a circular vortex but has more an elliptical shape (sketches of circular rotors are usually due to different scales of vertical and horizontal distances in rotor pictures found in publications). Typical vertical velocities are $\pm\ 3\,\mathrm{m/s}$ for moderate rotors as has been experienced by many glider pilots when entering the wave system through the rotor updrafts. As the rotor velocities also depend on the height of the mountain and on the strength of the approaching flow, vertical lift of the order of $10\,\mathrm{m/s}$ has been also observed in the rotor systems of large mountain areas like the Andes or the Sierra Nevada.

10 Travelling gravity waves

10.1 Introduction

We have focused our discussion above on mountain or lee waves as these waves are more or less stationary gravity waves induced by small and large mountains, the locations of which are known. If the stratification and wind speed remain nearly constant for hours, glider pilots will find lift areas over a suitably long period and hence mountain waves are most suitable for wave soaring.

In Section 5.4, it was pointed out that stationary gravity waves can be found if the phase speed of the waves are of equal magnitude, but of opposite direction to the approaching air flow (see Fig. 5.9). If this is not the case, the waves can move with or against the wind depending on their phase speed (denoted by c). As a rule of thumb, this phase speed is given by the relation $c = NL/2\pi$, where N is the Brunt-Vaisala frequency and L is the wavelength. Let us take, for example, the situation in the ICAO standard atmosphere, where $N = 0.011\,1/\mathrm{s}$ (see Table 3.1 in Section 3.5). If we take $L = 10\,\mathrm{km}$, the phase speed will be $c = 16\,\mathrm{m/s}$ (about 30 kn) and must be added to or subtracted from the wind speed depending on the wave direction to obtain the absolute wave speed with respect to a stationary observer on the ground.

In fact, gravity waves can be found nearly everywhere in the atmosphere, even over the oceans. All that is required is a source to trigger vertical excursions of air parcels which need not be the upslope or downslope ridge of mountains. We have already indicated the possibility of gravity wave launching by thermals impinging on the inversion at the top of the convective boundary layer during daytime conditions in Section 5.5 and these so-called thermal waves are discussed in the next section. More exotic gravity waves as lift sources for soaring flight are solitary waves which will be presented in Section 10.3.

10.2 Thermal waves

Thermal waves, also called convection waves, occur in the stably stratified atmosphere above a convective boundary layer. They have been explored by glider pilots like H. Jaekisch or C. Lindemann only since the 1970s, more or less accidentally (see Kuettner et al. (1987) for references). Early scientific investigations of these waves were performed by Kuettner et al. (1987) using research aircraft and radiosonde observations. Complementary model simulations were performed by Hauf and Clark (1989). The principle behind the triggering of thermal waves was indicated in Fig. 5.10 (Section 5.5). Thermals in the convective lower layer of the atmosphere, which are, e.g., used for thermal flight, impinge on the inversion capping this layer. If the atmosphere is stably stratified above the convective layer, which is mostly the case, the undulating inversion acts like a wave maker in a wave pool. The observations suggested however that there must also be an additional increase of wind speed with height of at least 3 m/s per 1000 m throughout the inversion layer in order for convection waves to be formed. The meteorological situation favorable for thermal waves is similar to the case for rotor formation shown in Fig. 9.3, except

that there are no mountains involved. A schematic of boundary layer clouds triggering thermal waves above an inversion layer is given in Fig. 10.1.

If the thermals (or Cumulus clouds in moist boundary layers) are distributed more or less randomly, the gravity waves triggered above the inversion will not be as regular as in the case of mountain waves (Hauf and Clark, 1989). Exceptions are so-called cloud streets in the convective layer, where Cumulus clouds are more or less organized in cloud rows oriented in the wind direction. These cloud streets have long been used by sailplane pilots for long distance soaring under thermal conditions. If there is not only an increase of wind speed with height, but also a strong change in wind direction above the inversion, gravity waves above can be organized parallel to the cloud streets below. But this case seems to be rare, as a strong change in wind direction only occurs under special meteorological conditions.

In contrast to mountain waves, thermal waves are difficult to predict and hence can be soared only more or less accidentally. Thermal waves are also only occasionally made visible by Lenticularis clouds, because the atmosphere above a strong inversion layer often contains insufficient moisture for cloud formation making visual identification of wave crests and hence lift areas difficult. Nevertheless, soaring thermal waves above Cumulus clouds have been experienced by many glider pilots. The techniques for entering and soaring these waves are described in, e.g., Hertenstein (2005) or Eckey (2012).

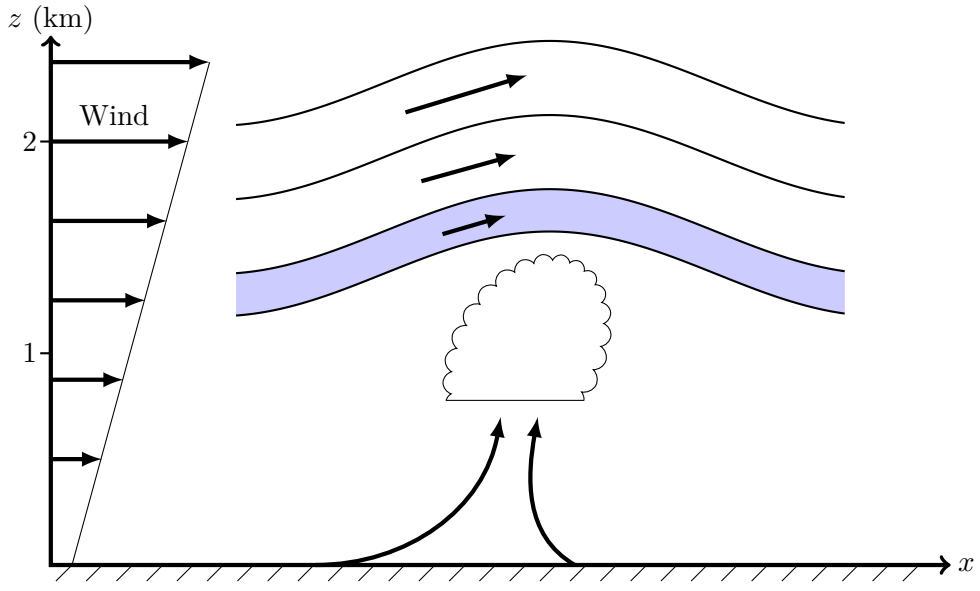

Fig. 10.1: Schematic of gravity waves (called thermal waves or convection waves) triggered by Cumulus clouds impinging on the capping inversion (shaded area) of a convective boundary layer. The necessary wind shear for wave formation is shown in the wind profile. Areas with upward lift for entering the wave are indicated by arrows.

10.3 Solitary waves

Solitary waves, also called undular bores, are perhaps the most exotic gravity waves used for soaring flight. In contrast to other gravity waves which usually are found throughout the troposphere, solitary wave are restricted to the lowest 1 - 3 km of the atmosphere. From a satellite perspective (Figure 10.2), they look like mountain lee waves, but in reality are not stationary as they move with typical speeds of about 30 - 50 km/h horizontally. The clouds produced by the updrafts of these waves look like those in Figure 10.2 showing a roll-like shape with horizontal extensions up to several hundreds of kilometres, where an airborne perspective and a surface view are shown in Fig. 10.3. These kinds of gravity wave occur at several places in the world, but most regularly (and to some degree predictable for soaring flight) in Northern Australia in the Gulf of Carpentaria (see Fig. 10.2), where they are called "Morning Glory". For references to this phenomenon, see, e.g., review articles by Christie (1992) or Smith (1988). With respect to soaring flight, the Morning Glory is treated in Eckey (2012) and Martinez (2012), where also many impressive photographs of the wave clouds are shown.

A sketch of the typical wave system of a Morning Glory (and other solitary waves) is shown in Figure 10.4. The wave front is moving at about 40 km/h in the horizontal and the vertical wind speed in front of the wave cloud can reach 2 - 4 m/s. This is comparable to wave lift in mountain lee waves, except that the lift areas are moving in the horizontal. The typical wavelength is about

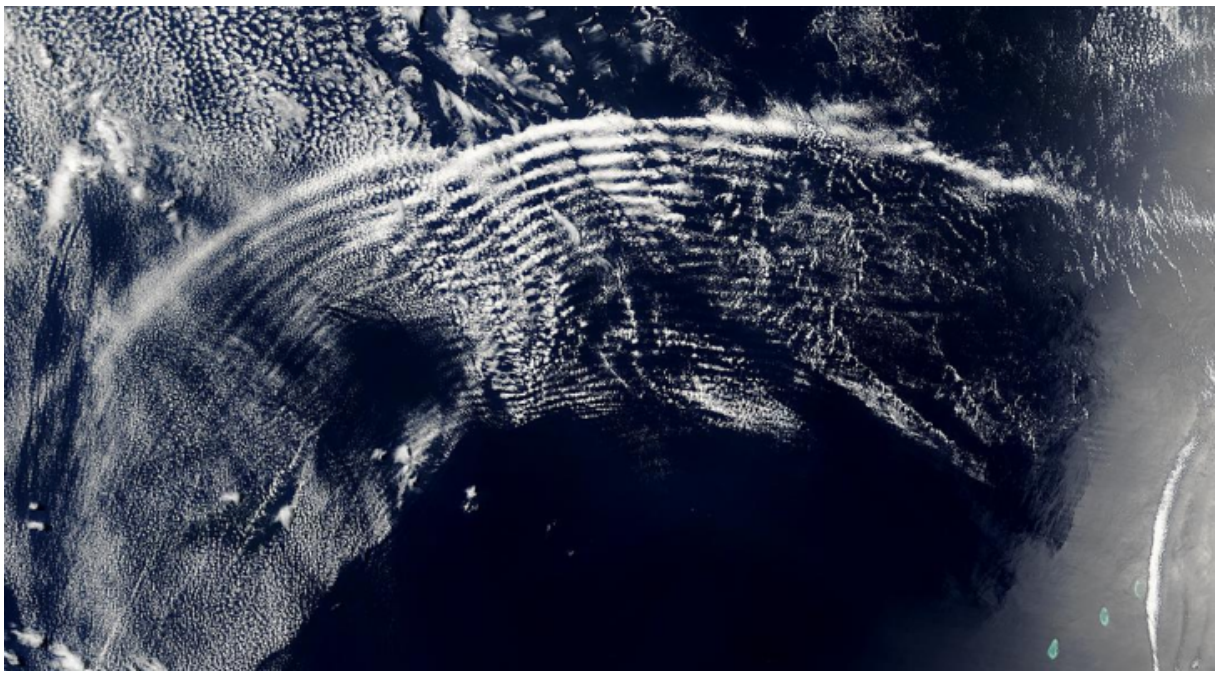

Fig. 10.2: Atmospheric solitary waves in the Gulf of Carpentaria, Northern Australia, made visible by cloud lines, as observed from a satellite. The waves are moving in the direction perpendicular to the first wave crests as indicated by cloud lines. The wavelength as measured by the distance between cloud lines is about 10 km. In this area, these waves are called the "Morning Glory".
Source: NASA Modis Rapid Response Team.

Fig. 10.3: The cloud rolls of the Morning Glory as observed over Northern Queensland from the ground (left) and from an airplane (right).
Photographs by Roger Smith.

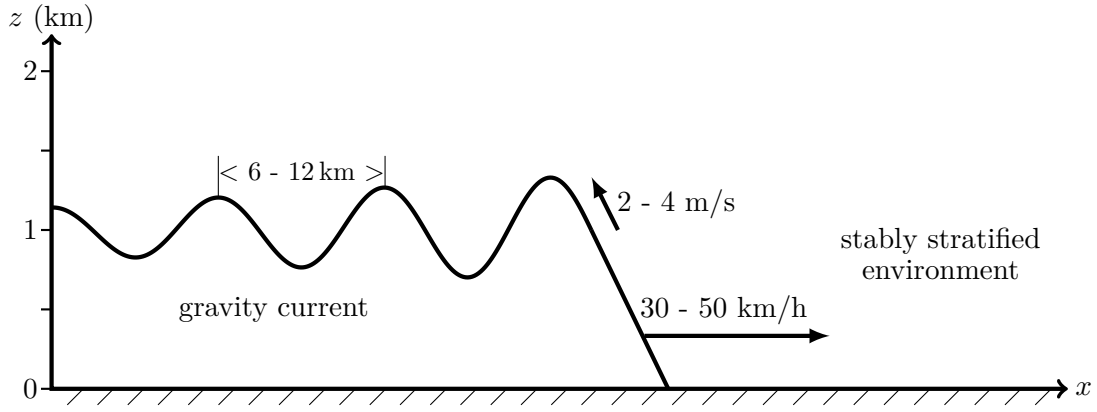

Fig. 10.4: Schematic cross section through an atmospheric solitary wave (like that shown in Fig. 10.2). The wavy outline indicates the gravity current moving into a stably stratified boundary layer. Typical velocities and spatial dimensions for these kinds of gravity wave are also provided.

6 - 12 km and the wave amplitude can reach 500 m. Soaring these solitary waves is analogous to wave surfing on ocean beaches, where the surfers are not just moving forward with the wave front but also sideways or parallel to the advancing wave crest. Although the Morning Glory wave in Australia has been known for a long time due its impressive cloud formation, it has only been used as a source of lift for soaring flight since 1989, starting with R. Thomson and R. White. Since then, the Morning Glory has been flown by sailplanes and powered gliders regularly, based mostly at Burketown in Northern Queensland, Australia (for more information, see the websites: `www.morninggloryaustralia.com` and `www.morningglorycloud.com`).

The physical origin of solitary gravity waves like the Morning Glory is not easily explained. In fact, these kinds of wave have kept theoreticians busy the last hundred years or so (see the recent collection by Grimshaw (2007) for details). Although several mechanisms have been discussed for the formation of the "Morning Glory" (see Christie, 1992 or Smith, 1988), the principle scenario seems to be the intrusion of a gravity current into a stably stratified atmospheric boundary layer

(the gravity current is indicated in Fig. 10.4). A gravity current, also called a density current, is a flow phenomenon which is formed when fluid layers of different densities are separated in the horizontal direction. A simple everyday example for a gravity current is if we spill some water on the kitchen floor, it will move sideways from its spill location. The reason is that the layer of water is much more dense than the surrounding air layer. According to the hydrostatic pressure law (see Section 2.4), the surface pressure in the water layer will be larger than the pressure in the surrounding air layer. Hence, there will be a horizontal pressure gradient which will accelerate the water into the direction of the surrounding air layer. The motion of the spilled water is one type of a gravity current, where the name gravity current stems from the fact that the hydrostatic pressure difference driving the current is induced by the gravity force.

Gravity currents can be found in many situations in environmental fluids (see Simpson (1997) for a collection). Examples include the sea breeze at coastal areas or the cold air outflows from thunderstorms impinging on the ground. Under special conditions concerning the propagation speed of the gravity current with respect to the surrounding wind speed, waves can be excited at the top of the gravity current (see Fig. 10.4) that extend over a limited distance into the stably stratified air layer above. For Morning Glory waves in Australia, these are mainly induced by colliding sea breeze fronts in the area of Cape York peninsula. In other areas of the world away from the coast, solitary waves may be induced by thunderstorm outflows travelling along the ground into a stably stratified boundary layer.

11 A short history of mountain wave soaring

The scientific research of mountain waves was very much connected with wave soaring in the early days of wave flight as described in the excellent monographs by Whelan (2000) and Martinez (2012) and so here we give only a short overview on the development of wave research and wave soaring. The first wave flight was performed by H. Deutschmann and W. Hirth in 1933 in the lee of the Riesengebirge Mountains in Central Europe. During these flights, Hirth also detected the rotors underneath the wave crests. His turbulent voyage through the rotor is described quite vividly in Whelan (2000). Following this event, the first systematic investigation of the mountain wave system of the Riesengebirge Mountains was performed by several glider pilots in 1937. The flight data were analysed by J. Kuettner (1939) and provided the first schematic of the lee wave system. His original map of the wave system is shown in Figure 11.1 and his pictures of the rotor system underneath the wave crests is shown in Figure 11.2.

From these early days of wave flight, glider pilots have used the mountain wave system for

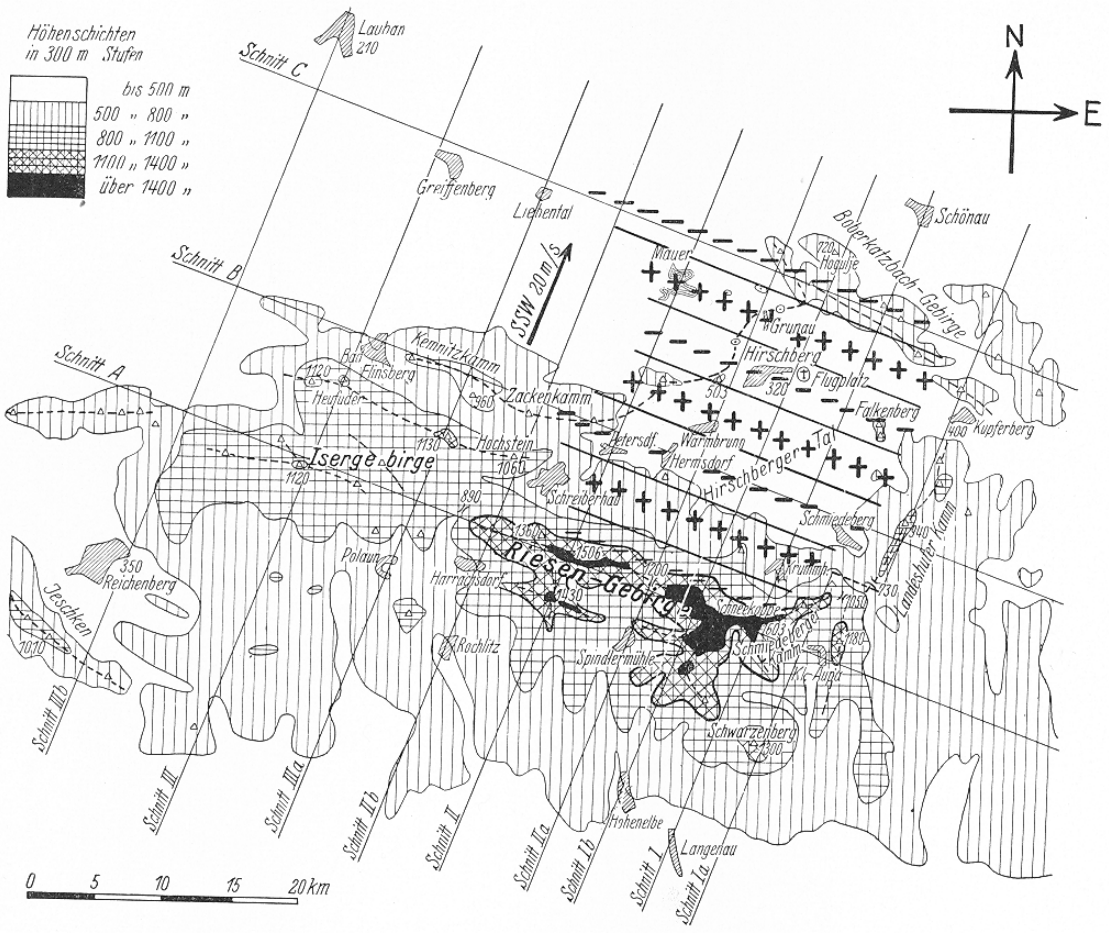

Fig. 11.1: Areas of upward (+) and downward (−) air motion in the lee of the Riesengebirge Mountains as derived from flight reports of various soaring flights on May 21, 1937. The wavelength of gravity waves as induced by the ridge of the Riesengebirge can be estimated from this map as 7 - 8 km.
From Kuettner (1939).

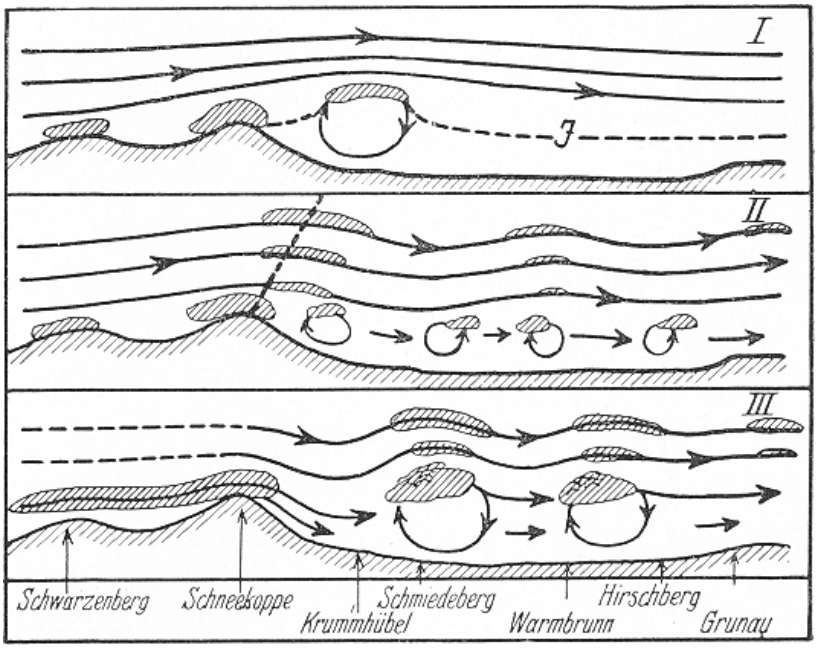

Fig. 11.2: Various interpretations of the flow above the Riesengebirge Mountains for the situation shown in Fig. 11.1. Schematic III including the lee waves and the rotors underneath was first proposed by Kuettner.
From Kuettner (1939).

extending their flights continuously with respect to distance and altitude. Kuettner was already able to soar up to 8 km altitude in the Riesengebirge wave. As early as 1940, the first flight by a sail plane to the edge of the stratosphere was conducted by E. Kloeckner, who reached the altitude of 11400 m above the European Alps. In the following years, other places in the world have been detected for wave soaring as described in, e.g., Queney et al. (1960). Here we mention only the Pennines in the UK (Manley, 1945) or the southern French Alps (Berenger and Gerbier, 1960). Later famous wave spots were found in the Sierra Nevada, USA (Whelan, 2000) and in the Southern Alps of New Zealand (Delore and Dew, 2005). The development of wave soaring in Canada is described in Wiese (1997).

In the years 1950 - 1955, mountain waves were subject to large field experiments named the Sierra Wave Experiment and the Jet Stream Experiment. A recent scientific retrospect of these experiments is given by Lewis and Grubisic (2004) and some of the wave flights performed with sailplanes during these field studies are described in Whelan (2000). Both field experiments took place above the Owens Valley at the flanks of the Sierra Nevada as this location was known for large amplitude mountain waves and strong rotors. Indeed, on one day a large amplitude mountain wave developed which kept a P38 powered aircraft aloft after its engines were shut down. The photograph of the enormous rotor cloud underneath the wave crest, as taken by the pilot B. Symons, has been the most published picture of a rotor (see, e.g., Whelan, 2000 and Martinez, 2012).

Very high altitudes up to 13 km have also been reached by sailplanes during these field experiments. Among them were flights by L. Edgar, K.E. Klieforth, J. Kuettner, B. Symons and B. Woodward. The wave system of the Sierra Nevada has been used since then by various pilots to challenge the altitude record for sailplanes. We mention only the last attempt by B. Harris, who placed the world record in 1986 at 14980 m. This was only broken in 2002 by S. Fosset

and E. Enevoldson in the lee of the Andes wave system with an altitude of 15440 m. In fact, besides the Southern Alps of New Zealand, the Andes have also become the place for chasing long distance records for soaring flight in recent years (see, e.g., Delore and Dew, 2005). The lee wave system of the Andes allows quite remarkable flights like the world record over 3009 km (a return flight from Chapleco, Argentinia) achieved by K. Ohlmann in 2003 or the record for a one way flight of over 2133 km (Kuettner Prize) flown by the same pilot in 2003 from El Calafate to San Juan in Argentinia (see Martinez (2012) or the website `www.mountain-wave-project.com`).

Despite these extraordinary flights performed in mountain wave systems, one should not forget that hundreds of glider pilots have performed successful wave flights since the early beginnings in 1933 using gravity wave systems triggered by large and small mountains nearby their home base. This kind of lift source for soaring flight will become even more attractive due to the advancement of knowledge of mountain wave physics and advances in forecasting mountain waves with recent numerical weather prediction models run by various national weather services as described in Section 8.

Appendix

The appendix is intended to give some more information on the formal treatment of internal gravity waves by means of physical equations and their mathematical formulation. Here we follow the usual notation of differences by using the symbol "∂" instead of "d" as used in the text for simplicity.

AI. The linear forms of the basic equations

In the following, we consider gravity waves as purely two-dimensional phenomena in the x - z coordinate plain. Hence, there are no variations in the second horizontal coordinate y in the direction parallel to the wave crests.

A basic state of the stratified atmosphere is defined with variables depending only on the vertical coordinate z:

$U(z)$ horizontal wind speed,

$\Theta(z)$ potential temperature,

$P(z)$ pressure.

Gravity waves are defined as *small* departures u, θ and p from this basic state as follows:

$$U_t(x,z,t) = U(z) + u(x,z,t),$$
$$\Theta_t(x,z,t) = \Theta(z) + \theta(x,z,t),$$
$$P_t(x,z,t) = P(z) + p(x,z,t),$$

where U_t, Θ_t and P_t denote the total (basic state + wave) wind, temperature and pressure fields, respectively.

The linearized equations mean that the wave quantities u, w, θ and p do not change the basic state $U(z)$, $\Theta(z)$ and $P(z)$. This concept is valid only for small perturbations;

$$p \ll P, \quad u \ll U, \quad \theta \ll \Theta.$$

For example, if the basic wind speed U is about 10 m/s, then the wind perturbation u induced by the waves should be about 1 m/s. As no mean vertical velocity exists in the basic state ($W = 0$), only perturbations $w(x,z,t)$ due to waves have to be considered.

The set of linearized equations for the formal description of wave motion is given below:

Momentum equation (equations of motion)

$$\frac{\partial u}{\partial t} + U\frac{\partial u}{\partial x} + w\frac{\partial U}{\partial z} = -\frac{1}{\rho_0}\frac{\partial p}{\partial x} \tag{A.1}$$

$$\frac{\partial w}{\partial t} + U\frac{\partial w}{\partial x} = -\frac{1}{\rho_0}\frac{\partial p}{\partial z} + \frac{g}{\Theta_0}\theta \tag{A.2}$$

Here, Θ_0 and ρ_0 are some typical constant values for temperature and density.

Heat equation (equation for potential temperature)

$$\frac{\partial \theta}{\partial t} + U\frac{\partial \theta}{\partial x} + w\frac{\partial \Theta}{\partial z} = 0 \tag{A.3}$$

With the definition of buoyancy

$$b = \frac{g}{\Theta_0}\theta,$$

this equation can be also written as

$$\frac{\partial b}{\partial t} + U\frac{\partial b}{\partial x} + wN^2 = 0. \tag{A.4}$$

Here, N is the Brunt-Vaisala frequency

$$N = \sqrt{\frac{g}{\theta}\frac{d\theta}{dz}}$$

.

Continuity equation

$$\frac{\partial u}{\partial x} + \frac{\partial w}{\partial z} = 0 \tag{A.5}$$

In equations A.1 – A.4, the first terms on the left hand side describe the temporal variations of wave properties u, w, θ or b. The second terms describe the advection (transport) of wave properties with the mean wind U and the third terms the advection (transport) of the mean wind U and temperature Θ by the vertical wave velocity w. In equations A.1 and A.2, the first terms on the right hand side (r.h.s) are the horizontal and vertical pressure forces, in A.2 the second term on the r.h.s is the buoyancy force.

AII. Wave equations

In order to find some analytic solutions for the equations A.1 – A.4, a so-called wave-ansatz is made for the variables u, w, p, and θ. For example, this is given for the vertical velocity w as

$$w(x, z, t) = w_0(z)\sin(kx - \omega t),$$

where $k = 2\pi/L$ is the wave number and $\omega = 2\pi/\tau$ is the frequency (L = wavelength, τ = oscillation period). The wave amplitude $w_0(z)$ has to be determined as a solution of the wave equations (see below) for a given combination of k and ω.

In seeking wave solutions to equations A.1 – A.4, it is usual practice to derive a single equation for the vertical velocity $w(x, z, t)$ from these equations. This is given for two special cases below.

(a) no background wind: $U(z) = 0$

$$\frac{\partial^2}{\partial t^2}\left(\frac{\partial^2 w}{\partial x^2} + \frac{\partial^2 w}{\partial z^2}\right) + N^2\frac{\partial^2 w}{\partial x^2} = 0 \tag{A.6}$$

The solutions of this wave equation are travelling gravity waves as discussed in Sections 5.1 – 5.3.

(b) stationary waves ($\partial F/\partial t = 0$, $F = u$, w, p, θ)

$$\frac{\partial^2 w}{\partial x^2} + \frac{\partial^2 w}{\partial z^2} + \left(\frac{N}{U}\right)^2 w = 0 \tag{A.7}$$

This is a simplified version where the curvature of the wind profile $U(z)$ has been neglected. The term N^2/U^2 is just the square of the *Scorer parameter* S introduced in Section 6.1.

The solutions of this wave equation are stationary gravity waves, especially mountain waves, which are discussed in Chapters 6 and 7.

AIII. Mathematical functions for the description of waves

Periodic functions

In Section 4.1, waves were defined as the periodic repetition of fluid properties (temperature, pressure, velocity) in space. The most simple formal description of waves can be given by means of sine or cosine functions. Here, we give some illustrations of these mathematical functions which will be named $\sin(\varphi)$ and $\cos(\varphi)$, where the argument φ is the Greek letter phi.

$$F_\mathrm{s}(\varphi) = \sin(n\varphi), \qquad \varphi = 0 \text{ - } 2\pi, \quad n = 1, 2, 3, ...$$
$$F_\mathrm{c}(\varphi) = \cos(n\varphi), \qquad \varphi = 0 \text{ - } 2\pi, \quad n = 1, 2, 3, ...$$

where π is the Greek letter pi with $\pi = 3.14$. The sine and cosine functions repeat themselves with the period 2π, hence $\sin(0) = \sin(2\pi) = \sin(4\pi)$ etc as is shown in Figures A.3 and A.4. The values of sin and cos are between -1 and $+1$ as is also shown in Fig. A.3.
Waves in real fluids are described by spatial and temporal variations. As the argument φ in the sine and cosine functions has to be a non-dimensional number, one has to introduce a wavelength L or wave period T to make the length x or the time t also non-dimensional. Waves and oscillations can then be formally described by:

$$F_\mathrm{s}\left(\frac{x}{L}\right) = \sin\left(\frac{2\pi x}{L}\right), \qquad F_\mathrm{s}\left(\frac{t}{T}\right) = \sin\left(\frac{2\pi t}{T}\right),$$
$$F_\mathrm{c}\left(\frac{x}{L}\right) = \cos\left(\frac{2\pi x}{L}\right), \qquad F_\mathrm{c}\left(\frac{t}{T}\right) = \cos\left(\frac{2\pi t}{T}\right).$$

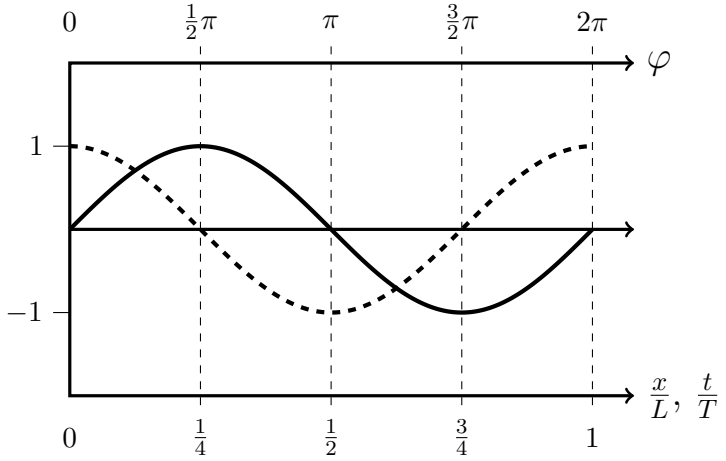

Fig. A.3: Functions $\sin(\varphi)$, solid line, and $\cos(\varphi)$, dashed line, for spatial (x/L) or temporal (t/T) coordinates for one wavelength L or one wave period T. Here, $\varphi = 2\pi x/L$ or $\varphi = 2\pi t/T$.

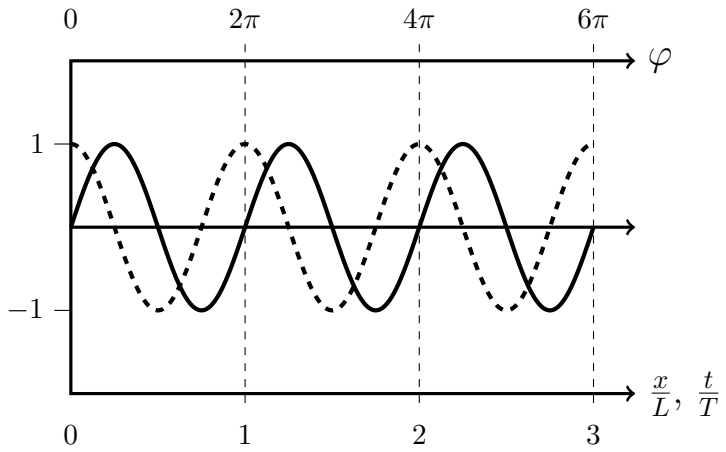

Fig. A.4: Examples of sine and cosine functions over 3 wavelengths or wave periods. Definitions are as in Fig. A.3.

These functions are displayed in Figures A.3 and A.4.

Waves as observed in the atmosphere or in the oceans can only in rare circumstances be described by a simple sine wave with one specific wavelength L (this case is called a *monochromatic* wave). In practice, waves are a superposition of several waves with different wavelengths (and amplitudes). The sine and cosine functions given above can then still be used for a formal wave description, one only has to sum up several of these functions with different wavelength L. The final result may provide a much more complicated wave structure than a monochromatic wave (see, e.g., the picture of water surface waves in Fig. 4.3).

Exponential function

Waves in the atmosphere do not extend infinitely in space but are limited to some horizontal or vertical distance and have a limited life time. This decay in space or time will modify the periodic wave behaviour as described by the sine and cosine functions above. Nearly all decay laws in physics can be described formally by the so-called *exponential function* exp or e:

$$F_{\mathrm{e}}(\varphi) = \exp(-\varphi) = e^{(-\varphi)}, \qquad \varphi = 0 \text{ ... any number.}$$

For $\varphi = -1$, $F_{\mathrm{e}}(\varphi) = e$, with e defined as the real positive number $e = 2.71$. The exponential function is displayed in Fig. A.5, where $F_{\mathrm{e}}(\varphi) = 1$ for $\varphi = 0$ and decays rapidly with increasing φ. Already for $\varphi = 3$ we have $e^{(-3)} = 0.05$, hence the exponential function has decayed to about 5% of its initial value.

If the exponential function is to be applied to waves and oscillations, one has to introduce a typical decay length L and a typical decay time T in order to obtain non-dimensional arguments (like the wavelength and wave periods for periodic functions sine and cosine). The exponential function can then be written as

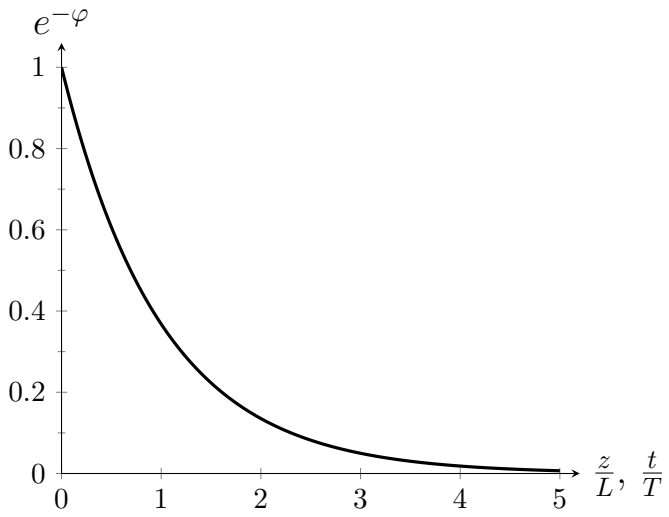

Fig. A.5: The exponential decay function $\exp(-\varphi)$ or $e^{-\varphi}$ with $\varphi = z/L$ or $\varphi = t/T$.

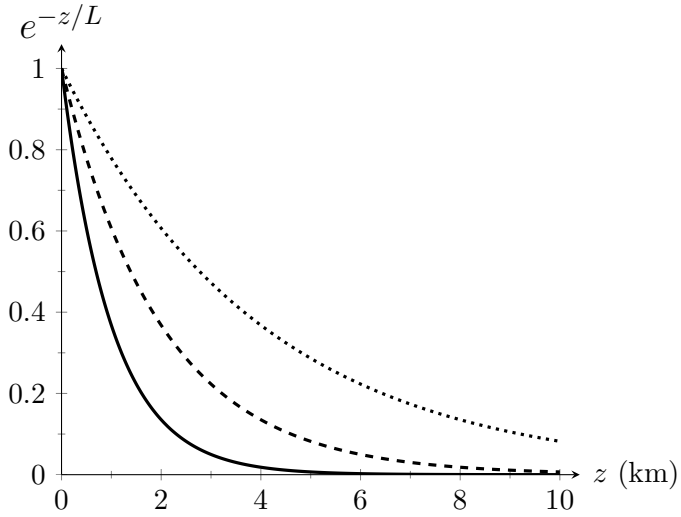

Fig. A.6: The exponential decay function $\exp(-z/L)$ for different values of the decay length L. $L = 1\,\mathrm{km}$: solid, $L = 2\,\mathrm{km}$: dashed. $L = 4\,\mathrm{km}$: dotted.

$$F_\mathrm{e}\left(\frac{z}{L}\right) = \exp\left(-\frac{z}{L}\right) = e^{(-z/L)},$$

where we have taken the vertical coordinate z as an example for spatial variations.

For temporal decay we obtain:

$$F_\mathrm{e}\left(\frac{t}{T}\right) = \exp\left(-\frac{t}{T}\right) = e^{(-t/T)}.$$

These functions are also displayed in Fig. A.5. In Fig. A.6, we give some practical examples for the decay of wave amplitudes in the atmosphere for different decay length scales L.

References (print and internet)

Books and scientific papers

Research on atmospheric gravity waves and mountain waves has been published in hundreds of papers. Here we present only a short list including articles in scientific journals and popular books.

1. Gravity waves and mountain waves

Baines, P. G., 1995: Topographic effects in stratified flows. Cambridge University Press, 515 pp.

Barry, R. G., 2008: Mountain weather and climate. 3rd edition, Routledge, 242 pp.

Durran, D. R., 1990: Mountain waves and downslope winds. In: Meteorological Monographs, **23**, 59-82. American Meteorological Society, Boston.

Durran, D. R., 2003: Lee waves and mountain waves. In: Holton, J. R., J. A. Curry. eds.; Encyclopedia of Atmospheric Sciences. Elsevier Science, 1161-1169.

Lighthill, J., 2001: Waves in Fluids, 2nd edition, Cambridge University Press, 524 pp.

Nappo, C., 2012: Introduction to atmospheric gravity waves, 2nd edition, Academic Press, 400 pp.

Queney, P. and 4 coauthors, 1960: The airflow over mountains. WMO-No. 98, TP.43. World Meteorological Organisation, Geneve, 135 pp.

Scorer, R. S., 1949: Theory of waves in the lee of mountains. Quarterly Journal of the Royal Meteorological Society, **75**, 41-56.

Sutherland, B. J., 2010: Atmospheric gravity waves. Oxford University Press, 394 pp.

Whiteman, C. D., 2000: Mountain meteorology: Fundamentals and applications. Oxford University Press, 345 pp.

2. Rotors

Doyle, J. D., D. R. Durran, 2002: The dynamics of mountain-wave induced rotors. Journal of Atmospheric Sciences, **59**, 186-201.

Grubisic, V., J. M. Lewis, 2004: Sierra wave project revisited: 50 years later. Bulletin of the American Meteorological Society, **85**, 1127-1142.

Grubisic, V., and 14 coauthors, 2008: The terrain-induced rotor experiment. A field campaign overview including observed highlights. Bulletin of the American Meteorological Society, **89**, 1513-1533.

Knigge, C., 2012: Untersuchungen von atmosphärischen Gebirgsrotoren mit Hilfe von Laborexperimenten und Grobstruktursimulationen. Dissertation, Fakultät Mathematik und Physik, Leibniz Universität Hannover, 155 pp.

Knigge. C., D. Etling, A. Paci, O. Eiff, 2010: Laboratory experiments on mountain-induced rotors. Quarterly Journal of the Royal Meteorological Society, **136**, 442-450.

Mobbs, S. D. and 8 co-authors, 2005: Observations of downslope winds and rotors in the Falkland Islands. Quarterly Journal of the Royal Meteorological Society, **131**, 329-351.

Sheridan, P. F., S. B. Vosper, 2006: A flow regime diagram for forecasting lee waves, rotors and down slope winds. Meteorological Applications, **13**, 179-195.

Vosper, S. B., 2004: Inversion effects on mountain lee waves. Quarterly Journal of the Royal Meteorological Society, **130**, 1723-1748.

3. Mountain waves and soaring flight

Dannhauer, K. H., 2011: Leewellenfluege am Harz. System Print Medien Leipzig, 303 pp.

Delore, T., R. Dew, 2005: Master of the wave. Delore Enterprises, 182 pp.

Dummann, J., 2009: A report on glider-pilot activities to document lee wave events in northern Germany and their aims. Technical Soaring, **33**, 109-116.

Eckey, B., 2012: Advanced soaring made easy. 3rd edition, eckey@internode.ou.net, 432 pp.

Hertenstein, R., 2011: Riding on air. Ridge, Wave and Convergence Lift. Bob Wander Soaring Books and Supplies, Minneapolis, 103 pp.

Kubitschke, N., 2011: Leewellen und Wellensegelflug im Mittelgebirge. Diploma Thesis, Institute of Meteorology and Climatology, Leibniz University Hannover, Germany, 94 pp.

Kuettner, J., 1939: Moazagotl und Foehnwelle. Beitraege zur Physik der freien Atmosphaere, **25**, 79-114.

Martinez, F., 2012: Ondas atmosfericas y vuelo sin motor. Historia, teoria y practica. Eqip, Bonn, Germany, 332 pp. (note: an English version entitled: Wave soaring: history, theory and practice, is announced for publication in 2014)

Marzinik, G. 2011: Wellenfliegen im Rheintal, Aerokurier **4/2011**, 124-126.

Palmer, M., 2004: Practical wave flying. Bob Wanders Soaring Books and Supplies, Minneapolis, USA, 80 pp .

Reichmann, H. 1993: Cross country soaring, 7th edition, Soaring society of America, Inc., 172 pp.

Whelan, R. F., 2000: Exploring the monster. Mountain lee waves: The aerial elevator. Wind Canyon Books, 196 pp.

4. Thermal waves and solitary waves

See also books by Eckey (2012) and Martinez (2012) listed under 3.

Christie, D. R., 1992: The Morning Glory of the Gulf of Carpenteria: A paradigm for non-linear waves in the lower atmosphere. Australian Meteorological Magazine, **41**, 21-60.

Grimshaw, R. H. J., 2007: Solitary waves in fluids. WIT Press, 208 pp.

Hauf, T., T. L. Clark, 2009: Three-dimensional numerical experiments on convectively forced atmospheric gravity waves. Quarterly Journal of the Royal Meteorological Society, **115**, 309-323.

Hertenstein, R. 2005: Thermals. Bob Wanders Soaring Books and Supplies. Minneapolis, 92 pp.

Kuettner, J. P., P. A. Hildebrand, T. L. Clark, 1987: Convection waves: observations of gravity wave systems over convectively active boundary layers. Quarterly Journal of the Royal Meteorological Society, **113**, 445-467.

Simpson, J. E., 1997: Gravity currents in the environment and the laboratory. 2nd edition, Cambridge University Press, 262 pp.

Smith, R. K., 1988: Traveling waves and bores in the lower atmosphere: the Morning Glory and related phenomena. Earth Science Reviews, **25**, 267-290.

5. Weather and soaring flight

Bradbury, T. 2004: Meteorology and flight. 3rd edition., A&C Black Publishers, 192 pp.

Piggott, D., 2004: Understanding flying weather., A&C Black Publishers, 96 pp.

OSTIV, 2009: Weather forecasting for soaring flight. WMO-No. 1038, World Meteorological Organization, Geneva, 78 pp.

Wallington, C. E., 1980: Meteorology for glider pilots. 3rd edition, Transatlantic Arts, 320 pp.

6. History

See also books by Delore and Dew (2005), Whelan (2000) and Martinez (2012) listed under 3.

Berenger, M., N. Gerbier, 1960: Experimental studies of lee waves in the French Alps. Quarterly Journal of the Royal Meteorological Society, **87**, 13-23.

Kuettner, J., 1939: Moazagotl und Föhnwelle. Beitraege zur Physik der freien Atmosphaere, **25**, 79-114.

Manley, G., 1945: The helm wind of Crossfell, 1937-1939. Quarterly Journal of the Royal Meteorological Society, **71**, 197-219.

Queney, P. and 4 coauthors, 1960: The airflow over mountains. WMO-No. 98, TP.43. World Meteorological Organisation, Geneve, 135 pp.

Wiese, U., 1997: Stalking the mountains. Stellar Craftworks, 220 pp.

Internet sources

Searching for information on mountain waves and wave soaring using the internet is quite convenient and provides additional information to the references listed above. In the following, some web pages are listed which are concerned with these topics.

Wave soaring activities in Northern Germany including pilots flight reports and presentations on various aspects of wave soaring given during the annual meeting of wave soaring enthusiasts are provided at:

`www.schwerewelle.de`

A collection of wave and rotor positions for various places in the world and information on wave research conducted with instrumented sail planes are given at:

`www.mountain-wave-project.com`

News on wave soaring can be found in the online magazine Soaring Cafe at:

`www.soaringcafe.com/tag/wave-soaring/`

An online teaching course on Mountain Waves and Downslope Windstorms is provided for free (registration required) by the education and training program COMET of UCAR, Boulder, CO, USA at:

`www.meted.ucar.edu/mesoprim/mtnwave`